Assessment of a Shredding Technology of Waste Printed Circuit Boards in preparation for Ammonia-based Copper leaching

Marc Patrick Prestele

Supervisors: Prof. Jochen Petersen & Dr. Thandazile Moyo

December 2020

Thesis presented in partial fulfillment of the requirements for the degree of Master of Science in Chemical Engineering at the Department of Chemical Engineering, University of Cape Town

Declaration

I, Marc Patrick Prestele, declare that this thesis was written, compiled and research was conducted by myself, unless where otherwise explicitly stated within the text. All sources obtained were correctly acknowledged and referenced. I further confirm that this thesis has not been submitted for any other degree or professional qualification in this or any other professional academic institution.

Signed by candidate

12.December 2019

Marc Patrick Prestele **Date**

Acknowledgments

Foremost I would like to thank my supervisor Professor Jochen Petersen for taking me under his wing as his student and letting me be part of the Hydrometallurgy family. I learned a great deal which helped me grow as a person. Thank you for your wisdom, guidance and for giving me the freedom to conduct this research on my basis while continuously encouraging me.

I would further like to express my deepest gratitude to my co-supervisor Dr. Thandazile Moyo, who never refused to assist, guide and teach me throughout the course of this research. Thank you for continuously bearing with me and never losing faith in me.

I need to express a heartfelt thank you to Kathija Shaik, without whom none of my hydrometallurgy laboratory-based experiments would have succeeded. I will never forget your continuous and never-ending support as well as the numerous lessons on how to conduct research properly. I will fondly remember the numerous hours in the lab and the many discussions about all kinds of topics.

I would also like to acknowledge the SARCHi chair for funding this project as well as the National Research Foundation for their financial support.

Another heartfelt thank you goes Joachim Macke without whom I could never have accomplished and finished the project. Your mechanical knowledge, fantastic work, and continuous help and support were greatly appreciated by me.

I also would like to thank a number of people for their guidance and help, including Ameen Jakoet for the advice on all electrical issues I encountered, Penny Louw for guiding me through the strength analysis, Tokoloho Rampai for helping me analyse and discuss said tests. Furthermore, I would like to thank the entire CMR staff for their greatly appreciated help and assistance. Last but not least I would like to thank Russel Geland, Sandeeran Govender and the rest of the UCT Analytical lab as well as Charney Small from CAF Stellenbosch for spending countless hours analysing my endless samples.

I would also like all the people in and around the Hydrometallurgy family who kept me sane and smiling throughout the two years. Special thank you to CK, Chad, Ruane and De Waal.

Finally, I would like to thank my family and friends for continuously encouraging and supporting me. To my mother Anke without whom I wouldn't be where I am today and my girlfriend Aleks, you were the rock who kept me going whenever I needed a little push, thank you both.

Abstract

The electronic waste (e-waste) stream grows at a global annual rate of 3-5%, with an expected 50 Mt to be discarded worldwide in 2020 alone. These large amounts of e-waste pose considerable environmental and health problems while also presenting socio-economic opportunities to most nations, especially to developing countries such as South Africa. E-waste presents a specifically unique challenge to developing nations as they suffer the challenges associated with e-waste, but do not have sufficient waste volumes to adopt business models used in developed countries to harness the economic opportunities presented by the growth of this waste streams. Recycling of e-waste requires huge capital and operating costs to run integrated recycling facilities and developing countries generally lack this funding. Furthermore, developing countries suffer from inadequate infrastructure, absent legislation and lacking capital investment which are necessary for the processing of e-waste regardless of it being regarded as a secondary resource or waste.

Printed circuit boards (PCBs) are a valuable fraction of e-waste, made up of tightly laminated metal-polymer composites containing several base and precious metals which makes them attractive to recyclers. Hydrometallurgy is a widely explored technology that allows for scalable operations for recovering metals from PCBs. However, for it to be effectively employed, the metals in PCBs need to be liberated or be accessible to leach agents. To date, this still heavily relies on energy-intensive pulverisation prior to the leaching and subsequent metal recovery stages. This paper explores the structure of the PCB, developing an understanding of how the structural design of the board translates to the difficulty in liberating or exposing the metals for leaching. The paper goes further to test and compare metal liberation techniques as well as compares energy consumption and costs associated with the techniques; with the view to identify a low energy and low capital investment method that would be suitable for adoption by small scale recyclers typical of those operating in South Africa.

The structural design of the PCBs was explored through an intensive literature survey and conducting a case study of the PCB manufacturing process of a local company as well as running tensile tests, drop weight impact tests and three-point bending tests on a batch of custom-made PCBs supplied by the local company. The metal liberation methods tested included the use of an industrial grab shredder to size reduce and delaminate the PCBs, use of a planetary ball mill and some instances including precursors such as freezing the PCBs in liquid nitrogen or soaking the boards in NaOH to remove the upper- and lowermost epoxy layers. The effectiveness of each method was then evaluated using a diagnostic ammoniacal leach test in which the extent of copper dissolution from the PCB is used as an indicator of the performance of the liberation method.

Results on the structural design of the PCBs showed that it would be suitable to use size reduction mechanisms that are based on impact stresses as the fibreglass and epoxy could absorb all other stresses at high intensity without failing.

In general, all treated or untreated PCBs underwent a maximum of six shredding passes, with results generally producing poor recoveries, not exceeding 27.5%. “Untreated” PCBs, referring to PCBs that only have undergone shredding in the industrial grab shredder, showed increasingly

higher copper recoveries with consecutively shredding cycles. The 6th cycle produced the highest copper recoveries of 6.80g (23.5%) after 72 hrs.

PCBs that had been soaked in NaOH and undergone six passes through the industrial grab shredder recovered a maximum of 27.5%. Interestingly, using a similar process but only shredding the PCBs in four passes showed similar results at 26.14% Cu recovery. Shredding the PCBs in four passes and subsequently milling them for 60 min (without NaOH treatment) showed lower Cu recoveries at 13.29% and this was not improved by extending the milling time to 120 min. This showed that the NaOH treatment was more effective in exposing the outer layers of copper relative to the shredding and milling.

It can be seen that apart from size reduction there is delamination of some of the shredded PCB pieces. However, this delamination is not always complete and Cu metal can still be seen covered by fibreglass and hence inaccessible to leach agents. It is concluded that the combination of the shredding and NaOH method has potential and it is recommended to incorporate a 2nd NaOH stage to further delaminate the inner layers of the PCB exposing the copper.

Table of Contents

Table of Figures

List of Tables

List of Equations

Nomenclature

Abbreviations

E-waste	Electronic waste
Mt	Million metric tonnes
PCBs	Printed Circuit Boards
EEE	Electronic and electrical equipment
Liberation	Physical separation of copper from dielectric material
WEEE	Waste electronic and electrical equipment
Delamination	Physical separation of the multi-layered PCB
SA	South Africa
wt%	Weight percent
ktons	Kilo tonnes
E-glass	Electrical grade glass
Pre-preg	Pre-impregnated
ED copper	Electrodeposited copper
RA copper	Rolled-annealed
ppm	Parts per million
ICP-AES	Inductively coupled plasma atomic emission spectroscopy
UV	Ultra-violet
IGS	Industrial grab shredder
Untreated	PCBs that were only shredded and did not undergo any other treatment
PBM	Planetary ball mill
PSD	Particle size distribution
Liq. N_2	Liquid Nitrogen
hrs	hours
min	minutes
sec	seconds
µm	micrometre

Chemical Formulas

Au	Gold
Ag	Silver
Pt	Platinum
Pd	Palladium
Cu	Copper
Cu^{+}	Cuprous ion
Cu^{2+}	Cupric ion
H_2SO_4	Sulfuric Acid
HNO_3	Nitric Acid
$HCl:HNO_3$	Aqua Regia
HCl	Hydrochloric Acid
H_2O_2	Hydrogen peroxide
$Cu(NH_3)_4^{2+}$	Tetraamminecopper(II)
$Cu(NH_3)_2^{+}$	Diamminecopper(I)
NH_4OH	25 % Ammonia Solution
$(NH_4)_2CO_3$	Ammonium Carbonate
$CuSO_4.5H_2O$	Copper (II) Sulphate Pentahydrate
NaOH	Sodium Hydroxide

I. Introduction

a. Background

Electronic waste (e-waste) is currently the fastest growing waste stream in the world, growing at an annual global rate of between 3 – 5%. It is expected that in 2020, approximately 50 million metric tonnes (Mt) of e-waste will be generated as a direct result of the increasingly faster global consumption of electronic products (Baldé et al., 2017). Overall, developing nations mostly struggle to deal with these vast amounts of e-waste, generally opting to discard the waste in landfill sites rather than to recycle it. E-waste recycling is considered to be beneficial both in terms of an economic and environmental context, advancing both the economy and the social welfare of developing nations at the same time (Grant & Oteng-Ababio, 2012; Ghosh et al., 2015).

The e-waste recycling industry is thought to be a lucrative business in developed nations due to the high amounts of base and especially precious metals present within it. The main component that can be found in virtually all types of e-waste is the tightly laminated high metal-containing Printed Circuit Board (PCB). Without this none of the electronic and electrical equipment (EEE) could function. Comprised of on average 30 % metals and 60 % non-metals, the PCBs hold the main portion of the economic valuable metal fraction of all e-waste. The most valuable metals, and therefore the economic driving force behind the recycling processes of PCBs, are precious metals such as gold, silver, and platinum (Baldé et al., 2017). However, unlike the precious metals which are present in relatively small amounts, copper is of relatively high abundance (± 20 wt%) within the PCBs (Wang et al., 2005; Yoo et al., 2009). As a result, the recovery of copper from PCBs is another economic motivator for the recycling of e-waste (Baldé et al., 2017).

Metal extraction from the tightly laminated PCBs is complicated as well as an energy-intensive process. PCBs are generally processed by either pyrometallurgical or hydrometallurgical process routes to effectively recover the valuable metals (Ghosh et al., 2015). Hydrometallurgical processing, unlike pyrometallurgical processing, requires pre-treatment of the boards for successful metal liberation through mechanical action. In general, complete pulverization of the PCBs to ≤ 2 mm is required to achieve the complete liberation of the copper and other metals from the dielectric material. Nevertheless, this process is regarded as the most energy-intensive and therefore expensive process step of the entire recycling stage (Ruan & Xu, 2016). This mechanical action is generally achieved through grinding, shredding, milling or pulverising of the boards to a range of fine particle sizes (Ghosh et al., 2015).

Presently pyrometallurgical processing of e-waste is the preferred recovery route for e-waste recycling as it generally can accept all forms of waste electronic and electrical equipment (WEEE) and yields metals of high purity grade. There exists an ongoing debate as to which, pyrometallurgical or hydrometallurgical processing of PCBs, is more environmentally friendly. However, this debate is somewhat irrelevant as pyrometallurgical processing also utilises hydrometallurgical down-stream process routes. Because of this, research into hydrometallurgical processing has increased over recent years (Ilankoon et al., 2018).

Both acidic and alkaline systems can be used to achieve metal recovery using the hydrometallurgical recovery process. Alkaline-based hydrometallurgical leaching and processing

of e-waste have become a more favoured process in recent years. This is primarily because of the lower operation costs, higher specific metal selectivity and reduced environmental impact (Cui & Anderson, 2016). However, to achieve copper recovery, the PCBs need to be reduced in size for the lixiviants to be able to access the metals held within the tightly laminated layers. Therefore, delamination, defined as the physical separation of the individual layers of a PCB, will expose the inner copper layers enabling copper extraction by lixiviants.

b. Problem Statement

Focus on base metal extraction, especially copper, from PCBs has increased over recent years due to the high abundance, ease of recovery and increase in economic value. The use of alkaline-based systems rather than acidic systems has proven to be effective in the recovery of copper. Especially the use of ammonia-based lixiviants in combination with salts such as carbonate, sulfate or chloride has shown greater specific copper selectivity with reduced environmental impacts (Koyama et al., 2006).

The recovery of copper by ammonia lixiviants still strongly depends upon the accessibility of the metals to the lixiviant. This, however, is complicated by the tightly laminated nature of the PCBs. The degree of copper liberation from the mechanical pre-treatment processes, therefore, plays an important role in the downstream effectiveness of copper recovery from PCBs. This mechanical size reduction is the most energy-intensive process of the entire recycling procedure and optimising this step is hence desirable (Ruan & Xu, 2016).

However, most published research neglects to report on the mechanical mechanism used for size reduction, nor does it state the amount of energy consumed during this stage of the recycling process. If reported, grab or cutting shredders are often utilized as the primary stage to introduce initial size reduction to the PCBs prior to further milling to finer particle sizes (Wang et al., 2005; Oliveira et al., 2010; Bizzo et al., 2014).

c. Objectives

The present research aims to investigate and develop an improved understanding of the following objectives:

1. Conduct preliminary failure analysis tests to characterize the physical properties of PCBs by analysing drop-impact, three-point bending, and tensile stresses
2. Evaluate the effectiveness of the clawing mechanics of an industrial grab shredder in terms of liberating the copper from the PCBs
3. Assess and compare the efficiency of pre- & post-treatments in terms of liberation of the copper from the custom-made PCBs
4. Record and interpret the energy costs that are associated with the size reduction process of the industrial grab shredder and other pre- & post-treatments
5. Utilize ammonia carbonate leach system to evaluate and compare the copper recovery from the variously treated processes
6. Test and validate the cost associated with the recycling processes investigated

II. Literature Review

a. The E-waste Challenge

The rapid expansion of the e-waste stream is caused primarily by increasingly faster turnaround time as well as shortened electronic product lifetime due to continued technological innovation and constant economic market expansions (Oliveira et al., 2010). As a result of this, 44.7 Mt of e-waste was generated globally in 2016 alone, of which 0.3 Mt is generated in South Africa. Based on current projections, it is estimated that the global e-waste generation will exceed 50 Mt by 2020 (Baldé et al., 2017).

i. E-waste Generation

These vast amounts of e-waste generated on a year to year basis pose considerable challenges to developing nations such as South Africa. These nations often do not have the suitable infrastructure and legislation in place nor the funds available for recycling facilities to deal with these vast amounts of e-waste. As a consequence, most of the generated e-waste is discarded inadequately in landfill sites or is illegally recycled in the informal sector through open-air burning (Grant & Oteng-Ababio, 2012). It must be noted that the metallic pollutants within e-waste are generally non-toxic and only become hazardous if ingested or exposed into the environment above certain concentrations in liquid, gaseous and dust forms. This informal and poorly documented handling of highly toxic e-waste contributes to the modern challenges faced by the waste industry in developing nations. E-waste recycling, therefore, offers an attractive alternative for this waste challenge, providing economic as well as environmental benefits to these nations (Ghosh et al., 2015; Baldé et al., 2017).

ii. E-waste Categories

E-waste, also referred to as waste electronic and electrical equipment, describes and includes all kinds of waste that are of electrical or electronic nature. These products were further classified into six major waste categories by Baldé et al. (2017) and are presented in Table II-2.

Table II-1: E-waste categories and example products (adapted from Baldé et al. (2017))

Group	Categories	Example products
1	Temperature exchange equipment	Refrigerator, Freezer, Air conditioner
2	Screens/Monitors based equipment	Laptops, TVs, Tablets, Monitors
3	Lighting equipment	Fluorescent lamps, LED lamps
4	Large equipment	Washing machines, electric stoves
5	Small equipment	Microwaves, Vacuum cleaners, Radios
6	Small IT & telecommunication equipment	Mobile phones, Printers, Routers

Table II-1 lists these six e-waste categories and example products included in each category. Recycling of the e-waste stream is a complex challenge because each of these categories has a wide range of different EEE products. Moreover, these six categories are fundamentally different, as each of the categories has a different lifecycle, culminating in various waste quantities, required recycling processes and environmental impacts if recycled inadequately. To further add to the complexity of e-waste, the products in each of the categories are characterized by a high variation in both weight and lifetime. These variations of the individual EEEs are displayed in Table II-2 (Baldé et al., 2017).

Table II-2: E-waste category, weight and estimated lifetime (adapted from Baldé et al. (2017))

EEE product	E-waste category	Weight of product (kg)	Estimated lifetime (years)
Refrigerator		35	10
Air conditioner	1	55	12
Freezer		35	10
Television (TV)		30	5
Desktops (PC)	2	25	3
Electronic games		3	5
Washing Machine		65	8
Tumble Dryer	4	35	10
Photocopier		60	8
Microwave		15	7
Vacuum cleaner	5	10	10
Radio		2	10
Mobile phone		0,1	2
Fax machine	6	3	5
Telephone		1	5

Management of the e-waste stream is, therefore, an incredibly complex process as each waste category requires its own unique management. Proper legislation, adequate collection infrastructure, and state-of-the-art recycling facilities are inevitable for the recycling of e-waste (Baldé et al., 2017).

iii. Recycling Rate

On a global scale, the e-waste stream continues to grow at an annual rate of between 3-5% (Das et al., 2009; Kumar, Holuszko & Espinosa, 2017). At the same time, the minable years of copper resources are estimated to only last for another 30 years. An alternative source for copper, therefore, needs to be allocated urgently. Copper recovery from e-waste materials through recycling is certainly an option that should be further investigated (Konishi et al., 2014). In the near future, the recycling and recovery of metals from e-waste will become even more of a necessity as it is today. However, recycling of this waste stream has proven problematic as

outlined earlier. Baldé et al. (2017) have reported that of the 44,7 million metric tonnes (Mt) of e-waste generated globally in 2016, only 20 % (8.9 Mt) was properly collected and reused or recycled, as shown in Figure II-1 (a). The fate of the other 80 % (35.8 Mt) is unknown. The authors' further state that developed nations tend to export their e-waste to underdeveloped countries, i.e. Ghana, but also that the WEEE is commonly treated with other general refuse waste and subsequently landfilled, incinerated or reused. The main reason, as stated in Figures II-1 (b), for this exceptionally high amount of undocumented e-waste is the fact that of the 195 countries that currently exist in the world, only 67 have national e-waste legislation in place. Discarding of e-waste is often considered to be a missed economic opportunity. The 44.7 Mt that were generated in 2016 are estimated to be containing raw materials worth approximately 55 Billion Euros. As of such, e-waste should be considered a secondary resource rather than waste (Baldé et al., 2017).

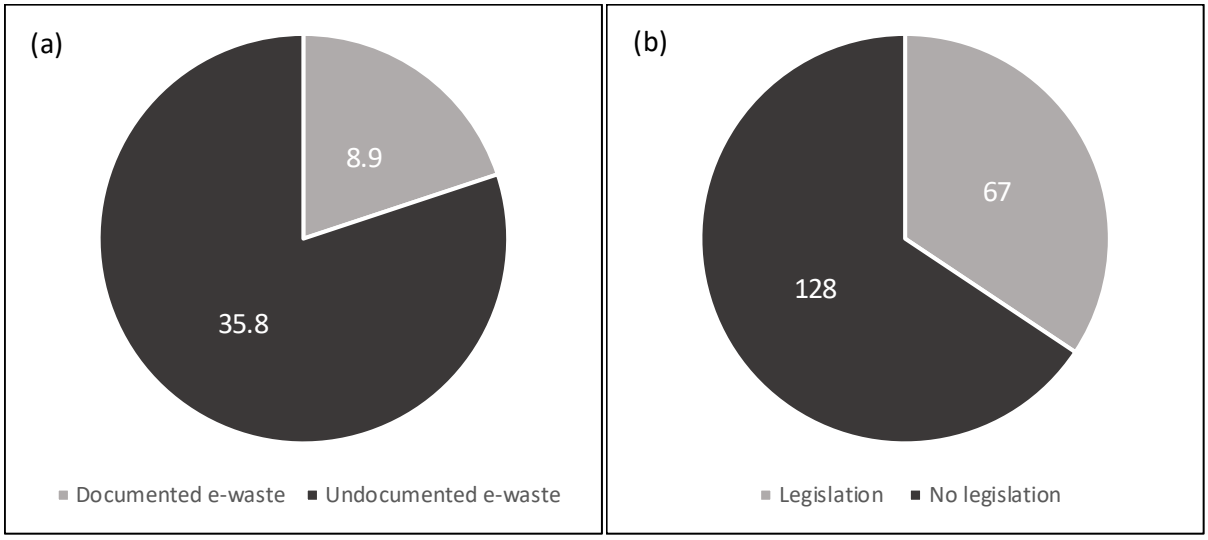

Figure II-1: Global e-waste data (a) - Global e-waste collection and recycling (Mt); (b) - Countries covered by e-waste legislation (adapted from Baldé et al. (2017))

Ore grades for most metals are in a steady decline, with easily accessible deposits slowly approaching end-of-life production. New deposits, on the other hand, are generally characterized by higher overburden, lower ore grade and growing expenditure required for extraction (Calvo et al., 2016). This is not only applicable to precious metals, but also for base metals. Bamber (2018) investigated the copper price and production trends from 1900-2018, highlighting that copper prices have increased 16-fold with copper being valued at $6400/t as of 2018. The author further placed emphasis on the sharp decrease in the average mined copper grade from a high of 2.5 % to under 0.5 % over the same time span. Furthermore, the copper price seems to be directly linked to the world population. As this number has been increasing exponentially since World War II, a supplementary and eventually alternative source of copper is necessary to supply future demand (Bamber, 2019).

iv. Importance of E-waste Recycling

However, mining is becoming increasingly more expensive because of the increase in necessary overburden removal, energy costs, emission charges and lower ore grade recovery (Rötzer & Schmidt, 2018). Global economies are therefore looking for alternative secondary resources, including the exploration of the recycling industry such as the e-waste industry (Calvo et al., 2016). Both papers agree that primary mining will continue to be the main production centre for all kinds of metals, but in order to continue to meet the world's resource demands, it needs to be offset by other industries, such as the urban mining industry (Calvo et al., 2016; Rötzer & Schmidt, 2018).

The recovery of valuable metals from WEEE is a complex and energy intensive process, yet, it is an easier and more economically favourable process than obtaining these metals from primary mining activities. The mining of there "urban ores", is therefore a favourable alternative to traditional mining. This is because e-waste contains considerably higher valuable precious as well as base metal concentrations compared to mined ore (Grant & Oteng-Ababio, 2012). The recycling of WEEE is however not as straightforward for developing countries as it is for developed countries. Developed countries employ integrated large scale, high capital cost, state-of-the-art recycling facilities that enable proper and effective recovery of valuable metals. South Africa on the other hand, like many other developing nations, lacks the capital, infrastructure and adequate legislation for proper recycling to successfully be implemented (Baldé et al., 2017).

v. E-waste Status in South Africa

As of 2019, South Africa (SA) has yet to pass an e-waste bill into law and, as a result of this, inadequate management of this waste stream has been observed (Baldé et al., 2017; DEA, 2018). Because e-waste is not considered a secondary resource in SA, much of the recorded e-waste that is generated each year has been discarded improperly or illegally recycled in the informal sector. The Department of Environmental Affairs (DEA) stated in the State of Waste Report: Second Draft (2018) that of the 360 000 t of e-waste generated in 2018 in SA, only 10 % of the WEEE generated that year was recycled, the other 90 % were disposed of in landfill sites (DEA, 2018). These numbers exclude the undocumented e-waste that is informally recycled in informal settlements. The lack of knowledge, absence of proper equipment as well as the high prices of the precious metals (Au, Ag, Pt, and Pd) within the e-waste are the driving forces for informal recyclers to apply unsafe and environmentally harmful measures to extract those metals. Through crude acid leaching or open-air burning, highly toxic metals (eg. As, Sn, Pb, Cr, Hg, Cd) and flame retardants (tetrabromobisphenol-A (TBBPA)) that form part of e-waste are released, posing a serious threat to the informal recyclers as well their immediate environment (Chatterjee & Kumar, 2009).

b. Printed Circuit Boards in E-waste

Without Printed circuit boards (PCBs), virtually none of the electronic devices could function and therefore most of WEEE contains PCBs. The focus of the recycling industry, therefore, lies in the recycling and eventual extraction of metals from these boards as they contain the highest abundances of the base, as well as precious metals.

i. Metallic Content

Because of the high heterogeneity of e-waste, it is difficult to pinpoint the exact weight percent (wt%) of PCBs within e-waste. Reported wt% Figures are displayed in Table II-3, placing the compositional percentage of PCBs within e-waste in the range of 2 - 12 wt% (Oguchi et al., 2011). This uncertainty of the actual mass of PCBs in e-waste is attributed to the high variability in weight and lifetime of different products within the six e-waste categories (Table II-4).

Table II-3: Weight percent of PCBs in e-waste

Author	Wt% PCB of e-waste	Author	Wt% PCB of e-waste
(Das et al., 2009)	6	(Oguchi et al., 2011)	12
(Widmer et al., 2005)	2	(Vidyadhar, 2016)	2
(Ongondo et al., 2011)	3	(Cui & Anderson, 2016)	3
(Luda, 2011)	8	(Hadi et al., 2015)	3
(Sohaili et al., 2012)	3	Average	5

Oguchi (2011) further investigated the PCB wt% of 21 types of waste electronic and electrical equipment. A snapshot of those WEEE products according to their e-waste category and their fractional weight percentage are displayed in Table II-4.

Table II-4: Type of e-waste and respective PCB wt% (adapted from Oguchi et al. (2011))

E-waste category	Type of WEEE	PCB wt% in e-waste
1	Refrigerator	0,5
	Air conditioner	2,7
2	LCD TV	11,6
	Notebook PC	13,7
4	Printers	7,4
	Washing machine	1,7
5	Stereo set	11,1
	Radio	10,4
6	Mobile phones	30,3
	Video game consoles	20,6

While PCBs wt% make up about only 0.5 % of refrigerators, their weight fraction spikes to about 30.3 % within mobile phones (Oguchi et al., 2011). However, even though their fractional composition is usually less than a tenth of the total mass, PCBs contain most of the valuable metals that make e-waste recycling economically viable. Most researchers place the PCBs compositional content at around 40% metals, 30% plastic, and 30% fibreglass. This however strongly depends on several factors including the type, the intended purpose, the age and the manufacturer of the individual PCBs (Wang et al., 2005; Yoo et al., 2009; Yamane et al., 2011; Birloaga et al., 2013).

ii. Economic Feasibility of PCB Recycling

Similar to the high variation in the reported wt% of PCBs in e-waste, there is also large variation within the reported metal content. Table II-5, adapted and expanded from Bizzo et al., (2014), displays the reported metal grade percentage of the most abundant base, precious and hazardous metals/elements in PCBs.

Table II-5: Metal content of waste PCBs (adapted & expanded from Bizzo et al. (2014))

Metal grade	**(i)**	**(ii)**	**(iii)**	**(iv)**	**(v)**	**(vi)**	**(vii)**	**(viii)**	**(ix)**	**(x)**	**(xi)**	**(xii)**
Cu (%)	19	20	22	12,5	19,7	28,7	12,6	19,2	23,5	28	27,5	14,2
Al (%)	4,1	4,1	-	2,0	2,9	1,7	2,4	7,1	1,3	2,6	1,3	-
Pb (%)	1,9	1,9	1,6	2,7	3,4	1,3	2,4	1,0	1,0	-	2,9	2,5
Sn (%)	1,1	1,1	2,6	4,0	3,7	3,8	1,4	2,0	1,5	-	3,4	4,8
Fe (%)	3,6	3,6	3,6	0,6	11,5	0,6	3,2	3,6	1,2	0,1	1,6	3,1
Zn (%)	0,8	0,8	-	0,1	2,1	-	-	0,7	1,5	-	2,9	0,2
Ni (%)	0,8	0,8	0,3	0,7	0,4	-	0,4	5,4	2,4	0,3	0,4	0,4
Au (ppm)	1120	1000	350	-	500	68	-	100	570	135	600	142
Ag (ppm)	5210	2000	-	350	500	79	-	70	3301	29	2600	317
Pt (ppm)	-	-	-	-	-	0	-	-	30	-	-	-
Pd (ppm)	-	50	-	-	-	33	-	-	294	-	-	-
Co (ppm)	-	-	-	-	300	-	-	400	-	-	-	-
Ti (ppm)	-	-	-	-	-	-	-	400	-	-	-	-
As (ppm)	-	-	-	-	-	-	-	-	-	-	-	11
Cd (ppm)	-	-	-	-	.	-	-	-	-	-	-	1183
Total Metals	**31,9**	**39,3**	**30,1**	**22,6**	**46,5**	**36,1**	**22,5**	**39,1**	**40,2**	**31,1**	**40,4**	**27,7**

(i) (Feldman, 1993); (ii) (Menetti & Tenorio, 1995); (iii) (Iji & Yokoyama, 1997); (iv) (Veit et al., 2002); (v) (Wang et al., 2005); (vi) (Creamer et al., 2006); (vii) (Das et al., 2009); (viii) (Yoo et al., 2009); (ix) (Oliveira et al., 2010); (x) (Guo et al., 2011); (xi) (Menad & Houwelingen, 2011); (xii) (Bizzo et al., 2014)

It is important to highlight that the precious metal grade content has decreased over the years, with Feldman (1993) and Menetti & Tenorio (1995) reporting values of 1000 ppm or above for gold, whereas most of the more recent articles report values of between 100 – 500 ppm (Bizzo et al., 2014). From Table II-5 it becomes further apparent that copper is the most abundant metal within PCBs, constituting between 12,5 – 28,7 wt% of the metallic fraction.

Copper content, on the other hand, displays no visual compositional trend. The primary reason for this is because the copper abundance in PCBs strongly depends on the purpose of the individual boards. The second most abundant base metals are aluminium, iron, and lead. The high base metals content implies that not only precious metals such as gold are the economic driving forces behind the recycling of PCBs, but that other base metals, especially copper, can also contribute to the economics behind the recycling (Pietrelli et al., 2014).

The tabulated data in Table II-5 also shows that the total metal content within PCBs usually ranges between 20 % and 50 %, averaging at 34 % for the analysed reports consulted. This high variation of the total metal content, as well as the documented variation of the individual metal contents, can be explained by the high heterogeneity of PCBs. A further reason for the variation is the difference is characterization techniques from the individual researchers.

As mentioned earlier, precious metals, especially gold, are the economic driving force behind the recycling process. Hagelüken (2007) expressed the value share of some of the metals present in PCBs in Table II-6. The value share of the precious metals, especially gold, considerably outweighs the value share of the base metals. However, because of the decline in gold content within PCBs, the value-share of the precious metals will decline simultaneously. Furthermore, with the copper content in the boards staying fairly constant and the increase in recycling of e-waste, more attention should be placed on the extraction of copper from the boards (Zhang & Xu, 2016).

Table II-6: Metal value share of waste PCBs (adapted from Hagelüken (2007))

Material in PCBs	Weight distribution (wt%)	Value share (%)
Fe	7	0
Al	5	1
Cu	20	14
Ag	1000 (ppm)	5
Au	250 (ppm)	65
Pd	110 (ppm)	15
Sum PMs	1360 (ppm)	85

iii. Environmental Benefits of PCB Recycling

Apart from the economic benefits that emerge with the recycling of PCBs, there are also several environmental benefits. Ayres (1997) and Veit (2002) compared the metal grade of PCBs with the ore grade generally found in standard mined ores. Table II-7, adapted and expanded from Pietrelli et al. (2014), compares the average mineral ore grade from mined ore to the metal grade that can be found within PCBs. The high-grade metal content within e-waste and particularly within

discarded PCBs, especially that of precious metals, is generally higher or at least equal to the mined ore grade. These further places emphasis on how e-waste should be handled as a secondary resource rather than waste. These high metal grades should also be seen as an incentive by all global economies to invest in proper recovery processes (Bizzo et al., 2014).

Table II-7: Environmental impact of PCB recycling

Metal	Mineral ore grade (%)	PCB metal grade (%)	Ecological burden ratio[ii]	Soil saved (ton/year)[ii]
Cu	0,5 – 2,0[i,ii]	12,5 – 28,7[iii]	50	42,1x10[iii]
Al	3,0 – 28,1[ii]	1,3 – 4,1[iii]	3,6	248,8
Fe	30 – 60[i]	0,1 – 11,5[iii]	1,7	55,71
Ni	0,7 – 2,0[i]	0,3 – 5,4[iii]	83,3	1,96x10[iii]
Au	1 – 15 ppm[ii]	68 – 1120 ppm[iii]	67x10[iii]	141,4x10[iii]
Ag	0,08[ii]	70 – 5210 ppm[iii]	1,3x10[iii]	3,8x10[iii]
Cd	40 ppm[ii]	31 – 130 ppm[ii,iii]	25x10[iii]	9,05x10[iii]

(i) (Ayres, 1997) & (Veit et al., 2002); (ii) (Pietrelli et al., 2014); (iii) maximum and minimum values according to individual metals from Table II-5.

Table II-7 also displays the ecological burden, defined as the ratio of mined metal to excavated rock, and the soil saved as a direct benefit of 100 % metal recycling for the Italian market as reported by Pietrelli et al. (2014). Assuming all PCBs are recycled in Italy, it would be possible to conserve 213 ktons of soil per year. Italy's gold mining industry inflicts the highest ecological burden, 141 ktons/year of soil to be exact, on the environment. An amount that could be considerably reduced by further encouraging the recycling of e-waste (Pietrelli et al., 2014).

Another further important benefit that recycling of end-of-life EEE products has over the mining of virgin ores are the large amounts of energy saved. These energy savings were adapted from Cui & Forssberg, (2003) and are tabulated in Table II-8. The Table lists several metals that are used within PCBs and their respective recycling energy savings compared to the production of primary mined materials (Cui & Forssberg, 2003; Khaliq et al., 2014). This also further alleviates the burden placed on the mining of ores from virgin materials. Introducing or increasing e-waste recycling will therefore not only alleviate pressure on the environment but also reduce the amount of energy that would be required to mine low-grade ores from virgin ores (Khaliq et al., 2014).

Table II-8: Energy savings from PCB recycling (adapted from Khaliq et al. (2014))

Metal/Material	Energy saved (%)	Metal/Material	Energy saved (%)	Metal/Material	Energy saved (%)
Aluminum	95	Iron & Steel	74	Plastics	> 80
Copper	85	Zinc	60	Paper	64

c. Printed Circuit Boards

This subsection outlines the general composition of PCBs as well as the general manufacturing process. It is subdivided into two sections, (i) manufacturing process and (ii) Components, including descriptions of the epoxy resin, the electronic fibreglass and the copper foil types typically used in PCBs.

i. Manufacturing Process

Printed Circuit Boards form the baseline component in all electrical and electronic equipment. Acting as the functional units of EEEs, these tightly laminated metal-polymer composites allow each of its compositional components (the metal and polymer layers) to retain their individual chemical, physical and mechanical properties. Similar to most composites, PCBs are mainly comprised of two phases, a matrix, and a reinforcing phase. Table II-9 lists the common base materials that are used for the cores of PCBs, according to classification by the National Electrical Manufacturers Association (NEMA) (Coombs Jr., 2008).

Table II-9: Types of PCB cores (adapted from Coombs Jr., (2008))

Terminology	Reinforcement	Resin	Flame Retardants
FR-2	Cotton Paper	Phenolic	Yes
FR-4	Woven Glass	Epoxy	Yes
G-10	Woven Glass	Epoxy	No
CEM-1	Cotton Paper/Woven Glass	Epoxy	Yes
CEM-2	Cotton Paper/Woven Glass	Epoxy	No

FR = Flame retardant; G = Glass epoxy; CEM = Composite epoxy materials

The manufacturing process of PCBs starts with the melting of raw glass materials in a furnace. Electrical grade glass (E-glass) is used in Printed Circuit Boards primarily due to its excellent fibre-forming capabilities. The formed continuous fibres are woven into fabrics of various patterns. The most common styles are 1080, 2116 and 7628 as displayed in Figure II-2 (a-d). Coupling agents are then added to the fibreglass, commonly in the form of an organosilane, which acts as a coating agent on the fibreglass surface, increasing the adhesive properties of the fibres and thereby ensuring higher adhesion at the matrix – reinforcement interface. Epoxy resin, originally derived from petrochemicals are formed by the polymerization of monomers from longer chains of organic molecules, so-called polymers. The fabrication of the epoxy resin and e-glass is referred to as A-stage (Ravikumar, 2008).

Additives such as curing agents, flame retardants, accelerators, and fillers are added to the matrix mixture as required by the design type of the board. Following the epoxy resin production stage, the fibreglass is embedded within the epoxy matrix to form the Pre-impregnated (Prepreg) composite (B-stage). The final stage of the PCB core production, the C-stage, includes the addition of rolled-annealed copper (RD-copper) layers under thermal pressure onto the prepreg. Multi-

layered circuit boards are made by the addition of several extra layers of copper and prepreg, with the number of layers corresponding to the number of copper foil layers. Each PCB has its own individual design, specified by the corresponding etching, stripping, drilling, and coating. The assembly process is completed through the application of a solder mask and the respective electronic components (Coombs Jr., 2008).

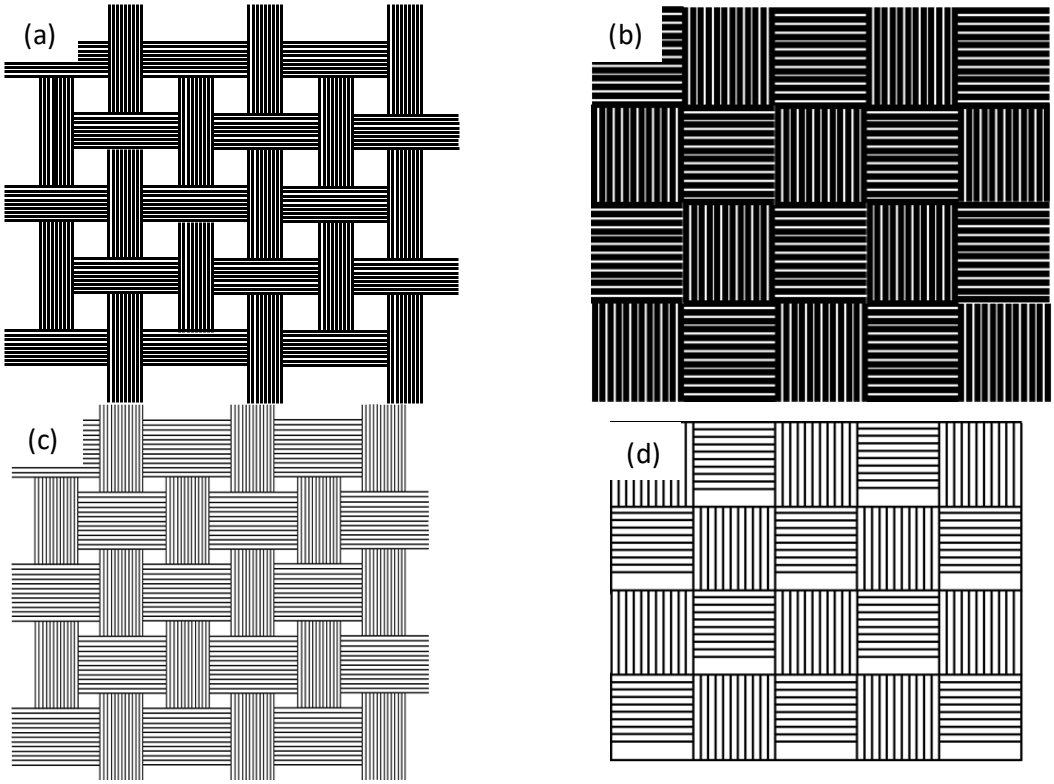

Figure II-2: Typical fibreglass weaving patterns in FR-4 cores (a) - 1080; (b) - 2116; (c) - 7628; (d) – 1506

ii. Components

The FR-4 composite, comprised of the thermoset epoxy resin with embedded woven E-glass fibres, is the most common type of core found in Printed Circuit Boards. This is primarily because of its extraordinary thermal, electrical and mechanical properties, allowing it to be suitable for a wide range of industrial applications including the computer, automotive and aerospace industries. Table II-10 summarises the basic components of a common FR-4 core PCB.

Table II-10: FR-4 core basic components (adapted from Ravikumar (2008))

Component	Purpose	Example Material
Reinforcement	Provide structural integrity (mechanical strength & stiffness)	Woven continuous Fibreglass (E-glass)
Matrix	Provide Reinforcement with support and protection	Epoxy resin (Thermoset plastic)
Coupling Agent	Increases adhesion properties on fibreglass	Organosilanes
Flame retardant	Decreases flammability	Tetrabromobisphenol A (TBBPA)
Curing Agents & Accelerators	Increases cross-linking and polymerization	Amine-based (Aliphatic diamines)
Conductive Material	Promote electrical conductivity	Electrodeposited & Rolled Annealed Copper foil

1. Reinforcement Phase

The reinforcing phase is a low-density material that provides strength and increases the stiffness of the composite structure. Even though the reinforcement phase is occasionally comprised of discontinuous particulates or fibres, in the case of PCBs and for most of the core types, it is usually found to be comprised of continuous glass fibres. The aspect ratio, length-to-diameter, of the fibres within the boards gives the composite its structural integrity. In general, the smaller the diameter and the longer the fibres, the greater the strength and flexibility of the composite structure.

Silica (SiO_2) is molten in combination with other mineral oxides, mainly Al_2O_3, CaO, and MgO, which are all required constituents of E-glass. The compositional ranges of E-glass used within FR-4 type PCBs are listed in Table II-11. During the early stages of E-glass production, while the glass is still viscous, the glass melt is rapidly drawn into fine diameter fibres and quickly cooled to avoid crystallization. Typically, these fibres have a diameter of between 3 - 20 μm and are subsequently woven into different patterns to increase the strength, stability, and stiffness. The most common weaving pattern is the plain pattern, with warp running lengthwise and the filling/weft running perpendicular to the warp, crossing over and under each other, as displayed in Figure II-2.

Table II-11: Elemental composition of E-glass (adapted from Coombs Jr. (2008))

Element	E-glass nominal weight percent (wt%)
Silicon Dioxide (Si_2O)	52 – 56
Calcium Oxide (CaO)	16 – 25
Aluminum Oxide (Al_2O_3)	12 – 16
Magnesium Oxide (MgO)	0 – 6
Boron Oxide (B_2O_3)	8 – 10
Sodium and Potassium Oxide (Na_2O & K_2O)	0 – 2
Iron Oxide (Fe_2O_3)	0.05 – 0.4

2. Matrix Phase

The matrix phase also referred to as the continuous phase, is usually a component of either polymeric, metallic or ceramic nature. In general, polymers have the lowest strength and stiffness, followed by metals with intermittent strength and stiffness. However, compared to the ceramics, which have the highest strength and stiffness of the three, polymers display a considerably higher ductile deformation behaviour whereas the ceramics display a more brittle behaviour. The primary function of the matrix is to support the reinforcing phase with proper orientation and spacing, but also to protect the fibres from abrasion. In the case of PCBs, the polymer and metal matrix composites form strong composite bonds with the fibres. During events where stress is applied to the composite structure, the matrix transmits the stress to the reinforcement phase through shear loading at the matrix-reinforcing interface (Coombs Jr., 2008).

The formation of polar or direct bonds between the epoxy resins' reactive sites and the polar sites on the substrate surface causes the resin to exhibit excellent adhesive properties. In general, inorganic compounds such as metals and fibreglass, display high polarity (high surface energy) whereas organic compounds, i.e. the resin, are found to be less polar (low surface energy). Because of the large difference in surface energies between the substrates and the adhesive (Table II-12), a strong attractive force is formed (Steven Label Corporation, 2019). The larger the difference in surface energies (Dyne/cm) between the various compounds, the higher the attractive forces between them. This permits the epoxy resin to wet the substrate surface and form strong bonds with the fibreglass and metals (Mereco, 2019).

Table II-12: Surface energies of PCBs components (adapted from Mereco (2019))

Material	Surface Energy (Dynes/cm)
Copper	1103
Glass	250 – 500
Typically cured epoxy	45

The matrix used for circuit boards is commonly epoxy resin, a type of thermosetting plastic. Thermoset plastics, unlike thermoplastics, cannot tolerate repeated heating cycles. By elevating

temperatures initially, the thermosets undergo chemical and physical reactions that result in the hardening of the material in a specific predetermined shape. The most commonly used epoxy resin in the printed circuit board industry is Diglycidyl Ether of Bisphenol-A (DGEBA), or short Difunctional Epoxy, which is derived through the reaction of Epichlorohydrin (ECH) and Bisphenol-A (BPA). By furthermore incorporating tetrabromobisphenol-A (TBBPA) to the Difunctional Epoxy, a brominated difunctional epoxy resin is formed that exhibits flame retardant capabilities (Coombs Jr., 2008).

3. Conductive Materials

Copper is the most commonly utilized metal in the PCB industry due to its high conductivity, availability, and price. There are many different types of copper foils available to the PCB industry, each with its own advantages and limitations. The overall purpose of the copper layers is to promote electrical conductivity between the individual layers of the PCB and the attached electronic components. Overall, there are two main types of copper foils most commonly used by the PCB industry, the electrodeposited (ED) and the rolled annealed (RA) copper foils. An important factor to note is the vertical grain structure of the ED and the horizontal grain structure of the RA copper foils. The two types of grain structures are displayed in Figures II-3 (a & b), adapted from Coonrod (2012). The red line in the two Figures represents the typical crack failure path experienced by the respective layers in stress environments (Coonrod, 2007).

The manufacturing process of ED copper foil starts with the dissolution of copper in sulphuric acid. The copper is then electroplated onto a stainless-steel drum, resulting in the drum facing side of the sheet to be smooth whereas the other, the solution facing side, to be of a coarse, rough nature (Coombs Jr., 2008). This rough side displays a generally vertical grain structure and aids in the bonding process, but in general, is unsuitable for small tracer lines and has been noted to exhibit bad bending resistance (Coonrod, 2012). RA copper foil on the other hand is manufacture by running an ingot of copper through a series of heated rollers, a foil of desired thickness and mechanical properties can be obtained. The grains are perpendicular, randomly orientated throughout the foil, suitable for thin tracer lines and are characterized by higher bending resistance. This type of copper foil is most commonly applied to the manufacturing of PCBs primarily because of its superior ductility over the ED copper. (Coombs Jr., 2008; Coonrod, 2012).

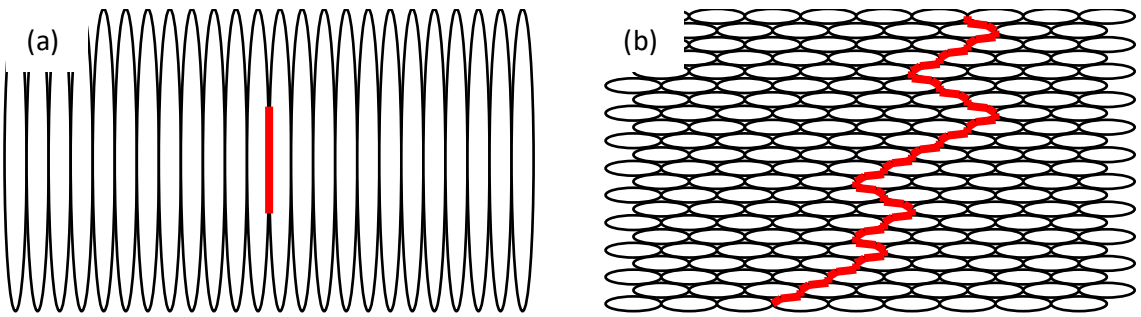

Figure II-3: Grain structure of two copper types (a) Electrodeposited copper; (b) Rolled-annealed copper (adapted from Coonrod (2012))

d. PCB Recycling

Even though there are numerous types of PCBs, the basic design layout, as well as the compositional structure, is the same, enabling recycling strategies to generally process all types of PCB. Within the e-waste recycling industry, there are three main recycling stages, beginning with the disassembly of the waste, followed by the upgrading stage and finally the refining and purification of metals stage (Cui & Anderson, 2016). The disassembly stage includes the separation of the high metal-containing materials such as PCBs from the larger bulk waste and to reduce the PCBs in size. This stage also aims to separate the metallic fraction from the non-metallic fraction by making use of several mechanical recycling processes (Ruan & Xu, 2016). The upgrading stage targets recovery of valuable fractions of the PCBs by making use of either mechanical, pyrometallurgical and hydrometallurgical recycling processes. These three routes often appear interlinked within the recycling industry as a combination of the processes results in better metal recovery. The final stage, the refining stage, deals with the refining of the metals by purification methods such as electrowinning to further purify the metals to high grades (Cui & Anderson, 2016). The diagram in Figure II-4 aims to visually show these stages with their respective processes.

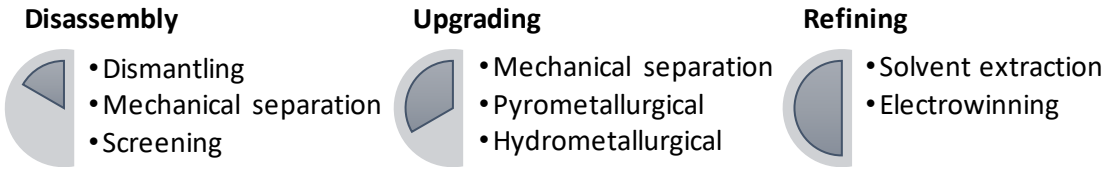

Figure II-4: Typical PCB recycling stages

i. Mechanical Separation Process

The mechanical recycling process is the main process that PCBs undergo in the disassembly stage. On their own, mechanical processes can be employed for the separation of metals from non-metals or can be used in subsequent combination with either the hydrometallurgical or pyrometallurgical processes in the following upgrading stage (Yoo et al., 2009). Due to the high density, strength and heterogeneous nature of PCBs, described in section II-b, mechanical size reduction as a precursor for downstream processing is a vital stage necessary for the hydrometallurgical recycling stream (Ruan & Xu, 2016). Various tools for size reduction are utilized in research as well as in the industry, including mechanical machines such as the crusher, ball mill, hammer mill, cutting mill, stamp mill and disc mill (Wang et al., 2005; Yoo et al., 2009; Yamane et al., 2011; Hanafi et al., 2012; Birloaga et al., 2013; Pietrelli et al., 2014).

Research has further shown that shearing or impact action forces are the most adequate forms of size reduction for e-waste (Ruan & Xu, 2016). However, attention must be placed on the level of size reduction, as excessive crushing will result in the pulverization of metals, resulting in inadequate downstream separation and further consume unnecessary amounts of energy (Ghosh et al., 2015). At the same time, insufficient crushing can result in poor liberation of the metals from the plastics and ceramics, again hindering the subsequent downstream processing of the

PCBs (Ruan & Xu, 2016). For complete copper liberation from the complex composite structures that are PCBs, a minimum particle size of ≤ 2 mm must be achieved (Zhang & Forssberg, 1998).

Following the mechanical size reduction stage, the PCBs often undergo a screening process to separate the crushed particles into uniformly sized sample fractions. This further aids the effectiveness of the downstream processes by prior separation of metallic from non-metallic fractions (Ghosh et al., 2015). Rotating screens, vibratory screens or trammels are often employed for this screening process (Kaya, 2016). Effective separation of metals from non-metals can then finally be achieved through in-sequence installed magnetic, electric conductivity and density-based separation (Zhang & Forssberg, 1999; Ruan & Xu, 2016). However, the fine particle sizes required for those previously mentioned processes to work effectively require significant energy inputs (Kaya, 2016)

ii. Pyrometallurgical Recycling Process

This e-waste recycling method utilizes methods such as smelting, incineration, combustion, and pyrolysis to extract valuable metals (Khaliq et al., 2014). Currently, this is the most widely applied e-waste recycling process in the industry, with approximately 70 % of all recycled e-waste being processed via this method (Cui & Zhang, 2008). This is primarily because pyrometallurgical processing can accept nearly all types of end of life e-waste (Kaya, 2016). Typical pyrometallurgical recovery processes for e-waste include techniques such as the smelting in plasma arc furnaces, incineration and high-temperature roasting under the addition of selected gases for non-ferrous metal recovery (Ghosh et al., 2015). Although pyrometallurgy is often viewed as the traditional method of metal recovery from e-waste, there are major limitations of this processing route (Kaya, 2016), outlined in Table II-13. The main drawback of this processing route is the generation of environmentally harmful gases, therefore requiring substantial emission control systems (Ghosh et al., 2015).

iii. Hydrometallurgical Recycling Process

For the hydrometallurgical extraction process, PCBs are generally dissolved in an acid or alkaline-based system, resulting in an impure metal-rich solution. This pregnant solution then undergoes solvent extraction to upgrade the metal purity. There are several methods that can be used to extract the metals from the solutions, but electrowinning is certainly the most commonly applied method during the refining stage (Cui & Anderson, 2016). Base metals, primarily Copper, play a major role in the economics of WEEE recycling as base metals are the most abundantly found metal group in e-waste. Moreover, the recovery process of base metals enriches the presence of precious metals within the solid residue, significantly promoting their recovery in subsequent leaching stages (Kaya, 2016).

Solution controls include pH, temperature and stirrer frequency (Khaliq et al., 2014). The overall process includes several stages. Starting with the purification of the pregnant solution, whereby filtration of any gangue material out of the media is achieved. This is then followed by processes such as solvent extraction, ion exchange and cementation that separates out the targeted metal

from the remaining solution (Khaliq et al., 2014; Ghosh et al., 2015). For final high-grade metal recovery, electrorefining or similar chemical reduction processes are employed (Ghosh et al., 2015). Table II-13 tabulates the advantages and disadvantages of this recovery process.

Table II-13: Advantages and limitations of the three PCB recycling processes

Recycling Processes	Advantages	Limitations
Mechanical methods	Effective separation of metallic from the non-metallic fraction[viii]	The liberation of metals and non-metals at different size fractions[viii]
	Available as Manual, automatic or semiautomatic[iii]	Loss of metal to dust or due to insufficient liberation[vi]
	Low capital and investment costs[vi]	Thermal degradation of non-metals[iv]
		Agglomeration of metals and non-metals due to localized pyrolysis[v]
Pyrometallurgy	Able to accept any form of e-waste[i]	Pollution by the generation of toxic gases[viii]
	Extraction of metals with high purity grade[viii]	Extremely complex specific metal selectivity[viii]
	Minimal metal loss to dust[ii]	High energy consumption[viii]
		Necessary subsequent processes for high purity grade[vii]
Hydrometallurgy	Easy control over reactions in the system[viii]	Toxic acidic and alkaline waste solutions[viii]
	Specific metal recovery possible[viii]	Consumption of large amounts of chemicals[ix]
	Environmentally friendlier than pyrometallurgy[viii]	
	Uncomplicated base metal recovery[viii]	
	Simple leaching of precious metals from the solid residue[viii]	

(i) (Sum, 1991); (ii) (Theo, 1998); (iii) (Li et al., 2004); (iv) (Barontini et al., 2005); (v) (Li et al., 2010); (vi) (Tuncuk et al., 2012); (vii) (Khaliq et al., 2014); (viii) (Ghosh et al., 2015); (ix) (Tunsu et al., 2015)

e. Methods of Size Reduction

E-waste, as well as PCBs, are characterized as complex heterogeneous composites with the material characteristic of high hardness and high strength as outlined in section II-b. This indicates that forms of shearing forces and/or impact forces are the most optimal acting forces to introduce size reduction to these composites. Table II-14 summarizes the type of crushers, the resulting particle sizes, the time of the size reduction process and leachates used by various researchers in literature.

Table II-14: Common methods of PCB size reduction

Author	Size reduction mechanism	Min. crushing size (mm)	Max. crushing size (mm)	Time (min)	Leachates (Ratio)
(Veit et al., 2002)	Cutting mill	< 0,25	1,00	-	N/A
(Wang et al., 2005)	Jaw crusher Roller crusher	< 0,30	> 12,00	- -	N/A
(Veit et al., 2005)	Cutting mill	< 0,25	1,00	-	N/A
(Hino et al., 2009)	Planetary Ball mill	< 0,25	> 2,00	-	N/A
(Oliveira et al., 2010)	Grab shredder Cutting mill	0,11	> 3,68	-	Aqua Regia
(Long et al., 2010)	High-speed universal crusher	< 0,105	4,00	-	N/A
(Yamane et al., 2011)	Hammer mill	< 0,106	2,00	-	Aqua Regia
(Kasper et al., 2011)	Hammer mill Knife mill	< 0,50	1,00	- -	Aqua Regia
(Hanafi et al., 2012)	Cutting mill Cutting scissors Ball mill Disc mill	< 0,074	> 0,20	- - 120 40	H_2SO_4 & HNO_3 (2.5:1)
(Oh et al., 2003)	Cutting mill	< 1,00	-	-	H_2SO_4 & H_2O_2
(Birloaga et al., 2013)	Planetary Ball mill	-		15	Aqua Regia
(Bizzo et al., 2014)	Cutting mill	< 9,00	-	-	Aqua Regia
(Pietrelli et al., 2014)	Ball mill	< 0,425	-	-	HNO_3, HF & HCL
(Petter et al., 2014)	Hammer mill Knife mill	< 1,00	-	- -	Aqua Regia
(Oyelami et al., 2016)	Hammer mill	< 2,00	-	-	HNO_3 &
(Terena et al., 2017)	Knife mill	0,075	0,075	-	Aqua Regia
(Kim et al., 2018)	Pulveriser	< 2,00	-	-	Aqua Regia

N/A = if not applicable for research; - = not stated

As it can be seen in Table II-14, the preferred type of crushers for this type of material are hammer mills, shredders and to an extent ball mills (Ruan & Xu, 2016). It should be mentioned that most papers found in literature do not mention the type of equipment used for size reduction. As suggested by Ruan & Xu (2016), the authors that reported on the equipment used the most utilized tools work on the basis of impact or shearing actions. Furthermore, most researchers then dissolved the crushed PCBs in Aqua Regia (3:1) or similar acid-based compounds with the main objective being gold recoveries, which is mostly plated on the surface and on contacts of the PCBs. However, when it comes to the analysis of copper, which is predominately found within the laminated layers of the PCBs, size reduction to fine particle sizes becomes an important factor.

It must be noted that in order to reach fine size reduction that completely liberates the copper from the plastic, high energy input is required. However, as outlined in Table II-14, only two of the reviewed researchers stated the amount of time the type of respective tool for size reduction was utilized for, to achieve a certain size fraction. This is an important fact as the time required for crushing directly translates to the energy that is consumed during the comminution process. This highlights how little emphasis is placed on determining the energy consumption of the actual recycling stage, regardless of the size reduction method utilized.

Oliveira et al., (2010) analysed the metal concentration of copper, zinc, lead, tin, and aluminium through 12 different size classes. Figure II-5 (a) shows the distribution by weight throughout the various size classes and Figure II-5 (b) displays the base metal grade percent according to each size class.

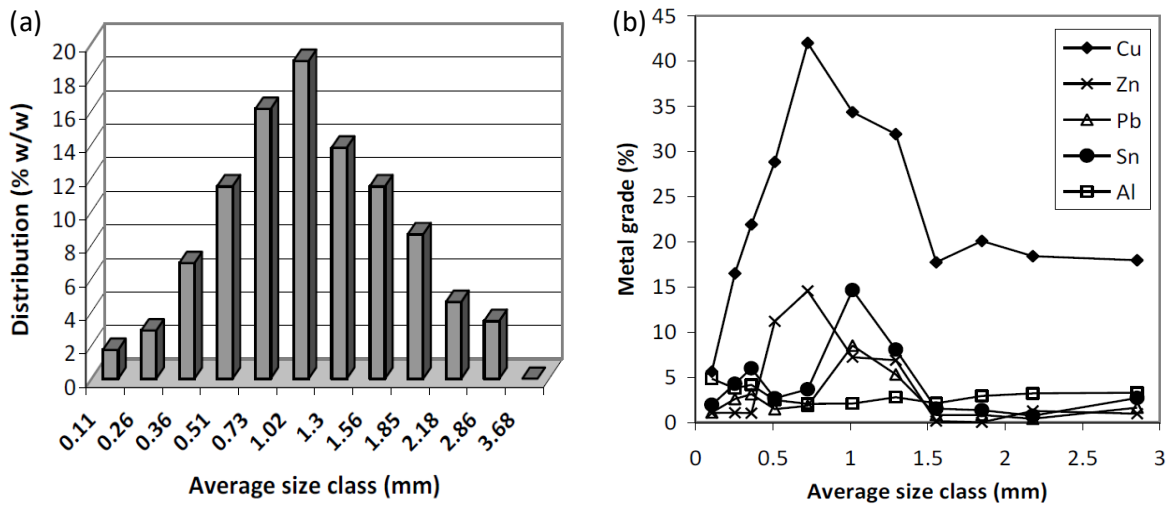

Figure II-5: Average size class vs (a) – Particle size distribution; (b) – Base Metal grade (Oliveira et al., 2010)

The particle size distribution shows a peak at 1,30 – 1,02 mm and decreases to the larger and smaller fractions. Metal concentrations in the respective size fractions differ considerably from the size distribution. For base metals such as copper, the highest concentration (40 %) was recorded at the 1,02 – 0,73 mm size class. Tin, as well as lead, have the highest recorded concentrations, 15 %, and 8 % respectively, in the 1,30 – 1,02 mm size class. Zinc's highest

concentration (15 %) with particle distribution falls within the same size class as copper. Aluminium behaves completely different than the other metals, having been recorded at maximum concentrations of approximately 5 % in the 0,36 – 0,26 mm range. Nickel and iron showed an increase in metal concentration towards the lower size fractions as seen in Figure II-6. Oliveira et al. (2010) therefore concluded that base metals tend to accumulate in the intermediate to lower size fractions of the researchers chosen size distribution classes. The researchers also found that precious metals, gold in particular, show no clear distribution pattern as seen in Figure II-6. The distribution of silver was seen to be very inconsistent; however, a general increasing trend towards the finer particle size distribution was observed (Oliveira et al., 2010)

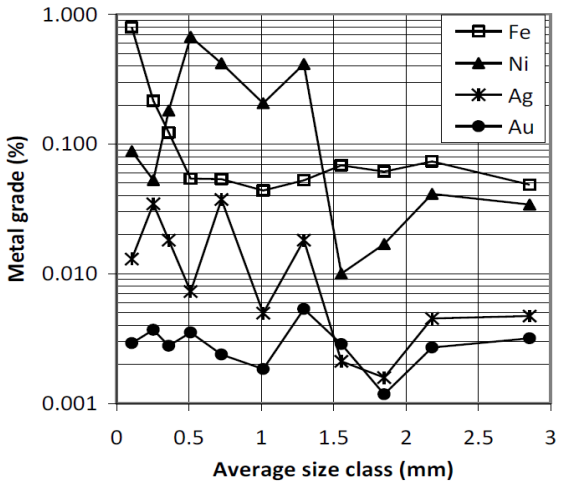

Figure II-6: Precious metal grade (Oliveira et al., 2010)

f. Hydrometallurgical Metal Recovery

For hydrometallurgical recovery, both acid-based and alkali-based systems can be employed for the recovery of base metals such as copper. Additionally, most metals including copper are present in WEEE in their metallic form which makes hydrometallurgical recovery a straightforward process. This is true as long as the PCBs were not pre-treated in any way or if, only underwent mechanical pre-treatment which resulted in no chemical alteration of the metals (Koyama et al., 2006). Table II-15 summarises the benefits and limitations of the two different systems.

Table II-15: Advantages and limitations of acid- and alkaline-based leaching

System type	Advantages	Disadvantages
Acid-based	Lower reagent prices[(v)]	Dissolution of metals involves acid of high concentration which further requires dilution for subsequent recovery[(ii)]
	Easier regeneration[(v)]	Corrosive solutions, require corrosion-resistant equipment[(vi)]
	Exceptionally high metal recoveries[(vi)]	Acids have poor specific metal selectivity, complicated downstream separation process[(i)]
		Low specific metal selectivity[(i)]
Alkali-based	Higher metal selectivity[(i)]	Iron and aluminum are not dissolved [(iv)]
	Cu (II) acts as oxidant, no additional oxidants needed[(i)]	Precious metal dissolution requires more complicated multi-stage processing[(iii)]
	Lower energy consumption[(i)]	

(i)(Koyama et al., 2006); (ii) (Maguyon et al., 2012); (iii) (Tuncuk et al., 2012); (iv) (Konishi et al., 2014); (v) (Ghosh et al., 2015); (vi) (Jadhav & Hocheng, 2015)

i. Acid-based Systems

Typical acids used for base metal extraction are sulfuric acid (H_2SO_4), nitric acid (HNO_3), aqua regia ($HCl:HNO_3$) and hydrochloric acid (HCl) in combination with other oxidants such as oxygen (O_2), hydrogen peroxide (H_2O_2), iron (Fe^{3+}) and chlorine (Cl_2) (Cui & Anderson, 2016). From those numerous acids, sulfuric acid is the favoured solvent predominantly because it's market price is lower than the other acids and has been proven to be an efficient solvent, especially for the recovery of copper (Ghosh et al., 2015). The various acidic components used for metal dissolution, their copper recoveries, and leaching conditions are tabulated in Table II-16.

Oh et al., (2012) studied the effects of sulfuric acid leaching in the presence of hydrogen peroxide as an oxidizing agent on the recovery of base metals. For this, the authors separated the PCBs into 30 % conducting and 70 % non-conducting materials. The 70 % of non-conducting materials were further separated into 42 % magnetic and 58 % non-magnetic fractions. The non-magnetic

fraction was then leached in a 2 M H_2SO_4, 0.2 M H_2O_2 for 12 hrs at 85 °C. The authors reported a maximum of 95 % recovery of Cu, Fe, Zn, Ni, and Al.

Table II-16: Acid-based leaching conditions

Author	Type of acid	Type of oxidant	Maximum Cu recovery (%)	Leaching conditions	
				Time (hr)	Temp. (°C)
(Oh et al., 2003)	H_2SO_4	H_2O_2	95	12	85
(Behnamfard et al., 2013)	H_2SO_4	H_2O_2	99	3	± 25
(Havlik et al., 2010)	HCl	O_2	90	3	900
			20	3	700
			5	3	300
(Castro & Martins, 2009)	HCl	-	33	3	60
(Vijayaram & Chandramohan, 2013)	HCl	-	24	3	60
(Patel et al., 2017)	HNO_3:HCl	HNO_3	± 95	12 min	± 25
			± 90	-	70
(Castro & Martins, 2009)	HNO_3:HCl	HNO_3	± 93	3	60
(Vijayaram & Chandramohan, 2013)	HNO_3:HCl	HNO_3	± 93	3	60

Behnamfard et al., (2013) investigated the effect of a two-stage sulfuric acid leaching process instead of the conventional single-step leach and reported similar results to Oh et al. (2003). During the first leaching step, finely milled PCBs were mixed into a solution of 2 M H_2SO_4 in the presence of H_2O_2 for 3 hrs at room temperature. The second step involved the redissolution of the filtered solid residue from the previous stage under the same conditions. The authors reported 85.76 % Cu recovery of the first leaching step, followed by an additional 13.99 % Cu recovered in the second leaching step. A total of 99 % of Cu was recovered through this two-stage method.

Havlik et al., (2010) opted to investigate the dissolution of the metals using hydrochloric acid as a solvent. The authors thermally pre-treated 5 g of milled PCBs by burning the samples at 300, 500, 700 and 900 °C for 0, 15, 30 and 60 min, respectively. Following the thermal pre-treatment, the remaining solid residue was then leached in a 1 M HCl solution at for a total of 180 min at 80 °C. The researchers reported Cu recoveries of up to 90 % for PCBs that were burned at 900°C and leached in HCl for 180 min. Cu recoveries for samples that weren't thermally pre-treated and those burned at 300 °C reached maximum recoveries of 5 % after 180 min. Thermally pre-treating the milled samples at 700 °C resulted in a maximum copper extraction of 20 % after 180 min. It thereby becomes apparent that HCl is only efficient in the recovery of copper when the PCBs were thermally pre-treated, effectively removing the plastic component from the system.

Castro & Martins (2009) carried out similar experiments to Havlik et al. (2010) by dissolving milled PCBs in HCl but in the absence of an oxidant. Prior to dissolution, the PCBs were dismantled and washed after being ball milled. The PCBs were dissolved in a 3 M HCl solution and samples were taken at 10, 30, 60 and 120 min at 60 °C after the start of the leaching process. Copper did not dissolve well in the absence of an oxidant, reaching maximum extractions of 33 % after 120 min. Similar observations were made by Vijayaram & Chandramohan (2013) who repeated the experiments under the exact same conditions, achieving slightly lower Cu recoveries of 24 %.

Patel et al., (2017) studied the effects that varying the amounts of nitric acid (HNO_3) in aqua regia has on the copper extraction from milled PCBs. The authors also adjusted the leaching time and the temperature during the experiments. Usually, aqua regia is made up of 30 % HNO_3 and 70 % HCl by volume. This solvent is considered to be the most efficient acid-based leachate. This is because of the high amounts of nitric acid present which acts as an oxidant. After pre-treating PCB samples at 600 °C for 15 min to remove all plastics, the boards were crushed in a ball mill. Copper showed the highest recoveries when HNO_3 content was at 15 – 20 %. For the effects of leaching time and temperature of the leaching tests, aqua regia content was kept at 10 % HNO_3 and 90 % HCl. Copper recoveries were recorded to be approximately 98% after a maximum leaching time of 12 min, whereas the Cu recoveries of ±95 % were recorded at 70 °C.

Castro & Martins (2009), in addition to investigating the effects of 3 M HCl, also studied the efficiency of copper leaching from waste printed circuit boards by dissolving them in aqua regia over time. Preparation of the samples and procedure of the experiment followed the same process as the samples that underwent dissolution in HCl. The only difference was that the solvent was mixed to a concentration of 3 M HCl + 1 M HNO_3. The highest Cu recoveries were reported to be ± 93 % after a total of 120 minutes of dissolution (Castro & Martins et al. (2009)). These results were confirmed by Vijayaram & Chandramohan (2013) who repeated the experiment under similar conditions. The authors reported a maximum Cu recovery of 92,7 % after 120 min at 60 °C.

ii. Alkali-based (Ammoniacal) Systems

Apart from the numerous earlier mentioned acid-based systems that can be employed for the base and precious metal recovery from PCBs, alkali systems can also be successfully employed to enable the recovery of such metals (Konishi et al., 2014). For the recovery of copper, ammoniacal media has been proven to be especially successful (Koyama et al., 2006; Konishi et al., 2014; Ghosh et al., 2015). The ammoniacal lixiviant is generally comprised of ammonia in combination with salts such as carbonate, chloride or sulfate. The ammonia leaching process is more suitable for copper extraction than acidic systems as these lixiviants show higher selectivity for copper, leaving metals such as iron (Fe) and aluminum (Al) undissolved. However, it has been shown that nickel (Ni) and zinc (Zn) are also dissolved in the ammonia-based lixiviant. As mentioned earlier, most metals present in PCBs are predominately found in their elemental form or as alloys, therefore requiring oxidative lixiviants such as oxygen (O) or Copper Oxide (Cu(II)O) for effective extraction (Tuncuk et al., 2012).

Figure II-7, adapted from Koyama et al., (2006), displays the potential-pH diagram of the Cu-NH_3-H_2O system. As indicated by the Eh-pH diagram, the Copper(II)tetraamine complex ($Cu(NH_3)_4^{2+}$) is only sTable in a pH range between 8 – 11. Outside of this range, copper has the tendency to precipitate out of the solution in the form of $Cu(OH)_2$ as per the following equation (Eq. (II-1)) (Radmehr et al., 2012):

$$CuCO_3 + 2NH_4OH \rightarrow (NH_4)_2CO_3 + Cu(OH)_2 \qquad \textbf{Eq. (II-1)}$$

The Cu(I) ionic species has a larger pH range from 7 – 12 in which it is complexed with ammonia to form the sTable Copper(I)diamine complex ($Cu(NH_3)_2^+$).

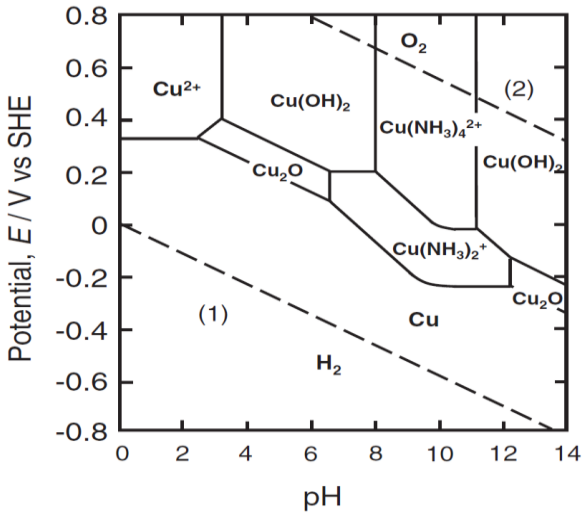

Figure II-7: Potential-pH diagram of the Cu-NH_3-H_2O system

Complexing agents such as NH_3 or CN^- are required for Cu(I) and Cu(II) to be sTable in neutral or alkaline solutions. As such, in the presence of excess ammonia (NH_3), both Cu(II) and Cu(I) can be found as sTable ionic species in these solutions in the form of Tetraaminecopper(II) ($Cu(NH_3)_4^{2+}$) and Diaminecopper(I) ($Cu(NH_3)_2^+$), respectively. The oxidation-reduction reactions occurring within these solutions are commonly expressed in the form of eq. (II-2) and eq. (II-3) for Cu(II)/Cu(I) and Cu(I)/Cu, respectively (Konishi et al., 2014):

$$Cu(NH_3)_4^{2+} + e^- \rightarrow Cu(NH_3)_2^+ + 2\,NH_3 \qquad \textbf{Eq. (II-2)}$$

$$Cu(NH_3)_2^+ + e^- \rightarrow Cu + 2\,NH_3 \qquad \textbf{Eq. (II-3)}$$

The Cu(II)-ammine complex ($Cu(NH_3)_4^{2+}$) is capable of oxidizing and thereby dissolving metallic copper (Cu^0) in ammonia-based alkaline solutions. This is principally because the oxidation-reduction potential of $Cu(NH_3)_4^{2+}/Cu(NH_3)_2^+$ is more positive than that of $Cu(NH_3)_2^+/Cu$ (Radmehr et al., 2012). In addition, because of the greater oxidation-reduction potential of $Cu(NH_3)_2^+/Cu$

compared to the potential of hydrogen evolution, the Cu(I)-ammine complex has a tendency to be rather reduced to metallic copper than to be oxidized to Cu(II). Therefore, the presence of $Cu(NH_3)_4^{2+}$ complexes in solution tend to increase the leaching rate of metallic copper from WEEE, whereas the $Cu(NH_3)_2^{+}$ ions are more inclined to suppress the reaction (Konishi et al., 2014).

It is evident from the previously described equations that pH is directly affected by the ammonia concentration within the lixiviant. When there is enough free ammonia in the solution, the Cu(II)-ammine complex is formed by the following reaction (Eq. (II-4)):

$$Cu(OH)_2 + (NH_4)_2CO_3 + 2\,NH_4OH \rightarrow Cu(NH_3)_4 + 4\,H_2O + CO_3 \qquad \textbf{Eq. (II-4)}$$

Koyama et al., (2006) further investigated the copper ion species behaviour in a kinetic leach test. As seen in Figure II-8 (a), as the Cu(I) concentration increases the Cu(II) ionic species simultaneously decreases. To further determine the exact leaching reaction occurring within the system, Koyama et al., (2006) investigated the stoichiometric ratio of the amount of Cu(I) that is produced compared to the amount of Cu(II) that is consumed during the reaction. Figure II-8 (b) shows this ratio, indicating that the ratio stays constant at 2, inferring that for every 1 mole of Cu(II) consumed during the reaction, 2 moles of Cu(I) is produced, yielding the following reaction (Eq. (II-5)):

$$Cu + Cu(NH_3)_4^{2+} \rightarrow 2\,Cu(NH_3)_2^{+} \qquad \textbf{Eq. (II-5)}$$

As mentioned earlier, the formation of copper(II)tetraamine by the above reaction (Eq. (5)) is the driving force that promotes the dissolution of the metallic copper (Koyama et al., 2006).

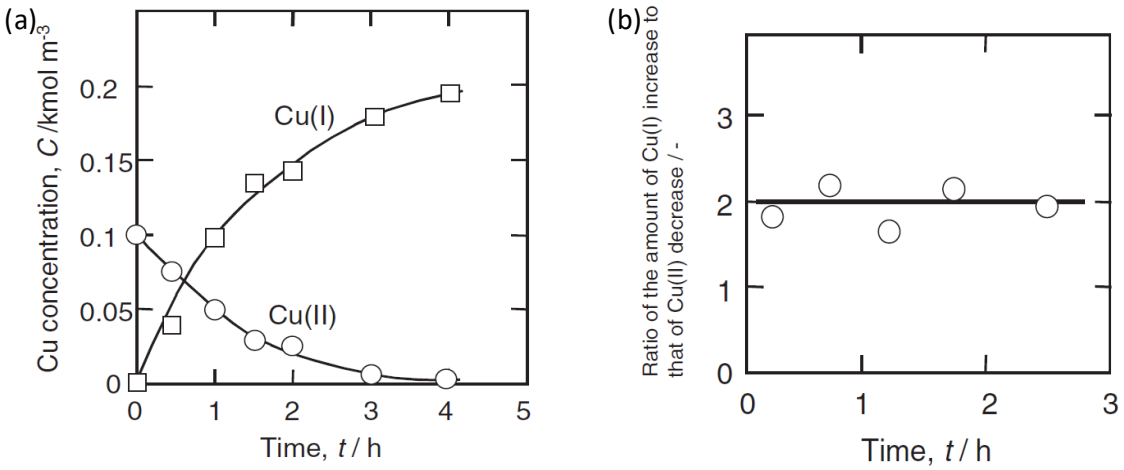

Figure II-8: (a) – Concentration of Cu(I) and Cu(II) over time; (b) – Ratio between Cu(I) increase and Cu(II) decrease (adapted from Koyama et al. (2006))

Moreover, in the presence of an oxidant (e.g. pressurized air), the generated Cu(I) is re-oxidized to Cu(II) in solution as display in eq. (II-6):

$$4\,Cu(NH_3)_2^+ + O_2 + 4\,NH_3 + 4\,NH_4 \rightarrow 4\,Cu(NH_3)_4^{2+} + 2\,H_2O \qquad \textbf{Eq. (II-6)}$$

The pH of the system is furthermore regulated by the ammonia buffer reaction (Eq. (II-7)):

$$NH_3 + H^+ \rightarrow NH_4^+ \qquad \textbf{Eq. (II-7)}$$

The overall metallic copper oxidation reaction within the aerated ammonia-based system is therefore presented in eq. (II-8):

$$2\,Cu + O_2 + 4\,NH_3 + 4\,NH_4^+ \rightarrow 2\,Cu(NH_3)_4^{2+} + 2\,H_2O \qquad \textbf{Eq. (II-8)}$$

Bari et al., (2009) further conducted an extensive study to examine several different leaching solutions with the aim to determine the best leaching agent for base metals, placing special emphasis on copper, nickel, zinc, and iron. The paper investigates lixiviants of both system types, acidic and alkaline. To compare the effectiveness of the leaching of the base metals, the researchers conducted the experiments in the presence of ammonia in a 5M solution and in the absence of ammonia. The results presented by Bari et al., (2009) show that alkaline systems display a higher selectivity to base metals when free ammonia is present within the solution. The authors further proved that ammonium carbonate and ammonium persulfate show the highest affinity to copper, recovering 93 % and 99 % of copper from the PCBs, respectively. Acidic systems exhibited a lower recovery of base metals compared to the alkaline systems, as well as a generally lower selectivity to specific metals.

g. Physical Material Properties

Within the PCB industry, there is a tremendously high number of different types of PCBs, each with its own physical, mechanical and material properties. As mentioned earlier, the boards are generally continuous fibre-reinforced polymer-metal matrix composites, often referred to as composite beams. These composites' mechanical behaviour is greatly depended on the strength of the supporting reinforcement phase and the relationship of matrix/reinforcement interphase (Wu & Cheng, 2014). Research has further shown that the ultimate strength of the composite boards is directly related to the interphase layers (Singh et al., 1999). The three failure analysis tests investigated in this study were the drop-weight impact, the three-point bending and the tensile tests. Standards such as the American Society for testing and Materials (ASTM) are generally used to ensure validity of the results obtained from these tests.

Reliability testing of PCBs is vital in terms of understanding the behaviour of the boards in various environments as it defines the failure modes. In general, the three main types of failure analysis tests investigated can provide information regarding the PCBs in different comminution environments. As such, the impact test can provide information regarding the PCBs behaviour in comminution environments where impact forces are the dominant means of size reduction, such as general ball mills. Tensile and three-point bending tests on the other hand offer insights into shear and tear type comminution environments, including grab shredders, hammer mills or stamp mills.

i. Three-point Bending Tests

Three-point bending tests provide information on the flexural properties of the composite beams, including strength, stiffness as well as the load/deflection behaviour. For composite beams, when a load is applied the beam will bend in the direction of the load that is applied. The material layer closest to the bend radius will be compressed, whereas the outermost layer to the bend radius will be stretched and undergo tension. The graph in Figure II-9 displays the general stress/strain curve for standard rolled annealed and electrodeposited copper (Coonrod, 2007).

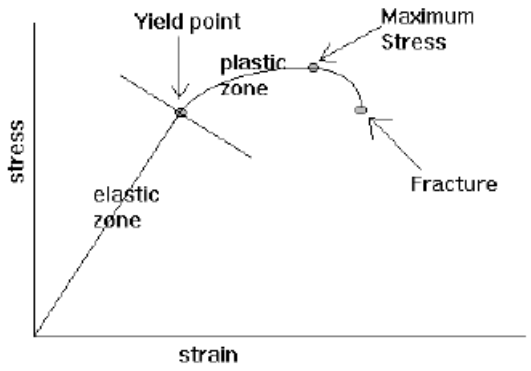

Figure II-9: Ductile behaviour of rolled annealed copper in response to flexural stress (Coonrod, 2007)

The elastic zone is the zone of deformation without permanent damage to the grain structure. If the load is released within this zone, the copper will return to its original shape. Once the yield point is reached and the stress/strain curve moves into the plastic zone, permanent damage is inflicted on the copper structure. Once maximum stress is reached the strain limit has been exceeded and the copper grain structure will actively fail. As can be seen by the red line in Figures II-3 (a & b), the grain structure crack initiation and propagation are worse for electrodeposited copper than for rolled annealed copper. This is because when a bend is applied, cracking will be initiated and propagate faster in ED copper than RA copper due to the sharp valleys on the tip of the grains which act as stress concentrators (Coonrod, 2007).

ii. Tensile Tests

By conducting tensile tests, it is possible to evaluate the strength of a material when a pulling or stretching force is applied to it. It can be applied to materials to test the materials' respective properties such as yield strength, modulus of elasticity, Poisson's ratio as well as the ultimate tensile strength and strain. Figure II-10 displays the tensile properties of fibres, the polymer (matrix) and the composite structure (Campbell, 2010).

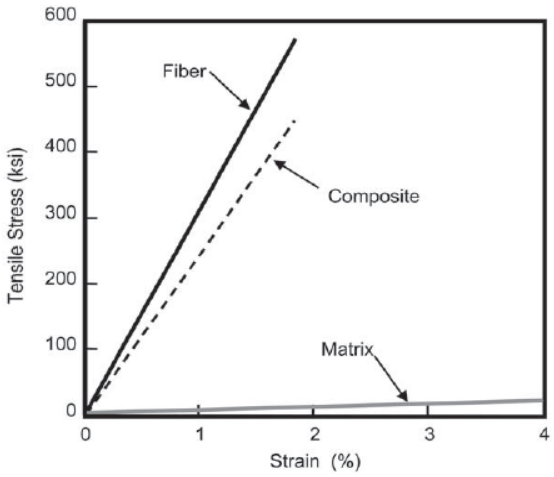

Figure II-10: Comparison of brittle behaviour of materials in response to tensile stress

As seen in Figure II-10, glass fibres have a tensile strength of about 500 kilo pounds per square inch (ksi) which is equivalent to about 3500 MPa. In comparison, a polymer has a typical tensile strength of around 10 ksi (70 MPa). The composite has a slightly lower tensile strength than fibres alone, however, by fusing the fibres with polymer the fibres are protected from abrasion and thereby offer higher structural support (Campbell, 2010).

iii. Drop-weight Impact Tests

Drop-weight impact tests provide insights on the damage resistance of materials to impact stresses. This applies to all kinds of materials, but each individual material has its own behaviour to the stresses. The complex composition of composite structures makes them unique in terms of stress responses. The resistance of composites to impact stresses is strongly dependent on several factors, including but not limited to the geometry, thickness, stiffness, and mass of the materials tested. These tests, therefore, provide answers to the impact stress behaviour of materials as well as the impact energy required to inflict damage to the structures. Impact testing is further used to determine a material's toughness rather than hardness as it describes the amount of energy a material can absorb before fracturing or breaking. The main reason as to why impact forces are effective in the delamination of PCBs is because delamination occurs between layers with different fibre orientations (González et al., 2012).

h. Research Approach

From the literature review, it is evident that leaching of size reduced PCBs in ammonia-based systems is an effective technique for copper extraction. Several researchers, including but not limited to Koyama et al. (2006) and Cui & Anderson (2016), have investigated and improved the efficiency of copper leaching from ammonia-based lixiviants. The literature review further clarified that most size reduction processes initially utilized various forms of grab shredders to reduce the tightly laminated PCBs in size. Furthermore, Oliveira et al. (2010) established the particle size distribution of milled PCBs and the thereby subsequently generated distribution of base and precious metals at particle sizes of less than 3 mm, but the copper distribution of larger particles remains yet to be investigated.

As indicated by Ruan & Xu (2016) the energy balance of the various size reduction processes applied to liberate copper from the PCBs remains yet to be identified. Moreover, most of the investigated research in the literature review conducted test work using pulverised PCBs with particle sizes of commonly ≤ 2 mm (Veit et al., 2002; Yamane et al., 2011; Terena et al., 2017). The degree of copper liberation and subsequent extraction from the PCBs strongly depends upon the means of size reduction and type of lixiviant applied. However, due to the laminated design of the PCBs, it can be assumed that the delamination of the layers could expose the inner copper layers. This can be achieved by shredding of the PCBs in a shear-type of environment, resulting in larger yet more delaminated PCB particles.

The copper leaching efficiency of PCBs generated by an industrial grab shredder in an alkaline lixiviant depends on the degree of exposure of the copper layers. Therefore, understanding the leaching behaviour of size reduced and delaminated PCBs, as well as the associated energy costs, are essential in optimizing the recovery process of larger PCB particles in an ammonia-based system. A cost-benefit analysis can then be conducted in order to identify the most beneficial size reduction processes for small-scale recycling operations in South Africa.

i. Hypothesis

Size reduction of PCBs during the recycling process is a highly energy-intensive but necessary process. By introducing size reduction to the PCBs via the tear and bend mechanism of an industrial grab shredder, copper is effectively liberated from the PCBs and made available for extraction. Through mechanical and chemical pre- & post-treating of the PCB, the viability of the copper liberation and subsequent extraction processes will be enhanced. Ammonia-based hydrometallurgical leaching will be an effective tool in terms of copper extraction from the PCBs.

ii. Key Questions

- Does delamination of PCB particles occur during shredding and if so, to what degree does it enable liberation of copper and subsequent extraction
- Does pre- or post-treatment of the PCBs affect copper liberation and recoveries?
- Which of the size reduction processes is the most energy-efficient?
- To what degree does pre- or post-treatment affect the cost-benefit analysis?
- How do the various size reduction processes affect the particle size distribution (PSD) of generated PCB chips and how does the copper concentration vary throughout the PSD?
- What are the associated material losses of the investigated size reduction process?

III. Materials and Methods

In this chapter, the experimental procedures, as well as the materials utilized, are outlined. The experimental work aimed to validate the stated hypothesis and carry out the study's overarching objectives. These overarching objectives were to mainly investigate the degree of copper liberation from PCBs by making use of an industrial grab shredder and to assess copper recovery in an ammonia-based leach system. The chapter is subdivided into sections outlining the materials, methods and analytical techniques applied.

a. Materials

i. Custom-made PCBs

Custom-made printed circuit boards (142 * 102 * 1,55 mm) were manufactured by Trax Interconnect (Pty) Ltd and used throughout this research without exception. Figure III-1 (a & b) display the top and bottom sides of the PCBs used. By ensuring that all the boards are of the exact same material composition, design and quality, reproducibility and accurate comparison of the obtained experimental data can be achieved. The specific PCBs represent the average design most commonly asked for by the company's customers. All components that are utilized within the composite, the fibreglass-epoxy Pre-Pregs as well as the copper foils are produced by a company in China.

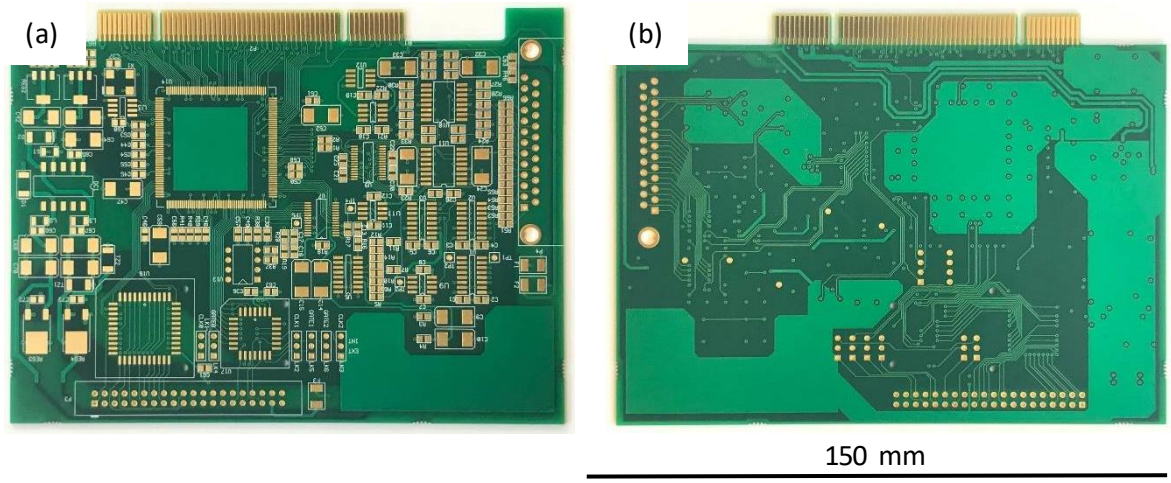

Figure III-1: Custom made PCBs (a) - Top side; (b) - Bottom side

The boards are unpopulated, non-flexible and comprised of metal, glass and other chemical compositional concentrations outlined in Figure III-2. On average, each board weighs approximately 52.24 g. The received PCB is a four-layered FR-4 core board, with intermittent layers of four different types of woven fibreglass. This fibreglass is set within a matrix of brominated difunctional epoxy resin. The boards have an overall thickness of 1.626 mm, where 0.937 mm is attributed to the FR-4 core (57 wt%) and the remaining 0.689 mm (43 wt%) are the below and above-attached copper foil and Pre-Preg layers. From the total composition of the PCBs, the copper foils only account for 0.142 mm (8.7 wt%). Table III-1 shows the cross-sectional make-up of the boards, while Figure III-2 displays a graphical cross-sectional view of the PCBs.

Figure III-2: Cross-sectional view of the custom-made PCBs (to scale)

The type of epoxy resin used for both the Pre-Pregs as well as the core is called Tetrabromobisphenol-A (TBBPA). E-glass is further utilized within the Pre-Pregs acting as the reinforcement phase. The general make-up of E-glass is listed in Table II-5. Two differently woven fibreglass types, 1080 and 7628, are used to give structural support to the Pre-Pregs, visually displayed in Figure II-2.

Table III-1: Cross-sectional make-up of the custom-made PCBs

Description	Material	Fibreglass weaving pattern	Copper type	Processed thickness (mm)		Additional information
Soldermask	Mixture of solvents and polymers	-	-	0.025		Liquid Photo-imageable
Copper Foil	Copper	-	ED RA	0.020 0.016	0.036	-
PrePreg	Fibreglass/Epoxy resin	1080 7628	- -	0.069 0.183	0.252	TBBPA E-glass
FR-4 Core	Copper	-	ED RA	0.018 0.017	0.035	-
	Fibreglass/Epoxy resin	7628 2116 1506 1080	-	0.930		TBBPA E-glass
	Copper	-	RA ED	0.017 0.018	0.035	-

The FR-4 core itself is comprised of an epoxy/fibreglass composite in the centre and capped off with two copper layers of equal thickness (0.035 mm) at the top and bottom. The Copper foils are made up of a combination of electrodeposited (ED) and rolled annealed (RA) copper. The epoxy resin used for the core is the same as the resin used for the Pre-Pregs. However, unlike the fibreglass of the Prepregs, the core itself is comprised of four instead of only two different weaving patterns. These two additional weaving patterns, 2116 and 1506, are also displayed in Figure II-2.

The head grade of the utilized PCBs was obtained by leaching a sample board in a solution of aqua regia ($HCl:HNO_3$) (4:1). The pulverization of the PCBs was achieved by first cutting the sample boards into 2 cm * 1.5 cm pieces and then subsequently milling the cut pieces in a ring mill. Minimal material loss occurred, mounting up to 0.523 g (Chirume, 2019). Table III-2 (adapted from Chirume (2019) lists the average elemental composition of four analysed custom-made boards.

Table III-2: Elemental composition of the custom-made PCBs

Element	Concentration (ppm)	Mass (wt %)	Element	Concentration (ppm)	Mass (wt %)
Al	531,21	7,37	Fe	259,43	3,37
Au	7,44	0,11	Mg	25,75	0,36
B	85,13	1,19	Ni	114,72	1,57
Ca	2027,61	27,11	Pb	29,68	0,39
Co	112,10	1,44	Si	15,40	0,21
Cu	3826,26	55,45	Zn	36,10	0,52

As shown in Figure III-3 (a-d), the design of the individual copper layers varies strongly from one to another. The major portion of the copper (69 %) can be found on the inner two layers (b & c), another 29 % can be found on the outer two layers (a & d) with the remaining 2 % found on coatings of holes drilled into the boards.

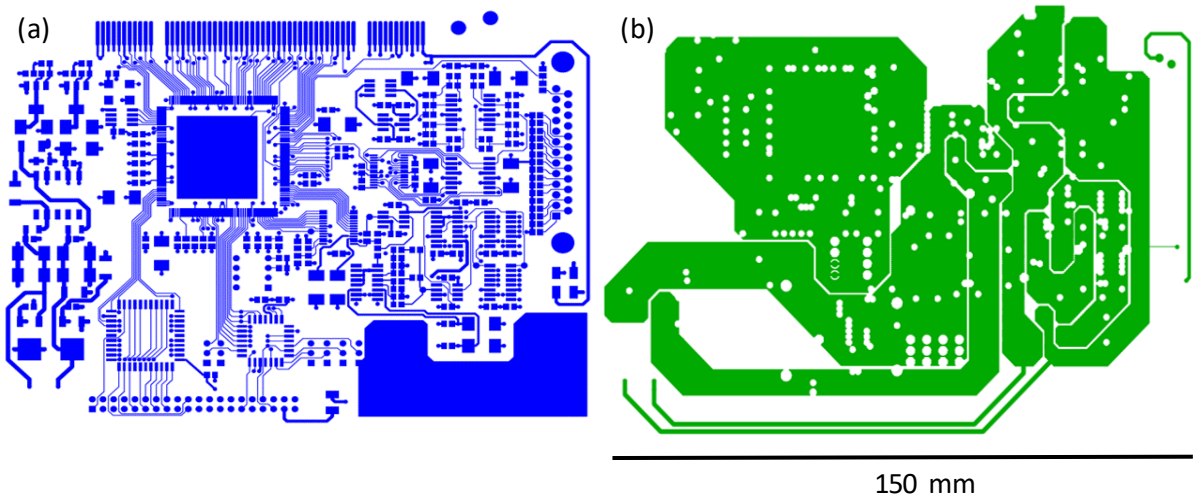

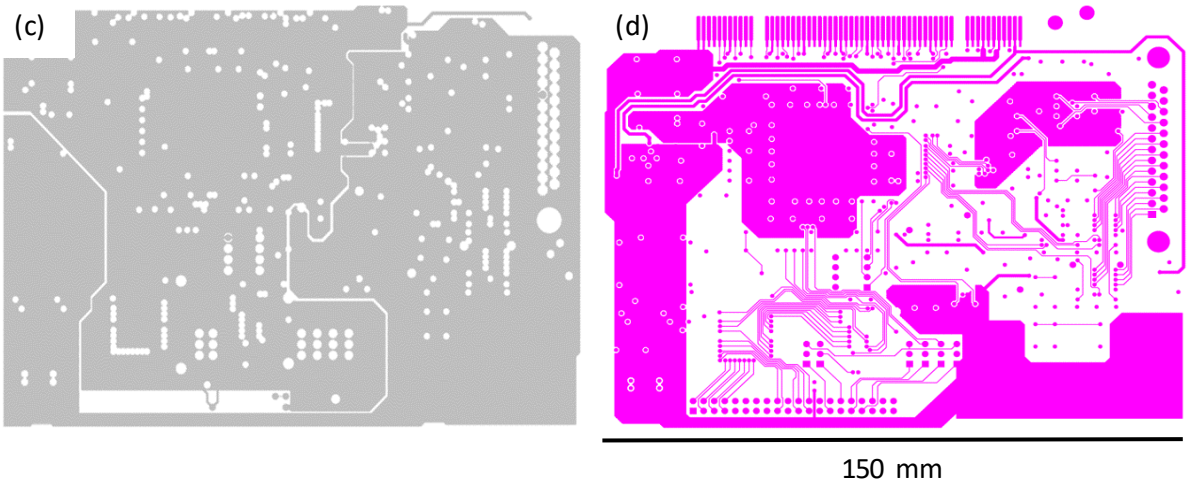

Figure III-3: Copper layers from custom-made PCBs; (a) Outer top layer; (b) Inner top layer; (c) Inner bottom layer; (d) Outer bottom layer

Table III-3 further summarizes the copper concentrations throughout the custom-made PCBs. Based on the results obtained by Chirume (2019), it can be concluded that most of the copper (19,99 g) can be found on the inner two layers. As identified in Table III-3, all copper layers used in the PCBs have the same thickness, however, as seen in Figure III-3 (a-d) the design of the individual layers varies strongly. This further motivates the need to access the inner copper layers during recycling operations in order to access high copper containing inner layers of the PCBs.

Table III-3: Copper content of custom-made PCBs

Layer	Weight Board (g)	Copper per board (%)	Copper (%)	Copper (g)
Outer Top layer (a)			11	3,19
Inner top layer (b)			25	7,24
Inner bottom layer (c)	52,24	55,45	44	12,75
Outer bottom layer (d)			18	5,21
Coating			2	0,58

ii. Reagents

Several reagents were used throughout the experimental procedure. Ammonium carbonate, 25% ammonia solution and copper (II) sulphate pentahydrate were the reagents used for these diagnostic leach tests. Moreover, sodium hydroxide, as well as liquid nitrogen, were utilized for the pre-treatment of the PCBs. All reagents except for liquid nitrogen were acquired from Merck Chemicals (Pty) Ltd. For the diagnostic batch reactor leach tests as well as the pre-treatment methods, the reagents were diluted in accordance with the required molar concentrations with deionized water. The exact molar concentrations and solution preparations are outlined in more detail in chapter III section v.

b. Equipment

i. Size Reduction

This subsection characterizes and outlines the equipment utilized to achieve the size reduction of the custom-made PCBs.

1. Industrial Grab Shredder

The industrial grab shredder (IGS) acted as the main grinding process by applying shear nd tear forces to introduce size reduction to the custom-made PCBs. The shredder was obtained from Filamaker Gmbh in Germany. The shredder has a length of 170 mm and a width of 140 mm, with 14 circular blades each of 8 mm thickness responsible for the shredding action. The shredder is shown in Figures III-4 (a & b). A total of 3 teeth can be found on each of the 86 mm in diameter wide blades that are spaced 120° apart from one another. The shredding action was facilitated by a 1.1 kW motor from SEW, running on a 50 Hz frequency controlled by a Siemens Basic Inverter (Sinamics V20), depicted in Figure III-4 (c).

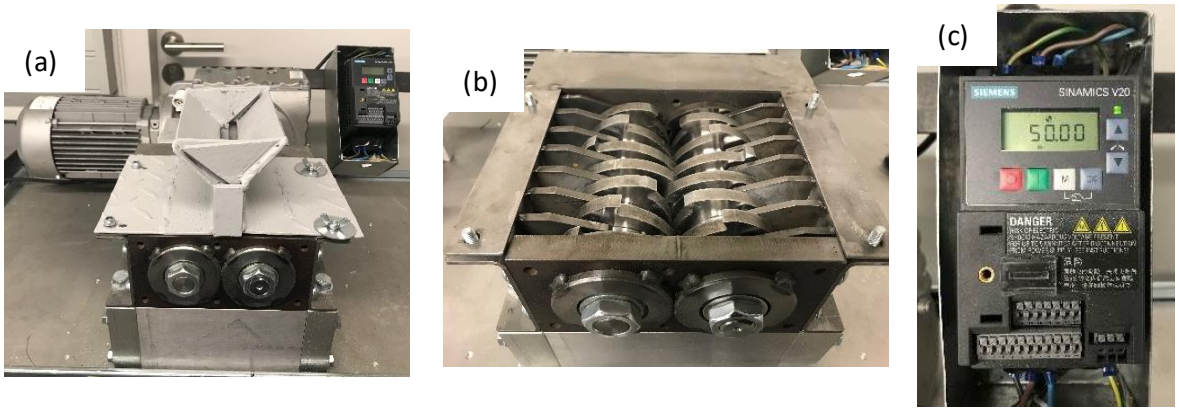

Figure III-4: S*hredding Equipment *(a) – Front view of Industrial grab shredder; (b) Industrial grab shredder without casing and safety cover; (c) – Siemens Basic Inverter

2. Planetary Ball Mill

A planetary ball mill (PBM) of model RETSCH 2000 was utilized as a subsequent finer particle size reduction process for some of the boards after the initial shredding of the boards. The planetary ball mill was chosen for subsequent grinding as it offers higher centrifugal forces and shorter grinding times to achieve finer particle sizes compared to the standard horizontally lying ball mill. The mill utilized was a 6.8 cm high agate cylinder with a radius of 3.6 cm, yielding a milling chamber able to hold an approximate total volume of 250 cm^3. The utilized PBM, as well as the agate milling chamber, is depicted in Figure III-5 (a & b). For all milling experiments, 12 agate milling balls were utilized as the grinding media. The process of the planetary ball mill is considered a post-shredding process as it introduces additional size reduction to the PCB in the form of abrasion.

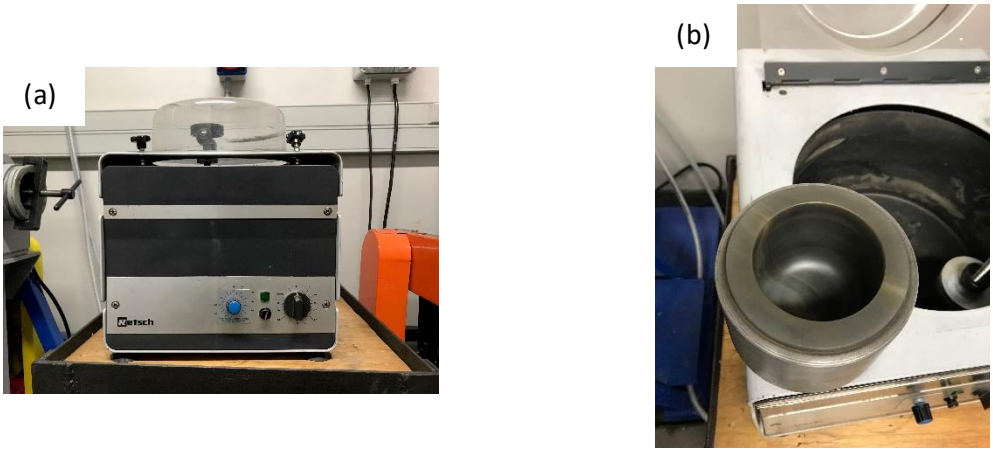

Figure III-5: Planetary ball milling equipment (a) - Planetary ball mill; (b) - Agate milling chamber

ii. Particle Size Distribution

This subsection aims to outline the equipment used to attain information regarding particle size distribution (PSD) of particles coming from various size reduction processes as well as the copper distribution thereof.

1. Screening

For the purpose of analysing the particle size distribution that was generated by both the industrial grab shredder and the planetary ball mill, an automatic sieve shaker, the Analysette 3 Pro, was employed to screen one size reduced board into six size fractions at a time. Several criteria were considered when the sieve sizes were selected. These included the availability of sieves during the experiment, the maximum thickness of the industrial grab shredder blades and the therefore subsequent maximum thickness of particles as well as the commonly applied sieve mesh sizes in literature listed in Table II-14. The shaker and the 4750 µm mesh are displayed in Figure III-6 (a & b).

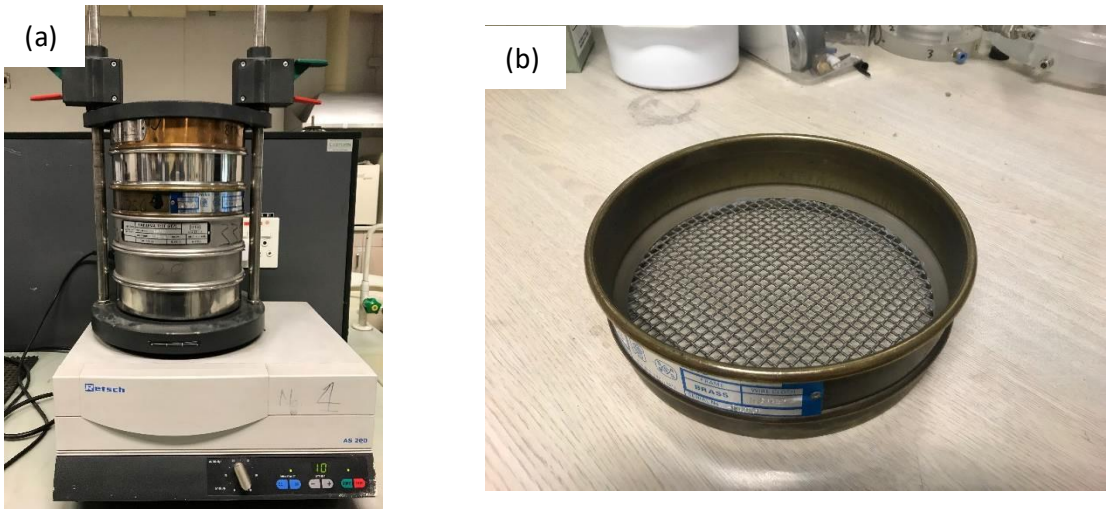

Figure III-6: Screening equipment (a) Analysette 3 Pro screener; (b) 4750 µm mesh

2. Pulveriser/Ring Mill

The pulveriser served two separate purposes. The first use of the mill was to shred one custom-made PCB once completely for further leaching. The shredded sample was then fed into the ring mill and then pulverised completely to ultrafine particle size. This was then followed by a diagnostic leach test which will be discussed in section III-v.

The other purpose of the ring mill was to pulverise the screened samples from each size fraction to ultrafine particles. As with the previous pulverization of the single board, the samples were completely pulverised in order to allow for analysis of the copper concentration in each of the size fractions. Figure III-7 (a & b) depicts the pulveriser as well as the grinding jars utilized.

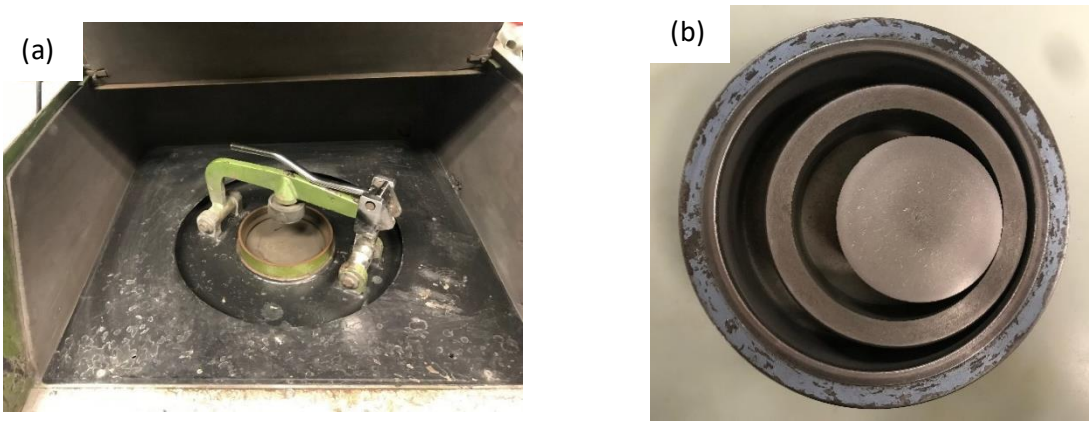

Figure III-7: Pulverising equipment (a) - Pulveriser; (b) - Grinding jars

3. Splitting

In addition to pulverization needed for the analysis of copper in each size fraction, the samples had to undergo splitting as only a certain sample size can be analysed. Therefore, to have a representative sample size analysed, the pulverised fractions underwent a splitting process by making use of the Dickie and Stockler (Pty) rotary splitter depicted in Figure III-8. This splitter separated the samples into 10 equally large samples.

Figure III-8: Dickie & Stockler (Pty) rotary splitter

iii. Batch Stirred Tank Reactors

Two 1 L overhead batch stirred reactors were used to determine the diagnostic leach and extraction efficiency of copper from the size reduced PCB particles. The experimental reactor set up is depicted in Figure III-9. The two reactors were set up in sequence with a circulatory water bath to regulate and maintain the temperature at the required level (°C). Overhead stirrers were employed instead of the conventionally used magnetic stirrers. This was primarily due to the nature of the PCB chips which blocked the bottom of the reactors causing issues for the magnetic stirrers. Furthermore, two Pyrex baffles were utilized within each of the reactors to prevent the potential formation of a vortex in the leach solutions. The chosen oxidant was supplied to the reactor in the form of compressed air with the supply line to each reactor fitted with a flow meter to control the flow rate.

Figure III-9: Batch stirred reactor set-up

iv. Energy Measurements

Through the entire mechanical size reduction processes, the energy consumption was monitored. For the planetary ball milling, the screening and the leach tests, the Power (P) consumed by the respective machine was measured using an ammeter to measure the current (I) flowing through the respective machine. A voltmeter was employed to monitor constant voltage (V) coming from the AC electrical power circuit. The power factor (P_f), a dimensionless number defined as the ratio of the real power that is required by the machines to do work and the apparent power that is supplied to the machine via the AC electrical power circuit, was determined to be 0.92 for the AC circuit of the building in which the research was conducted.

For all measurements, regardless of the equipment utilized to determine it, the equation (eq.(III-1)) for calculation of the consumed power remains the same and is defined as follows:

$$P = P_f * V * I \qquad \textit{Eq. (III-1)}$$

Where:

- P = Power consumed by process (W = J/s)
- P_f = Power factor of the AC electrical power circuit
- V = Electric potential difference between the plug point and the machine (V)
- I = Current flowing through the circuit (A)

The Shredder itself had an attached converter which allowed for direct reading of current flowing through it, thereby rendering the use of the ammeter unnecessary. The Digital Watt ammeter 1310, manufactured by Topward, is depicted in Figures III-10, respectively.

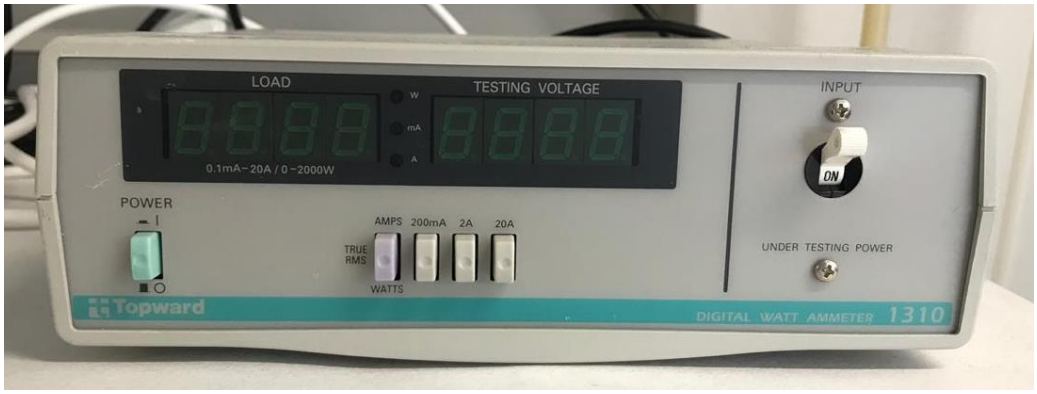

***Figure III-10: E*nergy reading equipment (Ammeter)**

Through the multiplication of the voltage with the current, measured in ampere (A), and the Power factor, the watts (W) consumed by the respective process were calculated. Furthermore, by taking note of the time required for each of the respective processes to complete, the kilowatt-hours (kWh) were determined. This value was then used in conjunction with the average Eskom

electricity prices (tabulated in Table VIII-13 in appendix E) to calculate the actual cost of running the mechanical size reduction processes.

The cost of shredding (CoS) required accurate determination of the time that is required for each individual shredding cycle (T), including the intermediate re-feed times (RFT). These re-feed times increased progressively depending on the shredding stage as indicated by Figure III-11. The 1st cycle, for example, did not require any re-feeding, the 6th cycle however required a total of five re-feeding cycles, adding a collective 75 sec to the shredding process (eq. (III-4)).

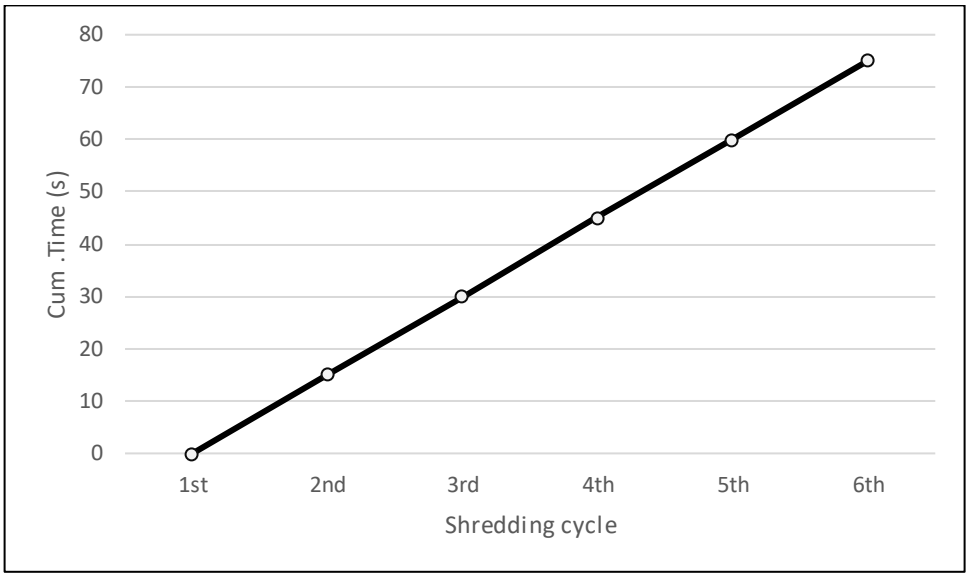

Figure III-11: Cumulative re-feed time increase per shredding cycle

The cumulative time required (TC) (eq. (III-3)) for the individual shredding cycle is then added to the cumulative re-feed time (RFTC) to determine the total time (TTC) necessary for each shredding stage (eq. (III-5)).

The total cumulative energy (E) was then calculated by cumulatively adding the total energy demands (TEC) for each shredding cycle together (eq. (III-2)). Following this, the energy consumed (kWh) by each individual shredding cycle was calculated by multiplying the total cumulative energy (kW) of each stage with the respective time (hrs) needed (eq. (III-6)). Finally, to determine the cost of shredding, the previously determined average cost of energy (CoE) for South Africa was multiplied with the energy consumed (eq. (III-7)). The average price of energy was determined to be R 1,55 per kWh (Eskom, 2019).

$$TEC = TE_1 + TE_2 + TE_3 + \ldots \quad \textit{Eq. (III-2)}$$

$$TC = T_1 + T_2 + T_3 + \ldots \quad \textit{Eq. (III-3)}$$

$$RFTC = RFT_1 + RFT_2 + RFT_3 + \ldots \quad \textit{Eq. (III-4)}$$

$$TTC = (T_1 + RFT_1) + (T_2 + RFT_2) + (T_3 RFT_3) + \ldots \quad \textit{Eq. (III-5)}$$

$$E = TTC * TEC \quad \textit{Eq. (III-6)}$$

$$CoS = E * CoE \quad \textit{Eq. (III-7)}$$

Where

- TE = Total energy (kW)
- TEC = Total energy cumulative (kW)
- T = Time required for shredding cycle (s)
- TC = Time required for shredding cycle cumulative (s)
- RFT = Re-feed time required (s)
- RFTC = Re-feed time required cumulative (s)
- TTC = Total time required for shredding cycle cumulative (s)
- E = Energy consumed (kWh)
- CoE = Cost of energy (R/kWh)
- CoS = Cost of shredding in terms of only energy (R)

v. Temperature Measurements

Temperature measurements were conducted using T-type thermocouples as depicted in Figure III-12. To be as accurate as possible about the temperature before and during the shredding process, the temperature increase over time was measured by making use of the RS Pro 5511 Digital Thermometer in conjunction with the T-type Thermocouples. After being frozen in Liq. N2, the PCBs underwent a single crushing cycle before undergoing the same ammonia leaching test as the standard PCBs.

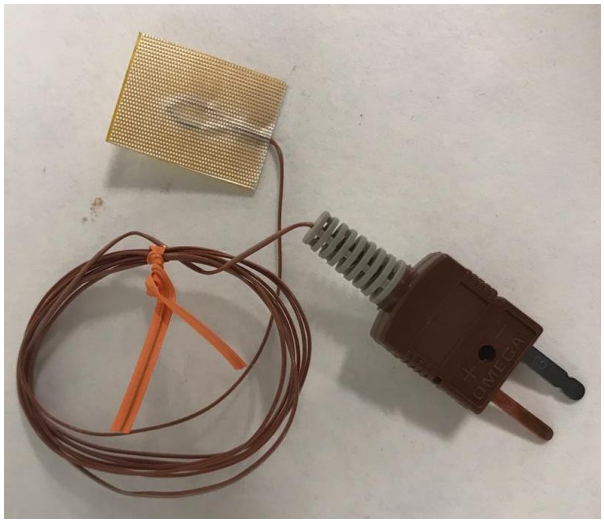

Figure III-12: T-type Thermocouple

c. Methods

A general overview of the experimental procedure is outlined in subsection c-i, providing a brief introduction of the following sections. Section c-ii describes the shredding procedures as the main size reduction processes, directly followed by subsection c-iii which describes the chosen pre-treatment processes. The penultimate section, subsection c-iv, outlines the post-shredding processes. Finally, subsection c-v will outline the preliminary failure analysis tests conducted on the boards. The focus of this work is on sections i-iv, as these preliminary material tests are only a preliminary study applicable to the specific boards used in this study.

i. General Overview

The entirety of the research revolves around the clawing mechanics of the industrial grab shredder and is as such termed the main size reduction process. The processes before and after the shredding process are therefore labelled pre-treatment and post-shredding processes, respectively. The pre-treatment stage included processes such as soaking of the boards in a sodium hydroxide (NaOH) solution to remove the upper- and lowermost solder mask. Another pre-treatment process involved is the freezing of the boards in Liquid Nitrogen (Liq. N_2). PCBs that were only shredded in the IGS without any additional pre- or post-treatments are referred to as "untreated". The post-shredding stage encompassed process actions carried out to the boards once the PCBs have undergone the shredding stage. These included processes such as screening of a PCB into six different particle sizes and the milling of the custom-made PCBs in a planetary ball mill to further reduce the shredded chips in size. The dominating post-shredding process, however, was the diagnostic leach test carried out to determine the copper recovery of each of the selected shredding cycles. An additional aspect investigated was the energy consumed by the various processes, predominantly by the shredder and the post-shredding processes. Figure III-13 depicts the overarching experimental procedure graphically.

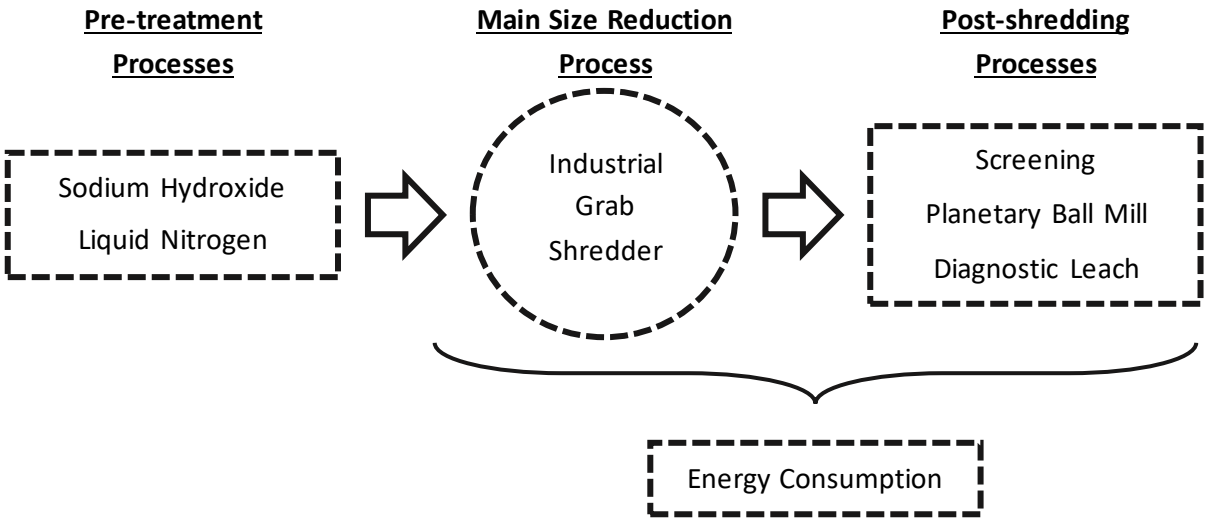

Figure III-13: Overarching experimental procedure

ii. Main Size Reduction Process

1. Industrial Grab Shredder

To investigate the effect of the clawing mechanics of the custom-made industrial grab shredder on the overall size reduction, delamination and ultimate liberation of copper of the custom-made PCBs were evaluated. The boards were fed into the shredder numerous times, up to a maximum of six repetitions. It was possible to quantify the degree of size reduction and delamination through progressive shredding of the PCBs. For calculation purposes, and on average 15 seconds long re-feed time that occurred in-between the successive shredding cycles were included. Table III-4 presents the shredding repetitions as well as the necessary re-feed times.

Table III-4: Shredding repetitions and associated re-feed times

Shredding repetitions (x)	Re-feeds necessary (x)	Cumulative re-feed time (s)
1	0	0
2	1	15
3	2	30
4	3	45
5	4	60
6	5	75

By feeding the custom-made PCBs into the shredder for the first time, major initial particle size reduction was introduced to the boards. This is graphically presented in Figure III-14. The shredded boards were collected below the shredder and refed into the shredder for the successive shredding stages. This was repeated depending on the required number of shredding cycles. Furthermore, the PCBs were weighed before they underwent the shredding and once the respective shredding cycle was complete for accurate mass balance.

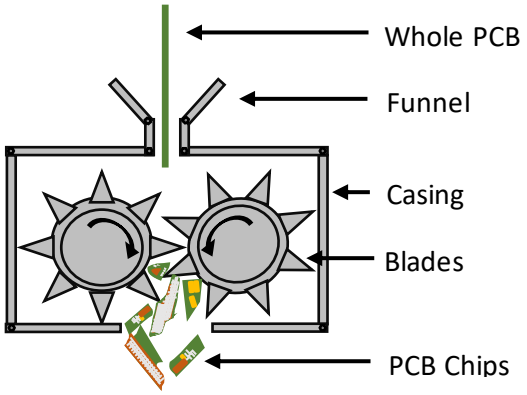

Figure III-14: Graphical representation of the interior of the industrial grab shredder

The 1.1 kW SEW motor was set to run on a frequency of 50 Hertz (Hz), as higher frequencies resulted in jamming of the shredder, as the shredder "suffocated" itself with small chips that got

stuck between the teeth at higher rotational speeds. Regardless of the frequency, jamming of the shredder occurred once the shredded PCB chips were small and numerous enough to fit into the gaps between the shredding blades. This typically occurred from the 3rd shredding cycle onwards and when re-feeding of the shredded chips occurred too fast.

iii. Pre-treatment Processes

The explored experimental procedures in this section include the pre-treatment of the PCBs in Sodium Hydroxide (NaOH) as well as the freezing of the boards in Liquid Nitrogen (Liq. N_2).

1. Sodium Hydroxide

Chirume (2018) undertook several pre-treatment experiments on the custom-made PCBs with the aim to increase copper recovery. The pre-treatment that was determined to be the most effective involved the soaking of the PCBs in Sodium Hydroxide (NaOH), resulting in the removal of the Liquid Photo Imageable Coatings (Solder Mask) on the upper- and lowermost copper layers. The results from Chirume (2018) were adjusted slightly as the removal of the solder mask proved more difficult than expected. The NaOH bath was prepared by dissolving 1280 g of NaOH chips in a 4 L container which was then filled up with deionized water and mixed with magnetic stirrers.

Whole boards were then placed into the 8 M NaOH bath and soaked for 24 hours without agitation. Once the pre-treatment was completed, the boards were rinsed with standard tap water to remove any remaining residue from the surface of the PCBs. The boards were immediately processed in the shredder after the soaking to avoid oxidation of the upper- and lowermost copper layers which were now exposed to air as the solder masks were removed.

2. Liquid Nitrogen

A further pre-treatment investigated was the freezing of a custom-made PCB in Liquid Nitrogen (Liq. N_2). The boards were submerged in Liq. N_2 and cooled down to approximately - 196 °C before initial shredding. The room temperature at the time of the experiment was recorded to be ± 18.5 °C. Moreover, due to the high heterogeneity in terms of material compositions of the boards and to ensure that the temperature change was constant throughout the entire board, four different localities on the boards were measured. These four areas are indicated in Figure III-15 (a-b).

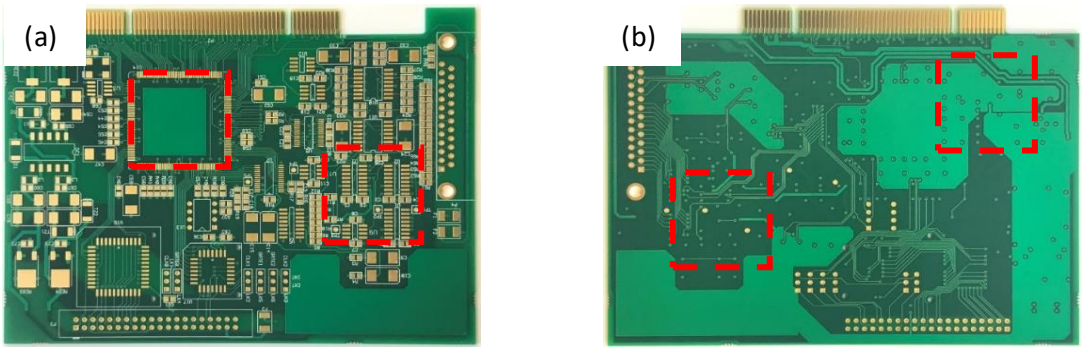

Figure III-15: T-type Thermocouple attachment area on PCB (a) – Topside; (b) – Bottom side

iv. Post-shredding Processes

This subsection outlines the post-shredding processes applied to the previously shredded PCBs. The experiments explored and discussed are the milling of shredded boards in a planetary ball mill (PBM), the screening of shredded and milled PCBs as well as the diagnostic leach tests conducted on the shredded and milled boards.

1. Planetary Ball Mill

To further test the effect of size reduction beyond the industrial grab shredder, two shredding cycles, the 2nd and 4th, were subjected to further size reduction in the planetary ball mill. The PBM's agate milling chamber was set up with alternating layers of PCB and agate balls. In total, 12 balls each with a diameter of 2 cm, were used for the milling process. Four balls were placed at the bottom of the mill, followed by approximately half of the shredded PCBs (± 25 g). Another further 4 balls were placed on top of the first half of the shredded PCBs. This then again was followed by the other half of the shredded PCBs (± 25 g) after which the remaining 4 balls were then placed above. Milling of the boards was done at between 70 – 80 % of the maximum rotational speed of 3500 rpm as higher speeds would result in overheating of the mill, causing short cut-outs during the milling. As tabularized in Table III-5, two milling times, 60 and 120 minutes, were chosen as the time limits for the milling cycle to ensure adequate pulverization.

Table III-5: Shredding repetitions and milling times for the Planetary Ball Mill

Shredding cycle	Milling time 1 (min)	Milling time 2 (min)
2	60	120
4	60	120

2. Screening

The screening process was applied to the respective six shredding cycles as well as the four PCBs that were milled in PBM. For the purpose of this study, the size reduced boards were screened into six size fractions. The 8000 µm size fraction was selected as the largest as this is the thickness of the IGS blades. Through conducting test shredding of the IGS, it was determined that the shredder does not produce particles considerably smaller than 2000 µm, which was therefore selected as the smallest size class. The remaining size fractions in between the largest and smallest were selected based on the availability of sieves in the laboratory as well as the recommended sizes in literature. These six size fractions are listed in Table III-6. The size reduced sample boards were fed into the screening process one at a time. The shaker was set to operate and screen the size reduced particles at a time interval of 10 seconds over a total screening period of 10 minutes, set to a maximum amplitude of 1.8 mm.

Table III-6: Sieve mesh sizes for the screening process

Shredded particle size fractions (µm)	Pulverisation time (s)
> 8000	70
8000 – 6700	50
6700 – 4750	40
4750 – 3350	30
3350 – 2000	25
< 2000	15

Following the screening procedure, the screened PCBs were weighed according to their size classes. The results were then normalized to the nominal weight percent (wt%). One set of PCBs that were shredded up to six times was screened and analysed for particle size distribution. On the other hand, another set with the same shredding characteristics was further processed to determine the copper distribution in each of the shredded particle size fractions.

3. Visual Analysis

Photographs were taken of the produced particles from each of the individual shredding cycles to quantify the degree of delamination as well as the generated particle shape and size. After each shredding stage, the generated particles were placed onto a white filter paper and distributed evenly across the paper. A scale of five centimetres (cm) was drawn onto the paper to enable size correlation. Each individual particle was turned in such a manner that if there was delamination present, the respective side would face upwards to be visible by the camera. Each photograph was taken from the same height and position to ensure correct visual accuracy.

4. Copper Distribution

For the determination of copper distribution throughout the previously outlined size fractions, the size reduced PCBs had to undergo a two-step process. This two-step process firstly included the pulverization of the prior shredded or ball milled samples and secondly, the splitting into smaller representative size fractions for subsequent analysis.

Pulverisation was achieved by milling of the samples to ultrafine particle sizes using a pulveriser. The size reduced PCB chips were placed into a grinding jar and distributed equally between the inner ring with a radius of 15 cm and centre cylinder of radius 12 cm. Pulverization occurred over a short period of time, depending on the particle sizes. For larger particles, the pulverization took slightly longer than for the smaller particle sizes. The pulverization times are also listed in Table III-6 and are the result of trial experiments conducted on test boards. Moreover, for the copper analysis, a minimum sample size of 1 g was required with the recommendation that each sample should preferably weigh 4 g. Because most samples exceeded the maximum weight, the samples were split and combined to a sample weight of 4 g by making use of the Dickie and Stockler splitter. By combining the split samples to the required sample mass, homogeneity and representativity throughout all the samples were guaranteed.

v. Diagnostic Batch Stirred Tank Leach Test

An ammonia-ammonium carbonate ($NH_3 + NH_4^+$) system was selected to extract the copper from the samples generated by the individual size reduction processes. The lixiviant was prepared by dissolving 192.12 g of Ammonium Carbonate in 298.4 ml of 25 % Ammonia Solution (Ammonium Hydroxide) in a 1 L Volumetric flask. Additionally, 0.329 g of Copper (II) Sulphate Pentahydrate ($CuSO_4.5H_2O$) was added to the solution to ensure an initial copper concentration of 100 ppm. The solution was then filled up to the 1 L mark of the Volumetric flask with deionized water. Thereafter, magnetic stirrers were utilized to mix the solution thoroughly until all solid particles were dissolved completely and the solution appeared in clear blue colour as seen in Figure III-16. During the mixing process, solution loss due to dissolution of the solids was compensated by addition for extra deionized water. Table III-7 outlines the conditions of the leaching lixiviant.

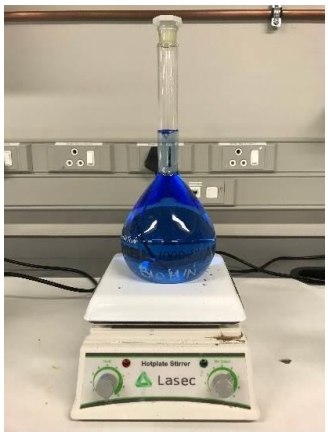

Figure III-16: Prepared ammonia-based lixiviant

Table III-7: Experimental lixiviant components and conditions

Lixiviant	Unit	Condition
Ammonium Carbonate	Molar (M)	2
25% Ammonia Solution	Molar (M)	4
Copper (II) Sulphate Pentahydrate	Parts per million (ppm)	100
Deionized water	Millilitre (ml)	± 700
Volumetric Flask	Litre (L)	1

Two separate 1 L in succession installed verhead batch reactors were selected as the leaching environment. Each reactor contained a water jacket around it, keeping the reaction at a steady temperature of 25°C. Once this temperature was reached, the respective size reduced board to be analysed was placed into the solution, where the PCB chips were evenly distributed across the bottom of the reactor. The liquid:solid ratio chosen for these experiments was 10:1. Overhead stirrers were utilized and ran at a constant rate of 100 rpm. Even though literature recommends higher mixing rates, it was observed that at an agitation rate of more than 100 rpm resulted in considerable splashing. This would have resulted in a loss of copper due to precipitation on the

reactor walls. The speed was therefore reduced and set to this low level in order to minimize the splashing of the solution onto the reactor walls. Moreover, to minimize solution loss to the reactor wall, a baffle placed inside the reactor further reduced the potential of a vortex to form within the solution. The chosen oxidant, compressed air, was supplied directly into the solution at a constant rate of 0.1 L/min to continuously oxidize the solution. A cross-sectional view of the reactor is depicted in Figure III-17. Table III-8 further lists the reactor settings.

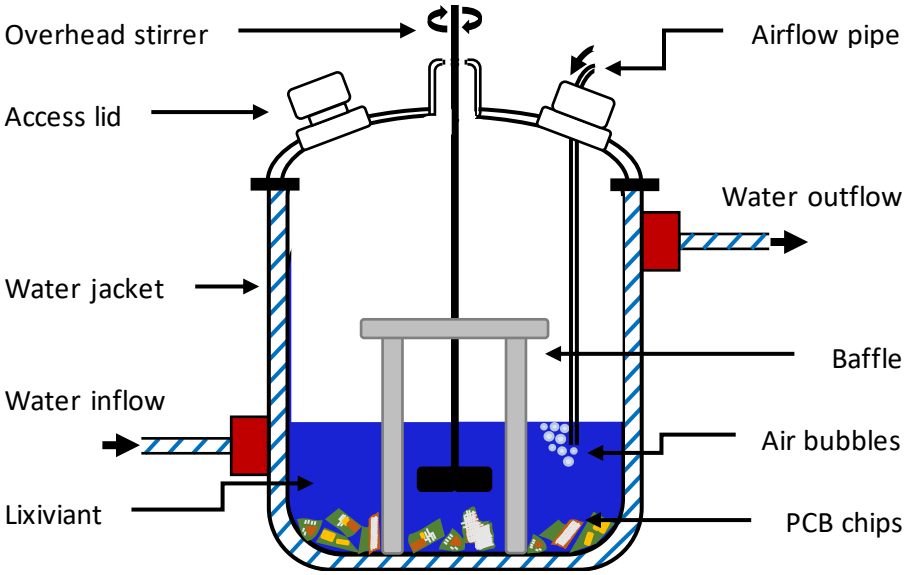

Figure III-17: Batch stirred reactor layout

Table III-8: Experimental batch stirred reactor set-up and conditions

Parameter	Unit	Condition
Reactor volume	L	1
Water-jacketed temperature	°C	25
Agitation	rpm	100
Airflow (O_2)	l/min	0,1
Liquid:solid ratio	ml:g	10:1
pH	-	10 (± 0.25)
Leaching time	hr	72

Initially, sampling of the solution occurred at 20-minute intervals for the first hour of each leaching test. After the sampling of the initial hour, samples were taken off hourly for the following six hours. Thereafter, one sample was taken daily for the next two days. The kinetic leach test of the PCBs, therefore, occurred over a 72 hrs time frame. To account for the loss in solution volume caused by sampling, either the initially created solution ($NH_3 + NH_4^+$) was added or NH_4OH if solution pH adjustment was required. Furthermore, to have accurate and represenTable data, the pH was maintained as close to 10 as possible. The sampled solutions were analysed for dissolved copper using Atomic Absorption Spectroscopy (AAS) analysis.

vi. Material Properties

In order to quantify the resilience of the boards to stress environments, three overall failure tests were conducted, namely Drop-weight Impact, Three-point bending, and Tensile tests. All three of these tests were conducted as closely as possible according to their specific American Society for Testing and Materials (ASTM) standards. For the statistical accuracy of each of the three following outlined tests, five specimens per area were tested. For all tests, the average value, standard deviation as well as the coefficient of variation was determined and reported.

1. Drop-weight Impact Test

The drop-weight impact testing was conducted on the Instron Dynatub 9210 and as close as possible in accordance with the ASTM D7136/D7136M (2015a) standard test methods.

a. Sample Preparation and Experimental Procedure

The 1.55 mm thick boards were cut into six 40 x 40 mm samples as indicated in Figure III-18 below; the circular dotted lines represent the areas of impact. The reason that six samples were selected covering most of a PCB instead of just one sample is because of the high heterogeneity of the boards in terms of copper layers, etching and holes.

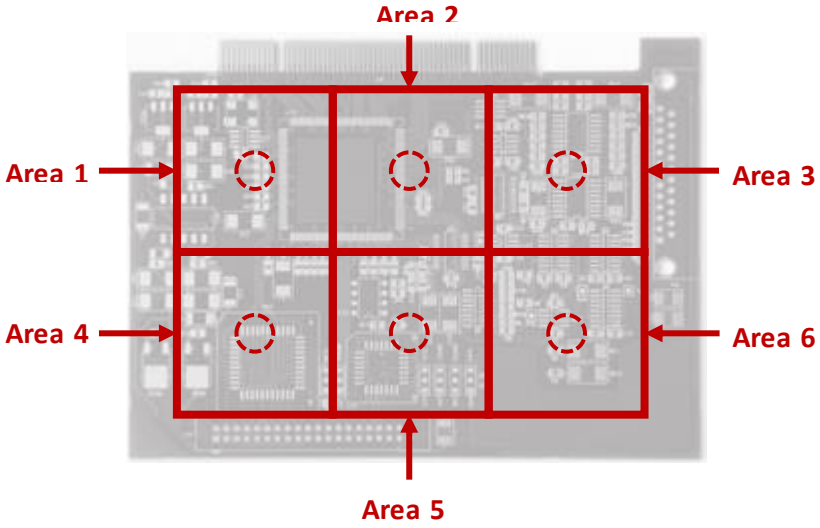

Figure III-18: Drop-weight impact sample design (Not to scale)

The ASTM D7136-15 provides clear instructions on the experimental set-up which were followed as closely as possible. The cut PCB samples were placed on the impact support fixture base on which they were tightly secured by the support plate and the support screws. Figure III-19 (a) displays the experimental set-up from a side view whereas Figure III-19 (b) provides a top view onto the set-up. The hemispherical impact striker tip was then raised and released from 209 mm above the sample as per equation III-8.

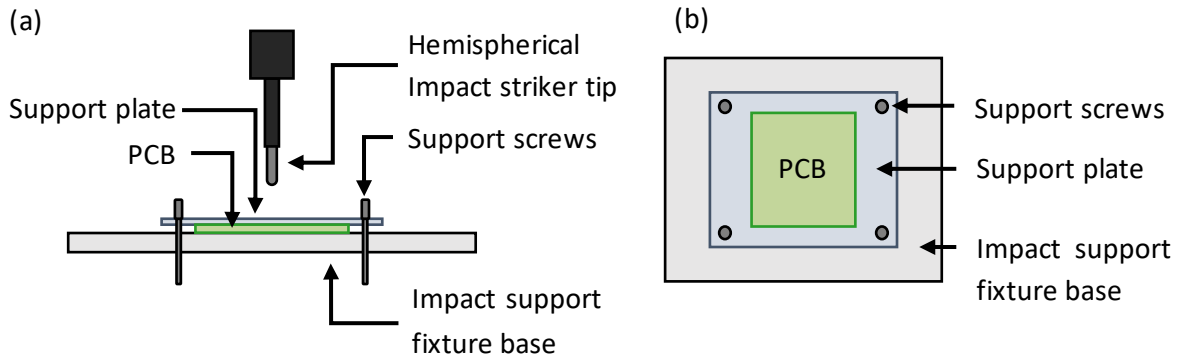

Figure III-19: Experimental set-up of Drop-weight Impact Test (a) – Side View of the Drop-weight Impact Test; (b) – Top view of the Drop-weight Impact Test

b. Calculations

Prior to the commencement of the tests, the potential impact energy (E) (eq. (III-8)) had to be calculated in order to determine the required drop height (H) (eq. (III-9)) for the experiments.

$$E = C_e h \qquad \textbf{Eq. (III-8)}$$

Where:

- E = potential energy of impactor prior to drop (J)
- C_e = specific ratio of impact energy to specimen thickness (6.7 J/mm)
- h = nominal thickness of specimen (mm)

$$H = \frac{E}{m_d g} \qquad \textbf{Eq. (III-9)}$$

Where:

- H = drop height (m)
- E = potential energy of impactor prior to drop (J)
- M_d = mass of impactor for drop height (5.0766 kg)
- g = acceleration due to gravity (9.81 m/s^2)

Moreover, the aim of this test was to determine the total absorbed energy of the boards. The equation utilized for this is presented in eq. (III-10) as indicated by the ASTM and the values were then integrated to determine total absorbed energy.

$$E_a = \frac{m(v_i^2 - v(t)^2)}{2} + m\ g\ \delta(t) \qquad \textbf{Eq. (III-10)}$$

Where:

- E_a = Absorbed Energy at time t (J)
- m = mass of impactor (5.0076 kg)
- v_i^2 = impact velocity (m/s)
- v(t)2 = velocity of impactor at time t (m/s)
- δ = impactor displacement at time t (m)
- g = acceleration due to gravity (9.81 m/s^2)

c. Limitations

There are several limitations that must be considered when analysing the data generated with the impact testing of the boards according to ASTM D7136-15. Firstly, the board's thickness (1.55 mm) falls outside of the recommended minimum thickness according to the standards. This further resulted in complications with the recommended minimum drop height of 300 mm, as the drop weight (5.0766 kg) could not be further reduced. The calculated drop height of 209 mm was therefore ignored and increased to 300 mm for the testing variables to be as close to the recommended standards as possible. Another factor that had to be considered was the fact that the ASTM recommended sample sizes to be 100 x 150 mm, however, the custom-made PCBs were only 98.6 x 142.2 mm. Moreover, the sample holders for the tests could only hold sample sizes of 40 x 40 mm, as these were the only holders available for the machine. Finally, the standards asked for carbide blades to be used during sample cutting as this provides smooth edges of the samples. However, the only machine able to utilize carbide blades was inoperable, and samples were therefore cut with a standard bandsaw.

2. Three-point Bending Test

The three-point bending tests were conducted on a Zwick 1484 and as close as possible in accordance with the ASTM D7264/D7264M (2015b) standard test methods. According to the ASTM, the recommended standard span-to-thickness ratio is 32:1, with a thickness of 1.55 mm and a width of 13 mm. The sample span width was therefore calculated to be 49.6 mm and 59.5 mm when including the recommended extra 20 % for extra length for the support span. The samples were cut out of the boards using a bandsaw. Six different locations were chosen to be tested as indicated in Figure III-20, three vertically and three horizontally. This was done primarily because of the high heterogeneity of the boards so the results are as representative as possible about the breakage behaviour of the entire board.

a. Sample Preparation and Experimental Procedure

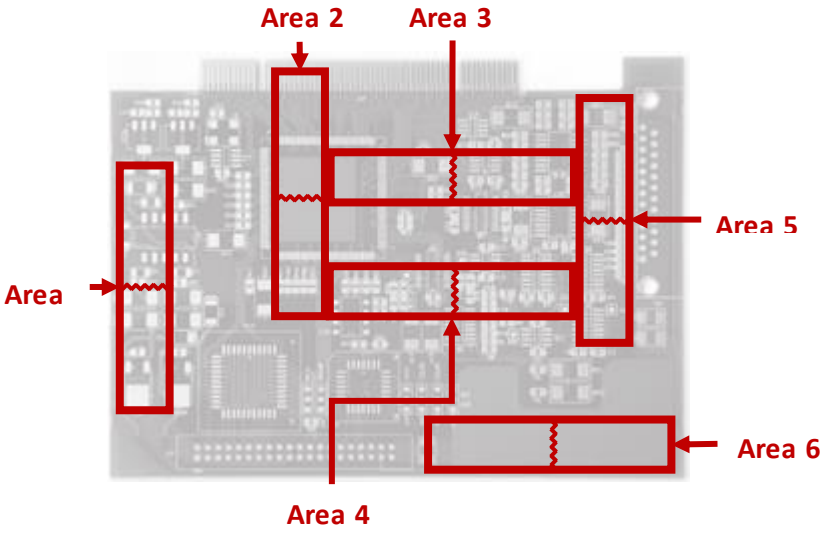

Figure III-20: Three-point Bending sample design (Not to scale)

The samples were placed into the Zwick after they were cut to the correct size and shape (59.5 x 13 x 1.55 mm). The support noses were spaced 49.6 mm apart from one another, with the roll loading nose placed exactly in the centre between the two support noses. The loading nose and support noses were aligned parallel and the PCB samples were placed perpendicular to the noses but central to the width of the noses. Figure III-21 graphically displays the experimental setup. The roll leading nose with a radius of 5 mm was then manually lowered just above the sample, after which it automatically moved at a rate of 1 mm/min once the experiment commenced. On average each experiment required approximately 10 minutes until failure occurred. The experiment was stopped automatically once failure occurred and the loading nose returned to its original starting position. Each sample individual failure identification code was subsequently recorded.

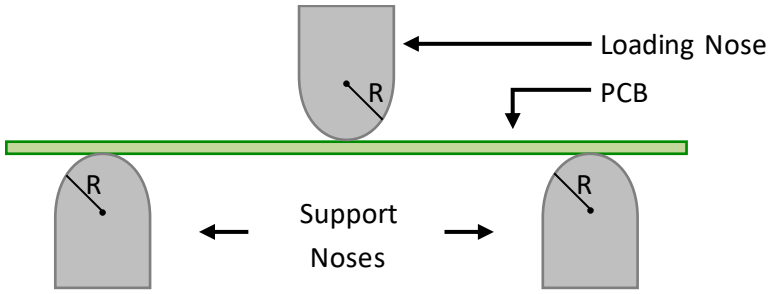

Figure III-21: Experimental Set-up of Three-point bending test

b. Calculations

The main purpose of this set of experiments was to determine the maximum amount of bending the custom-made PCBs could withstand. For this purpose, as recommended by the ASTM, the calculations used to determine the maximum flexural stress the boards can withstand in a three-point bending environment are outlined in eq. (III-11).

$$\sigma = \frac{3PL}{2bh^2} \qquad \textit{Eq. (III-11)}$$

Where:

- σ = stress at the outer surface at mid-span (MPa)
- P = applied force (N)
- L = support span (49,6 mm)
- b = width of beam (13 mm)
- h = thickness of beam (1.55 mm)

c. Limitations

As with the Drop-weight Impact Test, there are several limitations associated with deviations from the ASTM. The first deviation from the ASTM standard was the inability to use the recommended 4 mm thickness for samples as the boards only have a nominal thickness of 1.55 mm. Again, as with the impact test, the standards asked for carbide blades to be used during sample preparation. However, the only machine able to utilize carbide blades was inoperable, and samples were therefor cut with a standard bandsaw.

3. Tensile Test

As with the three-point bending tests, the tensile testing was also conducted on the Zwick 1484 and as closely as possible in accordance with its recommended ASTM D3039/3039M (2017) standard test methods. Sample preparation for this failure analysis test was conducted as recommended by the ASTM standards. This particular failure test however required higher amounts of preparation. For successful testing of the tensile properties, the test samples had to be equipped with tabs made of old PCBs by gluing them onto the test strips.

a. Sample preparation and procedure

For tensile tests of polymer matrix composite materials, the use of tabs for increased gripping of the tensile device is recommended. For the purpose of tabs, old PCBs with a thickness of 1.5 mm were cut into 25 x 75 mm long strips. These strips were then sandpapered to increase the effectiveness of the glue as well as the gripping force during subsequent tensile testing. The stripes were further tapered at ± 20° on one side in order to increase the grip of the wedge-operated grips.

To glue the tabs to the test samples, a composite glue (Spabond 340LV resin) was mixed with a fast hardener in a 2:1 ratio. Both the resin as well as the hardener were acquired from AMT composites. The glue was spread evenly across the tab strips at an approximate thickness of 0.5 mm and then placed on top of the boards. The boards and the attached strips were then clamped together for several minutes (± 1 hr) and left to dry in the same room for three days. Following the drying period, the glue had hardened, and the boards were cut into 25 mm wide strips for the tensile tests as indicated in Figure III-22. The orange square area represents the attached tabs, whereas the zigzagged lines represent areas of failure. Figure III-23 displays a side view of the created samples.

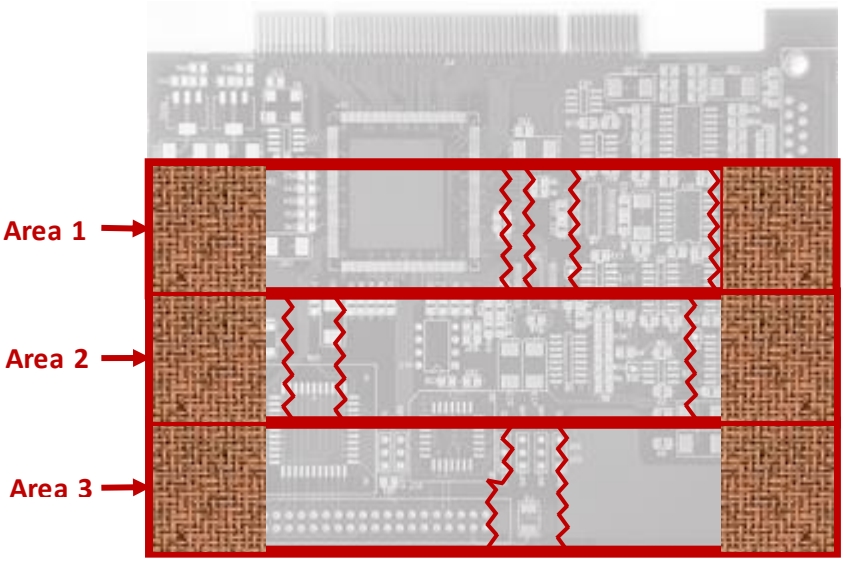

Figure III-22: Tensile test sample design (Not to scale)

Following the preparation of the samples as outlined in the sample preparation section, the cut samples are placed into the Zwick. The samples were firmly secured within the device by rigid wedge-shaped holders gripping onto the sandpapered tabs. The samples were also aligned with the long axis of the gripped specimen with the test direction. The head-speed of the tests was set to 1 mm/min. Loading was applied at the specified rate until failure occurred and subsequently stopped. Once failure occurred, each individual sample's failure identification code was recorded.

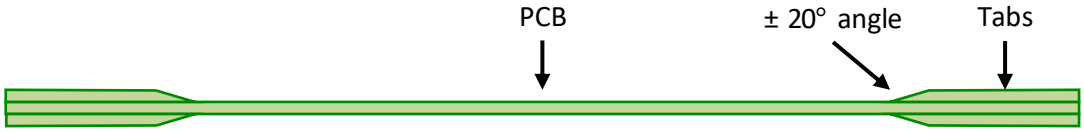

Figure III-23: Experimental design of the Tensile test

b. Calculations

The overarching aim of this test was to determine the maximum tensile stresses the custom-made PCBs can withstand before failure occurs. Based on the ASTM, the equation for ultimate tensile strength is outlined as follows in eq. (III-12).

$$F^{tu} = \frac{p^{max}}{A} \qquad \textit{Eq. (III-12)}$$

Where:

- F^{tu} = ultimate tensile strength (MPa)
- p^{max} = maximum force before failure (N)
- A = average cross-sectional area (mm^2)

c. Limitations

As with the drop-weight impact and the three-point bending tests, there are a few limitations associated with the tensile tests. Firstly, the ASTM standards asked for carbide blades to be used during sample preparation. However, the only machine able to utilize carbide blades was inoperable, and samples were therefor cut with a standard bandsaw. Moreover, an exact angle of 20 was not possible to be created as there was no equipment to measure the angle accurately during the angling process. Finally, the extensometer, a tool that measures the stretching of the PCBs during the test, was unavailable during the time of the tests and it was therefore impossible to obtain Poisson's ratio.

d. Analytical Techniques

i. Material Testing Methods

The materials testing experiments were conducted on two testing rigs. The three-point bending tests, as well as the tensile tests, were conducted on the Zwick. The data is presented in the form of standard force (N) versus standard displacement (mm). The rig used for the drop-weight impact testing is called the Instron Dynatub 3022. The data is generated in the form of standard force (N) vs standard time (ms).

ii. pH Measurements

Every leached sample's pH was also simultaneously measured using a CRISON Basic 20+ pH-meter. Calibration of the probe was done daily before readings were taken to ensure accurate and precise readings of the pH-meter by making use of three pH solutions, 4.01, 7.02 and 9.28. Furthermore, each reading was taken at least three times to minimize error and the average value was recorded as the final pH value of the respective samples.

iii. Elemental Compositional Analysis of Leached Solutions

The leached samples from the diagnostic leach test were analysed for total copper concentrations through atomic absorption spectroscopy (AAS) by making use of the Spectra 110 Atomic Absorption Spectrophotometer at the University of Cape Town (UCT) Chemical Engineering Analytical Laboratory. The Analytical Lab makes use of a four-point calibration standard curve with 5, 20, 30 and 60 ppm for copper analysis. The samples were diluted by factors of between 10 to 1000 and reported in ppm concentrations. This method has a precision of ± 10%.

To further verify the generated data, the samples were additionally analysed in the Genesys 150 UV-Visible Spectrophotometer from Thermoscientific. The samples were analysed based on a standard curve with standard Cu concentration of 0, 100, 200, 500 and 700 ppm. The optimal wavelength was determined to be 620nm, as recommended by Koyama et al. (2006). Samples that exceeded concentrations of 700 ppm were diluted so that the UV spectrophotometer was able to provide accurate data. All samples were analysed in triplicates to ensure accurate measurements. The calibration curve is depicted in Figure VIII-1 in appendix C.

iv. Elemental Compositional Analysis of Pulverised Solids

After splitting the samples and, where possible, combining of the splits to a sample mass of ± 4g, the samples were sent for total copper content analysis. The compositional concentrations of total copper distributed across the size fractions were analysed by making use of inductively coupled plasma atomic emission spectrometry (ICP-AES).

Approximately 0.1 g of each sample was digested in 5 ml HNO_3 and 2 ml HCl (Aqua Regia) and diluted to a final volume of 50 ml with deionized water prior to analysis in ICP-AES at the Central Analytical Facilities (CAF) at the University of Stellenbosch (US). Each individual sample was analysed with two replicates and the percentage error was below 1 % for all samples.

IV. Results and Discussion

This chapter aims to present, interpret and discuss the results obtained from the various conducted experiments. To recap, the main focus of the study relied on the evaluation of the IGS efficiency in terms of copper liberation from PCBs in the form of size reduction and delamination. The chapter is divided into three main subsections, with section IV-a focussing on the IGS, section IV-b evaluating the PBM, section IV-c characterizing NaOH pre-treated and section IV-d outlining the efficiency of pre-treating the PCBs in Liq.N_2 and complete pulverization post shredding.

a. Industrial Grab Shredded PCBs

For comparative reasons, the PCBs treated only via this method are referred to as the "untreated" processed PCBs from this point onwards. The two main points investigated were the shredder's efficiency in terms of energy consumption and its effectiveness regarding the liberation of copper through size reduction as well as the delamination of the PCBs. For accurate mass balances, all boards were weighed before and after their respective shredding cycles. The numerical data is tabulated in Table VIII-1 in appendix A.

i. Original Copper Content and Material Loss

On average, one custom-made PCB weighs approximately 52.24 g based on 38 weighed boards. As indicated by Figure IV-1, which displays the average cumulative material losses associated with the respective shredding cycles, it can be seen that size reduction through shredding generally did not cause major material loss. Shredding a PCB once resulted in a material loss of on average 0.11 g, whilst shredding a PCB six times resulted in a loss of ± 0.47 g.

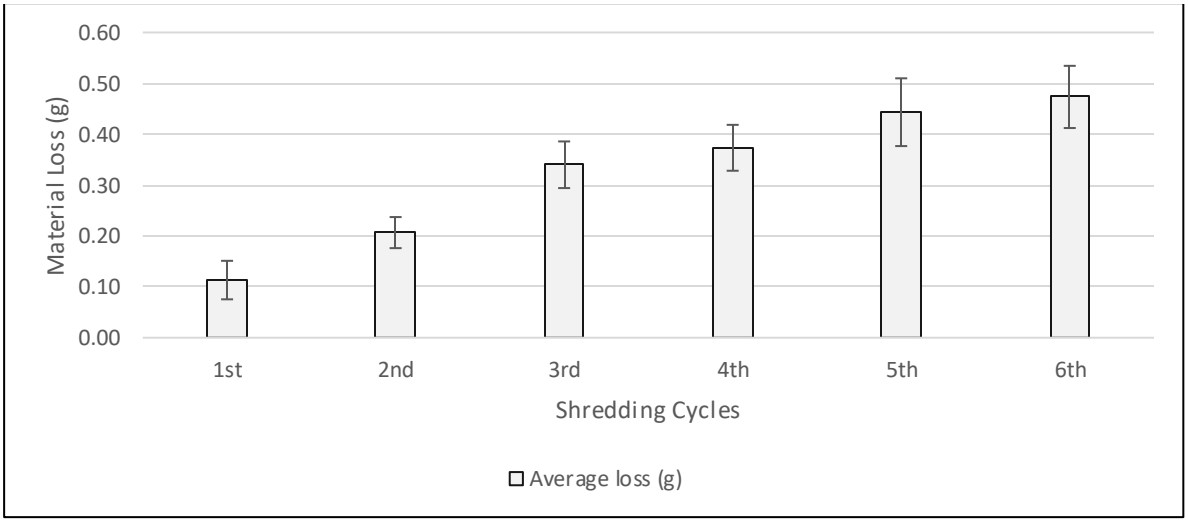

Figure IV-1: Average cumulative material loss during shredding

Between the first three shredding cycles some material loss (≤ 1 %) can be noted, increasing on a scale of ± 0.10 g per repetition. Through progressive shredding, an increased amount of smaller and delaminated particles is generated. There is also a marked associated increase in generated dust which was retained predominately on the shredder blades and increased with progressive shredding. This dust was then brushed off the blades for material loss calculation. Material loss between shredding cycles three and four as well as five and six is of no certainty as the error bars overlap. It is however evident that shredding cycles five and six have higher material losses than the previous shredding cycles. It must furthermore be noted that the total loss of material during shredding did not exceed more than 0.9 % of the total average weight of one PCB.

Chirume (2019) determined the copper concentration of the board to be approximately 55.45 %, which translates to ± 28.97 g. It was further determined by Chirume (2018) that the four copper layers of the custom-made PCBs display a large variation in copper content as tabulated in Table IV-1.

Table IV-1: Copper distribution according to copper layers of the custom-made PCB

Copper layer	Copper content (%)
Outer top layer 1	11
Inner top layer 2	25
Inner bottom layer 3	44
Outer bottom layer 4	18
Other	2

ii. Particle Size Distribution (PSD)

As mentioned in chapter III, the shredded PCBs were screened into six size fractions. The particle size distribution (PSD) of the individual shredding cycles at room temperature is displayed in wt% in Figure IV-2. The Figure also includes the PSD of the 1st shredding cycle under Liq. N_2 conditions. As expected, the PSD shifted to progressively smaller particle sizes with each successive shredding cycle.

As indicated by Figure IV-2, a general trend was observed in which the largest size fraction (≥ 8000 µm), classified as the coarse size fraction (Table IV-2), continued to transfer material with progressive shredding. The other size fractions, on the other hand, continued to gain material from the coarse size fraction or from the respective larger size classes. An exception to this was observed in the 4750 µm size class from the 3rd to the 4th shredding cycle. This was the only shredding cycle during which more material was lost from this class than gained from the ≥ 6700 µm size classes.

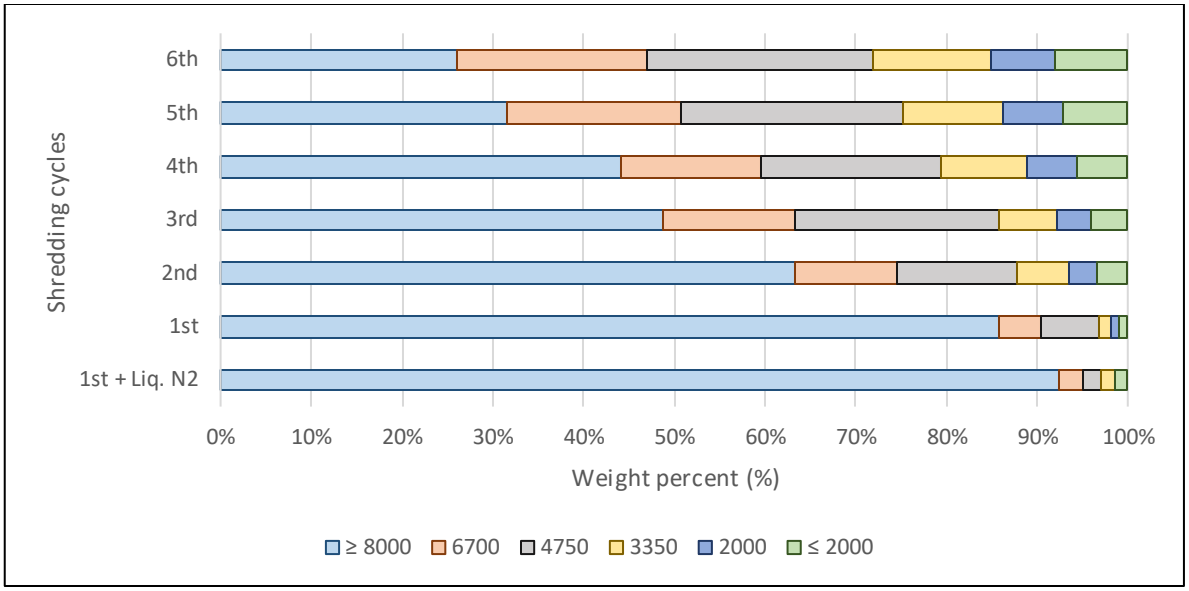

Figure IV-2: Particle size distribution of the various untreated shredding cycles at room temperature (25°C) and under liquid nitrogen (-196°C) conditions

Figure IV-3 further displays these changes, displaying the percentage change from one shredding cycle to the next. A major decrease can be noted from the 1st to the 2nd shredding cycle, during which the ≥ 8000 µm size class lost more than 40 wt% to the intermediate (6700 - 3350 µm) size fractions. A similar effect is seen from the 2nd to the 3rd as well as from the 4th to the 5th shredding cycles, where approximately 15 and 13 wt% were lost by the coarse size fraction, respectively. This is not the case for cycles three to four as well as five to six, where only approximately 5 wt% were lost. As expected, the other size classes continued to grow with successive shredding cycles except for the 4750 µm size class from the 3rd to the 4th shredding cycle. This size class loses 2.5 wt% and did not gain any other material from the two larger size classes.

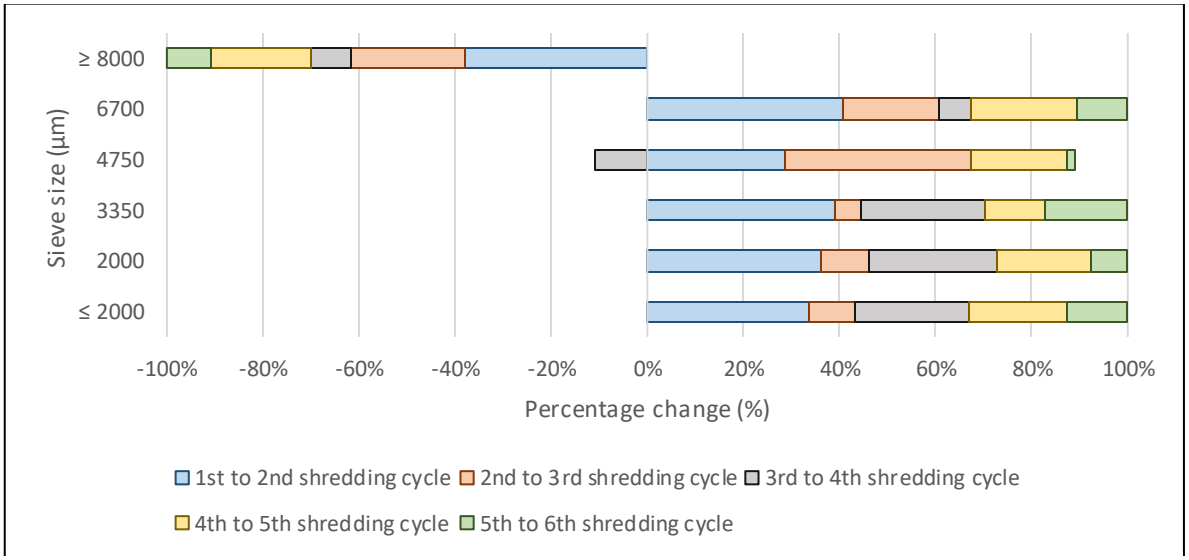

Figure IV-3: Percentage change in particle sizes for successive shredding cycles

The largest size class (≥ 8000 µm) lost up to 60 wt% of material from the 1st to the 6th shredding cycle. The 4750 µm size class gained the most material (18.5 wt%). This change in PSD from the 1st to the 6th shredding cycle is tabulated in Table IV-2.

Table IV-2: Increase and decrease of each size class from 1st to 6th shredding cycle

Size classes (µm)	Increase/Decrease (wt%)	Classification
≥ 8000	-59.69	Coarse fraction
6700	16.24	Intermediate fraction
4750	18.54	
3350	11.69	
2000	6.24	Fine fraction
≤ 2000	6.97	

iii. Visual Analysis

To quantify the degree of delamination, photographs of the shredded material from the individual shredding cycles were taken. Delamination has been defined as a particle where at least one side of the inner PCB chip has been exposed. The generated particles in Figures IV-4, IV-5 & IV-6 (a-f) were separated according to size and delamination, with all delaminated particle sides turned facing up towards the camera. From the images, it became apparent that there are considerable changes within the generated particles between the various shredding cycles from the industrial grab shredder. Delaminated particles were classified as a particle which has at least 50% of the inner copper clad exposed.

To be able to better quantify the degree of delamination, the number of non-delaminated and delaminated particles larger than 2000 µm were counted and placed into context with the visual analysis. This, as well as the total particle count larger than 2000 µm, is tabulated in Table IV-3.

Table IV-3: Non-delaminated and delaminated particles generated by the individual shredding cycles

Shredding Cycle	Non-delaminated particles (#)	Non-delaminated particles (%)	Delaminated particles (#)	Delaminated particles (%)	Total particles
1st	65	76	21	24	86
2nd	110	67	53	33	163
3rd	124	60	82	40	206
4th	113	47	125	53	238
5th	132	44	165	56	297
6th	128	39	203	61	331
1st + Liq. N_2	18	29	44	71	62

After the 1st shredding cycle, the majority of generated particles were of elongated shape and exceeded sizes in lengths of 3 cm or more. Moreover, in comparison to the non-delaminated particles, the number of delaminated particles was relatively small with an insignificant number of fines produced. This indicates that the 1st shredding cycle predominantly acts as a mechanism of size reduction rather than delamination. The 1st shredding cycle also generated the most particles compared to all subsequent cycles, indicating its purpose to be predominantly associated with size reduction. Table IV-3 supports this, indicating that of the 86 generated particles only 21 were delaminated.

A considerable change in generated particles could already be observed with the onset of the 2nd shredding cycle, displaying a general increase in the number of particles generated and an overall decrease in particle size as supported by the PSD in Figure IV-2. The number of non-delaminated particles outweighs the number of delaminated particles, almost doubling the number of particles present compared to the 1st cycle. This stipulates that the 2nd cycle favoured size reduction over delamination.

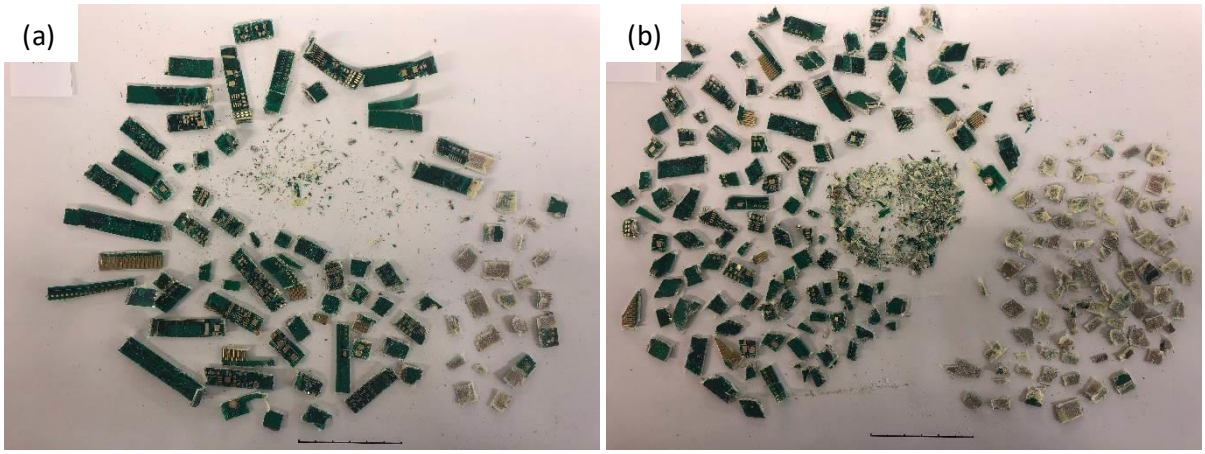

Figure IV-4: Visual analysis of individual shredding cycles; (a) – 1st Shredding Cycle; (b) – 2nd Shredding Cycle

A similar trend in changes relating to particle shape and size as well as delamination and the number of particles generated was observed from the 2nd to the 3rd shredding cycle. With the 3rd shredding cycle, the generation of new particles decreased compared to the 2nd cycle. As with the previous cycle, the number of non-delaminated particles outweighed the number of delaminated particles. It must further be noted that the particle shape changed from the originally dominating elongated shape from the 1st and 2nd shredding cycles to relatively square shaped particles with the 3rd shredding cycle.

As indicated by the PSD in Figure IV-2 and Table IV-3, from the 3rd to the 4th shredding cycle, only a few new particles were generated, with most of the shredding resulting in an increase in the number of delaminated particles. As seen by Table IV-3, there are now more particles present that were delaminated rather than non-delaminated. Based on this, it can be stated that the 4th cycle favoured delamination over size reduction.

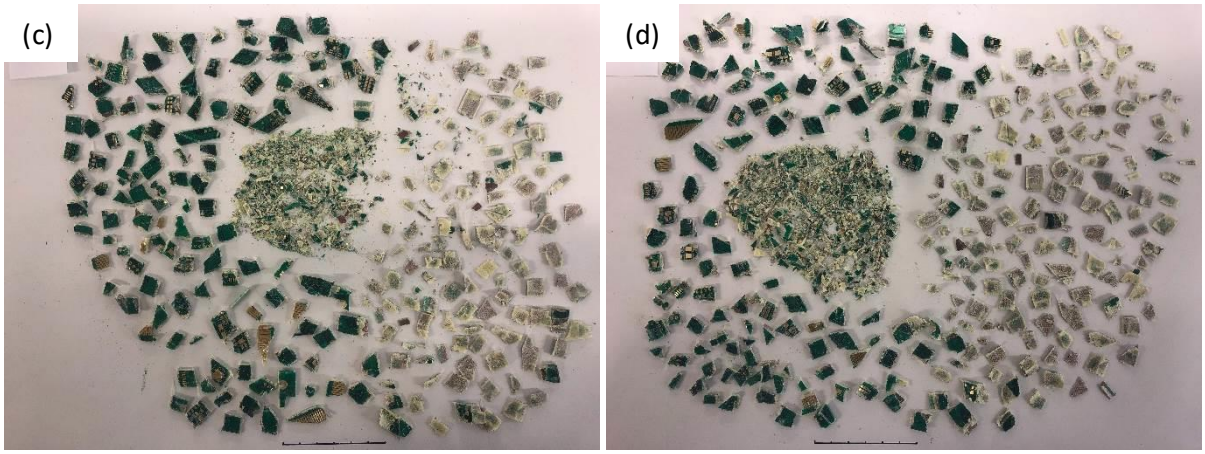

Figure IV-5: Visual analysis of individual shredding cycles; (c) – 3rd Shredding Cycle; (d) – 4th Shredding Cycle

The 5th shredding cycle introduced higher amounts of newly generated particles and only slight changes between the delaminated to non-delaminated ratio. There was also another marked increase in the number of fines produced, indicating that size reduction rather than delamination was the favourable action of this shredding cycle. The highest ratio of delaminated to non-delaminated was obtained by the 6th shredding cycle, generating a 2:1 ratio. This cycle also produced the highest amount of fine particles (≤ 2000 µm).

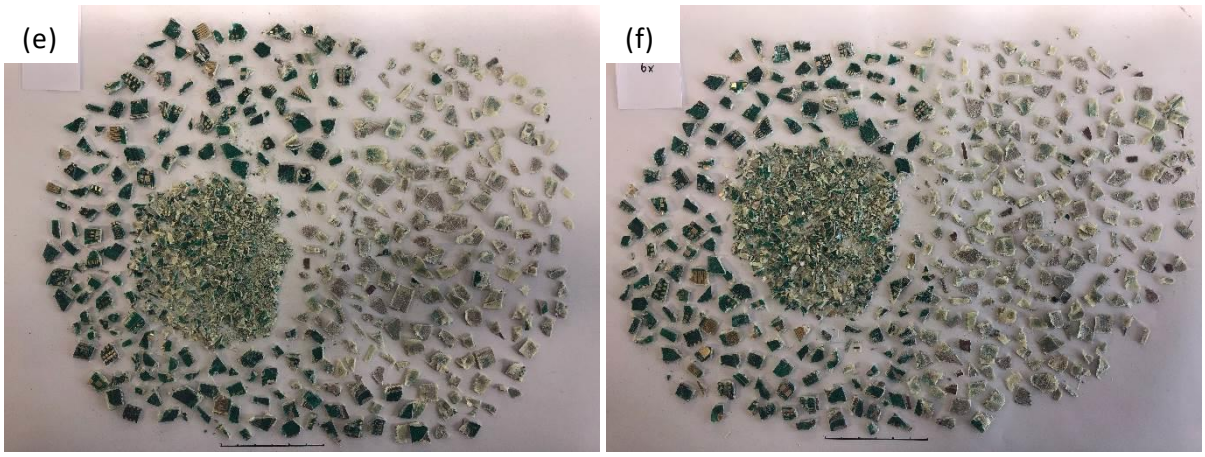

Figure IV-6: Visual analysis of individual shredding cycles; (e) – 5th Shredding Cycle; (f) – 6th Shredding Cycle

It must be noted, however, that delamination tends to occur predominantly at the centre of the PCB's FR-4 core. This has been identified as a key liberation mechanism based on visual observation. In this section of the PCB, four layers of tightly woven fibreglass are present, covering the inner copper layers. These woven fibreglass layers protect the copper layer from any potential lixiviant that aims to extract the copper. The copper found within the finer size fractions (≤ 2000 µm) is generally completely dissociated from the fibreglass or epoxy resin, making it available to extraction.

Overall, the shredder blade's shape and thickness were the controlling factors on the size reduction, degree of delamination as well as on the general shape and size of the generated particles. The "teeth" of the shredder, as displayed in Figure III-4 (b) in chapter III, had a considerable impact on the delamination, effectively biting into the boards and tearing the layers apart. By increasing the number of blades while simultaneously decreasing the thickness, a higher degree of delamination, as well as finer particles, could be generated.

iv. Copper Distribution

A further aspect evaluated included the characterization of the copper distribution in the six size fractions analysed in the PSDs of the untreated PCBs displayed in Figure IV-4. The results are presented in the following graphs in Figure IV-7 (a-f) plotted according to the six size fractions. The primary y-axis presents the size fractions wt%) and the Cu conc. (%), obtained by aqua regia digestion as outlined in chapter III section d (iv), is plotted on the secondary y-axis. The Cu content of each size fraction can be found in Table VIII-11 in appendix D.

The PCBs' copper distribution throughout the six shredding cycles is presented in Figure IV-7 (a-f). The results showed that the copper distribution is directly correlated to the particle size distribution. The liberation of the copper generally occurs at ≤ 2 mm, with PCB particles of larger sizes generally retaining the copper within the layers. As expected, and correlating with the results from the PSD, the copper content was highest in the larger size fractions and smallest in the finer fractions. Overall, copper changes follow the changes in PSD with most copper migration recorded in the coarse (≥ 8000 µm) size fraction and most gain recorded in the intermediate (6700 – 3350 µm) fractions.

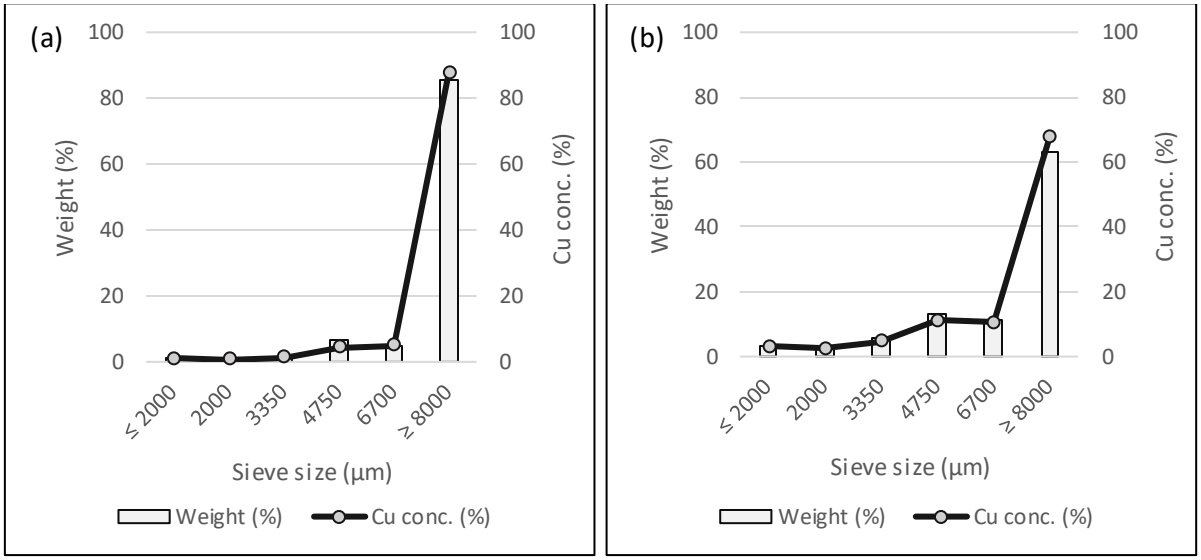

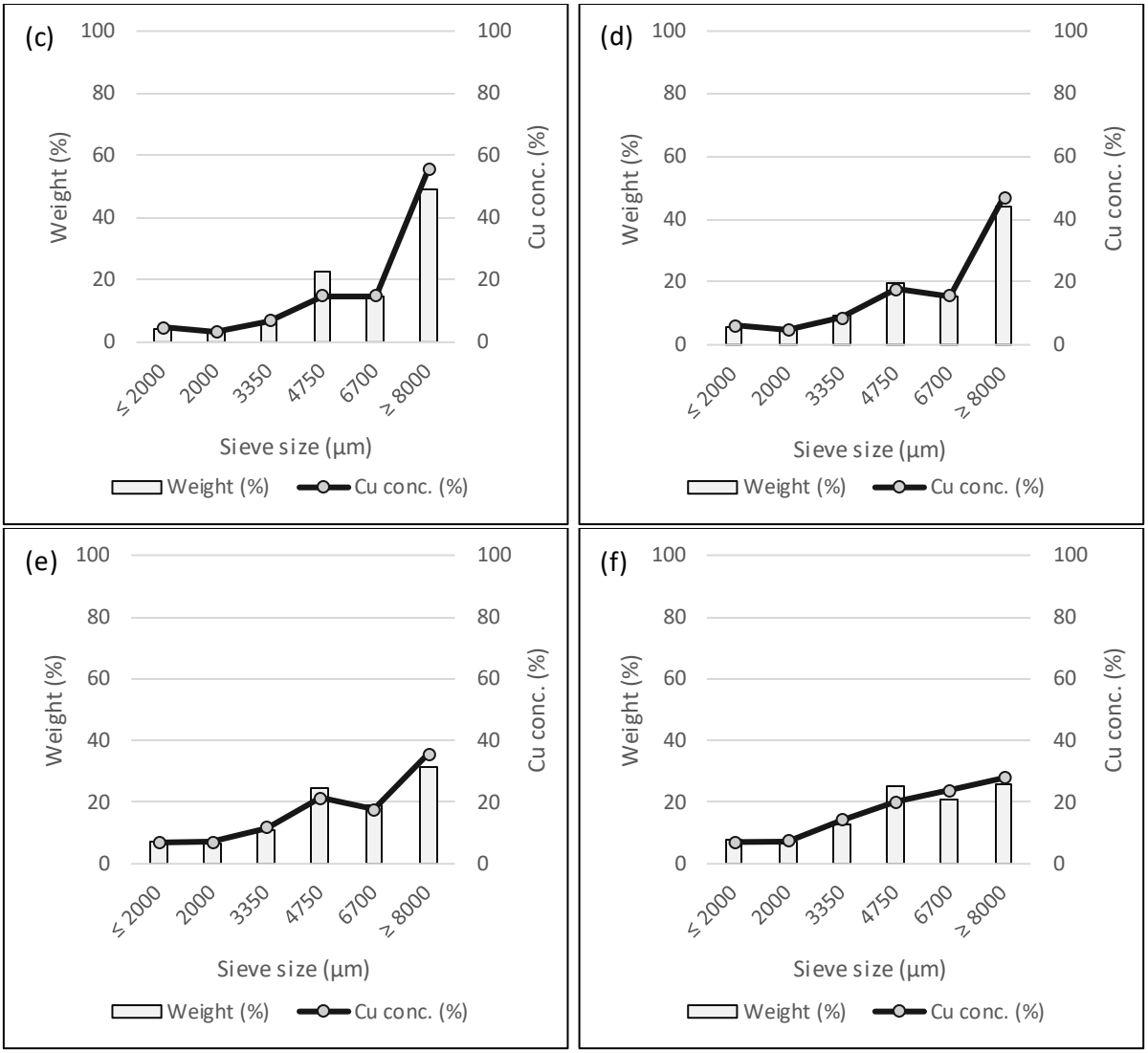

Figure IV-7: Copper concentration and weight percent of custom-made untreated PCBs according to shredding cycle (a) – 1st cycle; (b) – 2nd cycle; (c) – 3rd cycle; (d) – 4th cycle; (e) – 5th cycle; (f) – 6th cycle

Of the total copper content, 24.2 g (88%) were found in the ≥ 8000 µm for the 1st shredding cycle, the remaining 3.34 g were distributed mainly throughout the intermediate size fractions and only minor amounts in the fine fractions. This correlates well with the PSD of the 1st cycle. With the onset of the 2nd cycle, the copper content of the coarse size fraction drops to 18.9 g (68 %), with most of the copper transferred to the intermediate size fractions (16 %). Even though less and less copper is transferred from the coarse size fraction with progressive shredding, the trend was repeated from the 2nd to the 3rd and from the 3rd to the 4th shredding cycles, transferring 12.4 % and 8.6 % of copper to the smaller size fraction, respectively. As with the previous shredding cycles, most of the copper is gained by the intermediate size fractions, (6700 µm and 4750 µm fractions). For the 4th to 5th shredding cycle, 11.4 % more copper was moved from the coarse fraction than for the previous cycles, the main portion of this loss is gained by the intermediate fraction (8.5 %). From the 5th to the 6th cycle a low of 7.8 % of copper was transferred of which 7.4 % is gained yet again by the intermediate fraction and a mere 0.4 % by the fine fraction.

v. Energy consumption

The energy consumption of the individual shredding cycles was measured in order to determine the cost of shredding. This was done by recording the ampere change over time during each shredding cycle. By subsequently implementing the recorded values into eq. (III-1), it was possible to deduce the power consumed by the industrial grab shredder for each individual shredding cycle. These measured power profiles for the individual shredding cycles are displayed in Table VIII-9 in appendix C. As indicated in these Figures, all power profiles start and end at a power consumption of 118.5 W. This is due to the industrial grab shredder idling on an average power of this value. The measurements were taken in triplicates to ensure statistical accuracy and precision.

The individual power profiles were then combined in succession to create a general power consumption profile for the IGS including the required intermediate re-feed times. This power profile is presented in Figure IV-8. As mentioned in chapter III, the re-feed time is characterized as 15 seconds that are required for the shredded material to be removed from beneath the shredder and refed into the shredder.

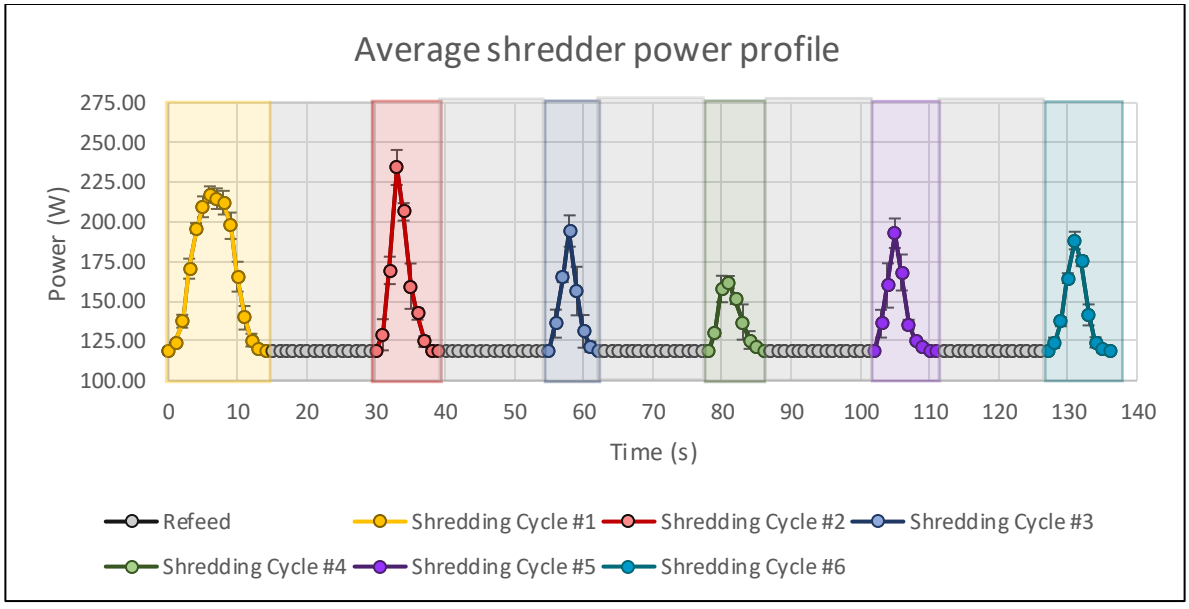

Figure IV-8: Power profile of all shredding cycles in succession including intermediate re-feed times

The energy consumption of the 1st shredding cycles reached a maximum of 221 Watts (W). The 2nd shredding cycle, on the other hand, reached a higher peak consumption average of 234 W. This spike is attributed to the higher number of elongated particles, as seen in Figure IV-4 (a). These elongated particles intertwine each other during this cycle, causing slight blockages in the shredding chamber requiring more energy input from the shredder for a short period of time (± 2 s). The peak consumption of the individual cycles experiences a drop over the following two shredding cycles, sinking to a low of 165 W for the 4th shredding cycle. This can be explained by the fact that the particles become successively smaller and more delamination occurs, requiring

less energy input. Nevertheless, these peak consumptions increase with the 5th and 6th cycles, as an increase in the number of particles causes blockages similar to that of the 2nd shredding cycle.

Furthermore, it must be noted that the shredding time decreases considerably from a maximum of 14 seconds for the 1st cycle, dropping to about six seconds for the 4th cycle. The 1st cycle requires the most time due it being the preliminary size reduction cycle. The time required decreases thereafter as the size of particles progressively decreases. The time required for shredding then increases again to just above eight seconds for both the 5th and 6th shredding cycles. This is the result of particles having reached such small sizes that they actively block the shredder chamber, requiring more time and effort to bring about size reduction and delamination (Figure IV-9).

The 1st shredding stage was also conducted under liquid nitrogen conditions, in which the boards were frozen to temperatures near – 196 °C. The shredding cycle required slightly less time, taking 13 seconds compared to the 14 seconds under normal room temperature conditions, but the total energy required for shredding was slightly higher. The absence of error bars for the Liq. N_2 pre-treated PCBs is the result of all three experiments taking exactly 13 sec each.

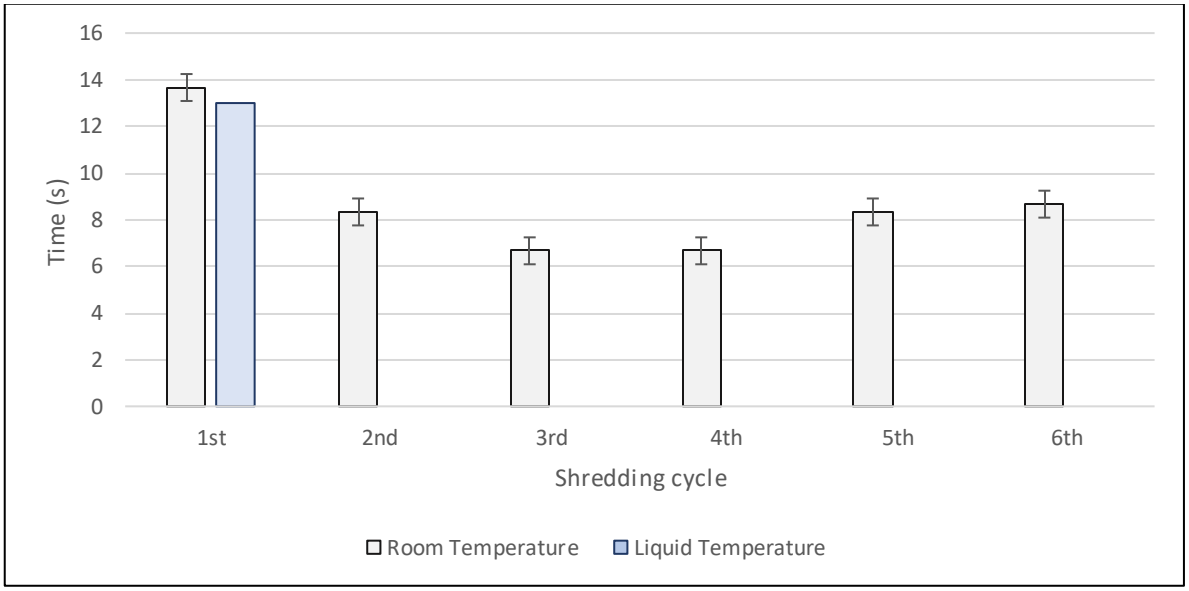

Figure IV-9: Total time required by each individual shredding cycle to be completed at room temperature (25°C) and under liquid nitrogen (-196°C) conditions

To determine the total power consumed by each individual shredding cycle, the area beneath the curve was integrated. The resulting total energy consumption is displayed in Figure IV-10. The data correlates well with the observed data from the individual power profiles tabulated in Table VIII-9, appendix C. The graph displays a decrease in required energy from the 1st to the 4th shredding cycles, after which an increase was recorded for the 5th and 6th cycles.

The high energy of about 2200 J for the 1st cycle was due to this cycle's main purpose being in size reduction rather than copper liberation in the form of delamination. Even though the peak consumption was lower for this cycle than for the 2nd cycle, the time required for completion is about 4 sec longer, therefore consuming more energy. Even though the energy profile peaks

during the second cycle (Figure IV-8), a decrease in energy required of ± 1000 J from the 1st to the 2nd cycle is recorded in Figure IV-10. This is due to the short period that these high energy values are required, minimizing the total energy consumed.

The energy consumed then drops to around 1000 J for the 3rd shredding cycle. This was followed by little change (± 40J) from the 3rd to the 4th shredding cycle's energy consumption. However, a marked energy consumption increase existed from the 4th to the 5th shredding cycles, increasing to about 1240 J. Similar to the increase in power during this cycle (Figure IV-8), the associated total energy increased. This is principally caused by the longer time required for completion of the 5th cycle's smaller particles increase, unlike the 2nd shredding cycle, during which the time required shortened. As with the 3rd to the 4th shredding cycles, only minor changes in energy consumption (± 30 J) from the 5th to the 6th cycles were recorded.

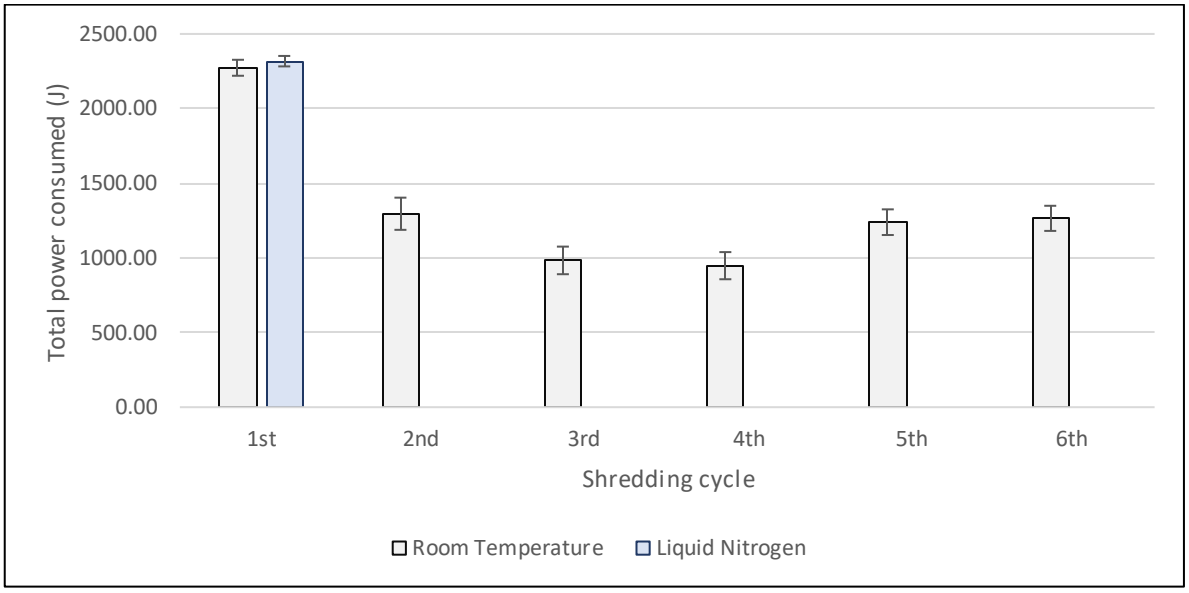

Figure IV-10: Total power consumption of individual shredding cycles at room temperature (25°C) and under liquid nitrogen (-196°C) conditions

vi. Diagnostic Leach Test

Figure IV-12 displays the Cu extraction curves for the untreated custom-made PCBs under alkaline conditions in an ammonia-ammonium carbonate system. This section includes the leaching of PCBs that only underwent the shredding process and no additional processes, termed "untreated" PCBs. The recovered copper was calculated based on eq. VIII-1, adapted from Koyama et al., (2006) as indicated in Appendix B. Appendix B further lists the individual Cu recoveries (g) and Cu recovered (%) according to their respective shredding cycles including their corresponding pH profiles in Tables VIII-1 to VIII-4. A pH level of 10 (± 0.25) was maintained throughout the experiment as outlined in chapter III section v. Due to time limitations, only two shredding cycles (4th and 5th) were repeated in triplicates.

As mentioned in subsection IV-iii, repeated shredding caused progressively finer particles to be created as well as a marked increase in delaminated particles. This indicates that with repeated

shredding, higher degrees of the liberation of the inner copper layers that are tightly laminated within the boards can be achieved. This is supported by the leaching profiles obtained from the diagnostic leach tests (Figure IV-11). With an increase in progressive shredding cycles, more of the inner copper layers were exposed, inferring that progressive shredding resulted in particles that potentially allowed for more lixiviant to access the copper layers and increase subsequent leaching. This however remained to be confirmed as the tightly woven fibreglass layers above the PCBs covered the copper as indicated by Figure IV-11.

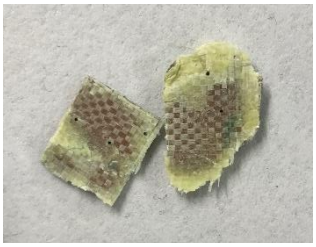

Figure IV-11: Delaminated PCB chips with a fibreglass layer covering the inner copper layer

1. Leaching Results

The Cu recoveries (g) of untreated processed PCBs are presented in Figure IV-12 and listed in Table VIII-4 in appendix B. The 1st shredding cycle had only minor success in terms of copper liberation. It mainly introduced initial size reduction with negligible fines or delaminated particles produced. The leached particles recorded a maximum recovery of 4.20 g of copper after 72 hrs, corresponding to 14.48 % total copper recovery. The results were similar to the ones achieved by Chirume (2019) in whose research the boards were cut into 5 x 5 cm pieces and leached in the identical alkaline system and conditions. Chirume (2019) recorded maximum recoveries of 3.17 g (11.3 %) after 43.75 hrs after which the curve plateaued and no further extraction was recorded. This indicates that shredding PCBs once results in marginally higher extractions compared to cutting off the boards into 5 x 5 cm pieces. These results further support the claim that the 1st shredding cycle primarily introduces initial size reduction with minimal effect on copper liberation.

The copper recoveries from the 2nd shredding cycle were considerably higher than those of the 1st shredding cycle, culminating in maximum recoveries of 4.96 g (17.12 %) after 72 hrs. This indicates that the increase in size reduction that is visible in the PSD (Figure IV-2) from the 1st to the 2nd shredding cycle allowed more lixiviant to reach and extract more metallic copper from the PCBs. As with the previous two cycles, the 3rd shredding cycle favours more size reduction that delamination, promoting higher extraction of Cu due to the higher amount of copper available.

The copper recoveries from the 3rd and 4th shredding cycles display similar trends and the results of the 3rd shredding cycle were within one standard deviation of the 4th shredding cycle. This thereby indicates that the extraction difference is not significant. Both Cu extraction curves recovered similar maximum concentrations of copper after 72 hrs, 5.75 g (19.85 %) and 6.08 g (20.99 %), respectively. Furthermore, as indicated by Table IV-3 and the PSD in Figure IV-2, the 4th

shredding cycle favoured delamination over size reduction and only produced marginally more fines (2000 µm - ≤ 2000 µm). Because the Cu recovery curves fall so closely together, it becomes apparent that delamination did not expose the copper as well as size reduction. The slightly better extraction of copper from the 4th cycle is attributed to the finer particles that were generated and provided copper to the lixiviant for extraction.

With the onset of the 5th shredding cycle, another marked increase in Cu extraction can be noted. The PSD in Figure IV-2 displays a marked decrease in the coarse fraction (12.54 wt%) from the 4th to the 5th shredding cycle, similar to the change in PSD from the 2nd to the 3rd shredding cycles (14.36 wt%). This loss leads to a marked increase in the intermediate and fine fractions, which, in combination with the increase in delaminated particles present as seen in Figure IV-4 (a), explains the increase in Cu recoveries in the earlier stages (7 – 24 hrs) of the leaching curve. Furthermore, the 5th shredding cycle favoured size reduction over delamination, producing considerably more particles than delaminated particles (Table IV-3). This supports the higher ultimate Cu extraction.

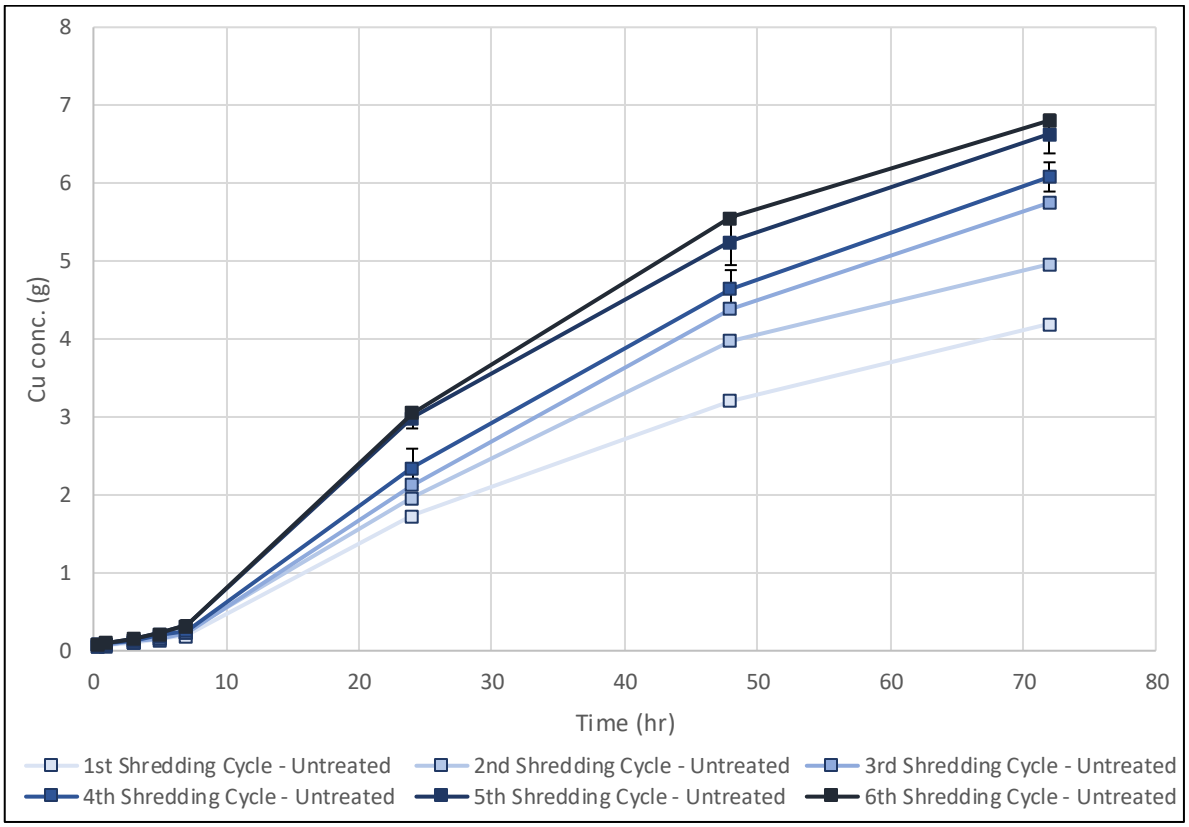

Figure IV-12: Cu concentration profile of untreated PCBs of six shredding cycles

This effect is marginally increased for the 6th shredding cycle recoveries, as only a minor amount is lost by the ≥ 8000 µm size fraction. This cycle, similar to the 4th cycle, also favoured delamination over size reduction, and as a result of this, only generated limited amounts of exposed copper particles. The main copper extraction was achieved from the increased fine particle size (2000 µm - ≤ 2000 µm). For both the 5th and the 6th shredding cycle, similar maximum recoveries of 6.63 g (22.89 %) and 6.80 g (23.49 %) was achieved after 72 hrs, respectively. However, the extracted

copper values of the 6th cycle fall within the error margin of the 5th shredding cycle, suggesting that the increased Cu recoveries are at best marginal.

In general, a marked increase in Cu extractions was noted for shredding cycles that favoured size reduction (1st, 2nd, 3rd, and 5th) over the respective previous cycle. Delamination favoured cycles (4th & 6th) proved to be ineffective in exposing more copper, resulting in the Cu extractions to be within the error margin of the previous cycle. Moreover, as seen in Figure IV-13, leaching of delaminated PCBs proved to be very effective in those cases where the tightly woven fibreglass was removed by the shredding action, exposing the inner copper layers.

Figure IV-13: Leached delaminated PCB chips

2. Reaction rates

All six copper extraction curves start with relatively slow reaction rates for the first 7 hours of the extraction process. These rates range from 0.02 g/hr for the 1st shredding cycle to 0.04 g/hr for the 6th shredding cycle as displayed in Table VIII-8, in appendix B. The slow rate is attributed to the relatively little metallic copper (Cu^0) accessible to the lixiviant for oxidization to Cu^{2+}. This was especially profound for the 1st shredding cycle as this cycle had a limited amount of copper exposed and available for extraction. These rates increased over the following 17 hrs, reaching each individual cycle's maximum rate of reaction up to a maximum of 0.09 g/hr for the 1st cycle and 0.16 g/hr for the 5th and 6th shredding cycles. As expected, the last two cycles show the highest rates because of the largest amount of fine and small particles, providing more Cu^0 to the solution causing oxidation to Cu^{2+}. Because Cu(II) is an oxidizing agent, it promotes the reaction within the system. It, therefore, acts as a catalyst, dissolving increasingly higher amounts of Cu^0.

There is an observed decrease in reaction rates between 24 – 48 hrs, as most of the liberated copper has been extracted by the lixiviant. Only unliberated copper therefore remains, which is more difficult for the lixiviant to access, effectively slowing the reaction rates down. This decrease in reaction rate is worst for the 5th and 6th shredding cycles, slowing down by 0.06 g/hr and 0.07 g/hr, respectively. The first four reactions (1st, 2nd, 3rd and 4th) also slowed down, however, the decrease in reaction rates is slower as for the last two cycles which slowed down on average by 0.02 g/hr. This is because of the previously slower reaction rates, resulting in more Cu^0 still being available for extraction.

For the last measured period (48 – 72 hrs), the reaction rates drop to between 0.04 – 0.06 g/hr, indicating that the reactions are approaching their completion. These lower extraction rates are thought to be the result of both the slow agitation speed in the system as well as the poor

exposure of Cu^0 by the PCB particles. Liberated copper, however, was found to be more limiting to the extraction process than agitation, as seen on Figure IV-14. The Figure also includes the 3rd shredding cycle untreated and NaOH pre-treated PCBs for comparison. Kridiotis & Rogerson (2019) conducted the leach experiment with the same compositional lixiviant, but inside a bottle-roller instead of the overhead batch stirred reactor in this study. The authors achieved considerably faster reaction rates compared to the untreated PCBs but ultimately only recovered marginally more copper after 72 hrs. Three times shredded and NaOH pre-treated PCBs displayed the highest Cu recoveries after the 72 hrs.

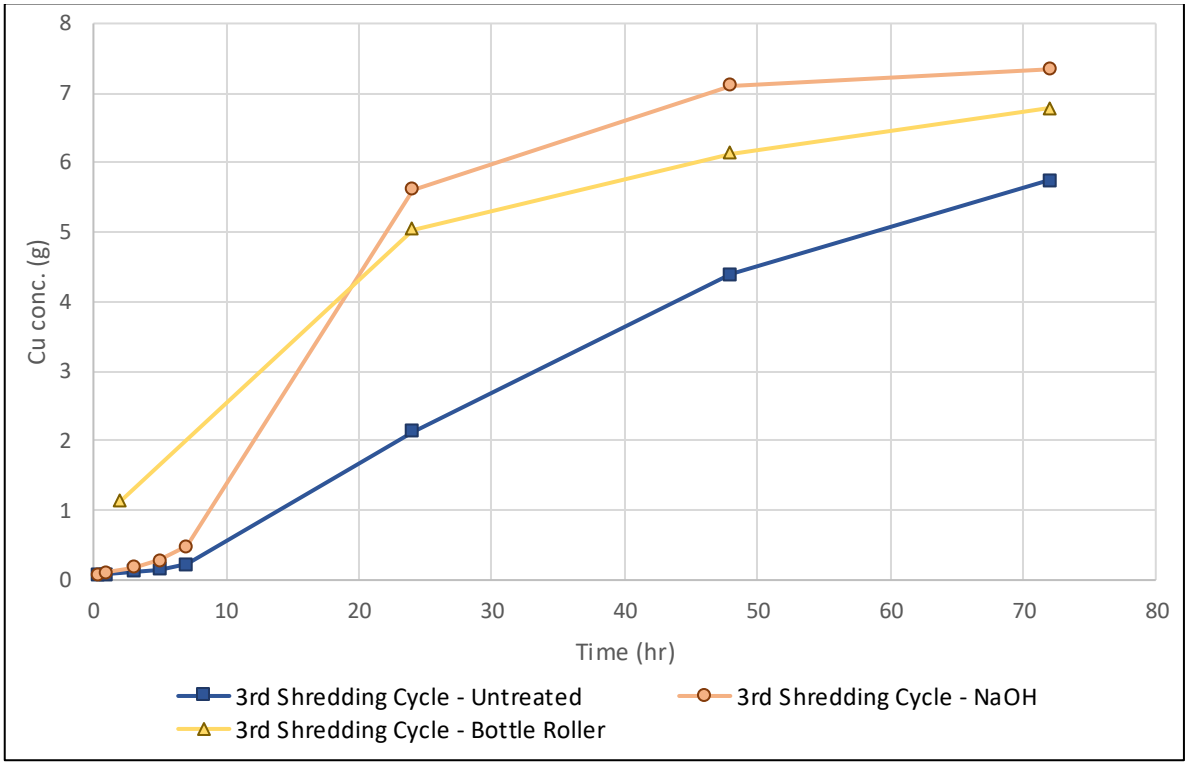

Figure IV-14: Cu concentration profile of 3rd shredding cycle untreated PCB, NaOH pre-treated PCB, and bottle-rolled PCBs

The higher initial Cu recoveries after 2 hrs of the bottle-rolled PCBs is the result of the experiment conducted with an initial 400 ppm Cu concentration instead of the used 100 ppm in the other two experiments. The bottle-rolled extraction achieved only about 1 g additional Cu over 72 hrs compared to the untreated PCBs that also underwent three shredding cycles but ± 0.60 g less than the NaOH pre-treated PCBs. The agitation of the ammoniacal leach system is therefore not a major factor in terms of copper recovery. This is because the size of the PCB chips generated by three shredding cycles still retrain most of the copper underneath the pre-preg, limiting the exposure of metallic copper to the lixiviant, limiting the subsequent effect agitation can have on the extraction process.

b. Planetary Ball Milled PCBs

i. Material Loss

As with the shredding action of the industrial grab shredder, there are also material losses associated with the milling of the PCBs in the PBM. Figure IV-15 compares the material loss from the PCBs that only underwent the respective 2nd and 4th shredding cycles to the PCBs that also underwent the subsequent 60- and 120-min milling. Similar to the shredding action, the losses that are associated with the milling of the boards, are marginal in comparison to the overall mass of the boards. This is primarily because the nature of the PBM is a closed environment with only minimal losses occurring during the transfer of the samples.

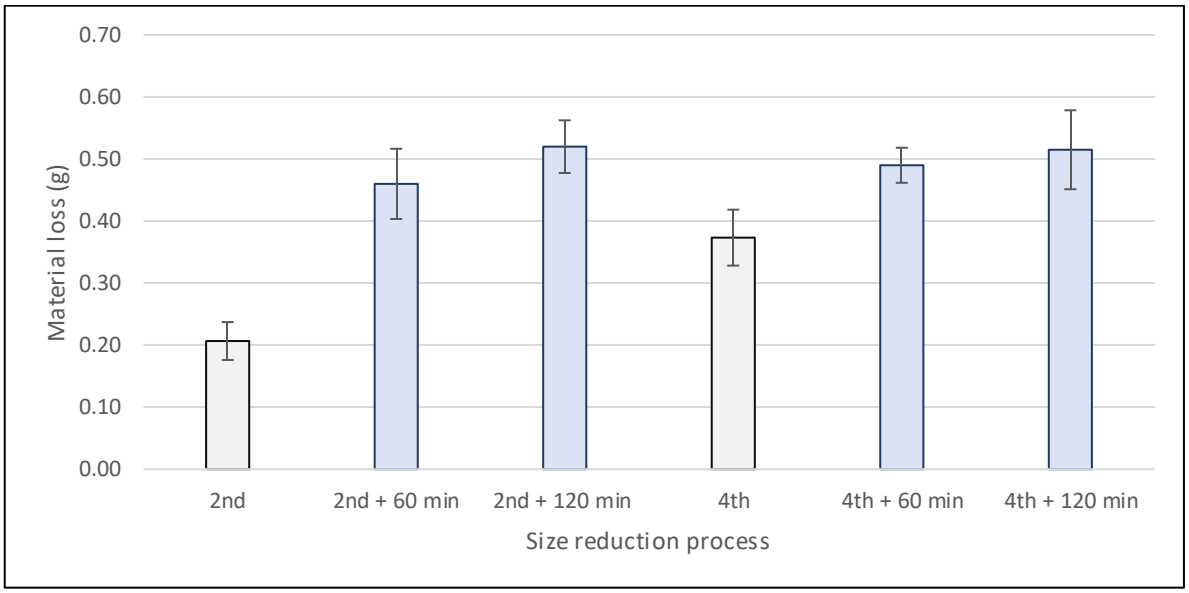

Figure IV-15: Average material loss during milling

It must be noted that the losses from milling are higher than that of the shredding action as indicated by Table VIII-2 in appendix A. However, as indicated by the overlapping error bars in Figure IV-15, the losses between the individual milling times from both investigated shredding cycles are insignificant. As with the shredding cycle, the total loss of material does not exceed more than 0.9 % of the total average weight of one PCB.

ii. Particle Size Distribution

Similar to the PSD of the untreated shredded PCBs, four boards that underwent subsequent milling in the planetary ball mill were also screened to determine the resulting PSD. The resulting PSD is displayed in Figure IV-16, with the untreated PSD of the 2nd and 4th cycle presented as a comparison. Subsequent milling of both shredding cycles had a considerable impact on the produced PSD. Milling times, however, had a greater effect on the particles of the 2nd shredding cycle than it had on the 4th shredding cycle.

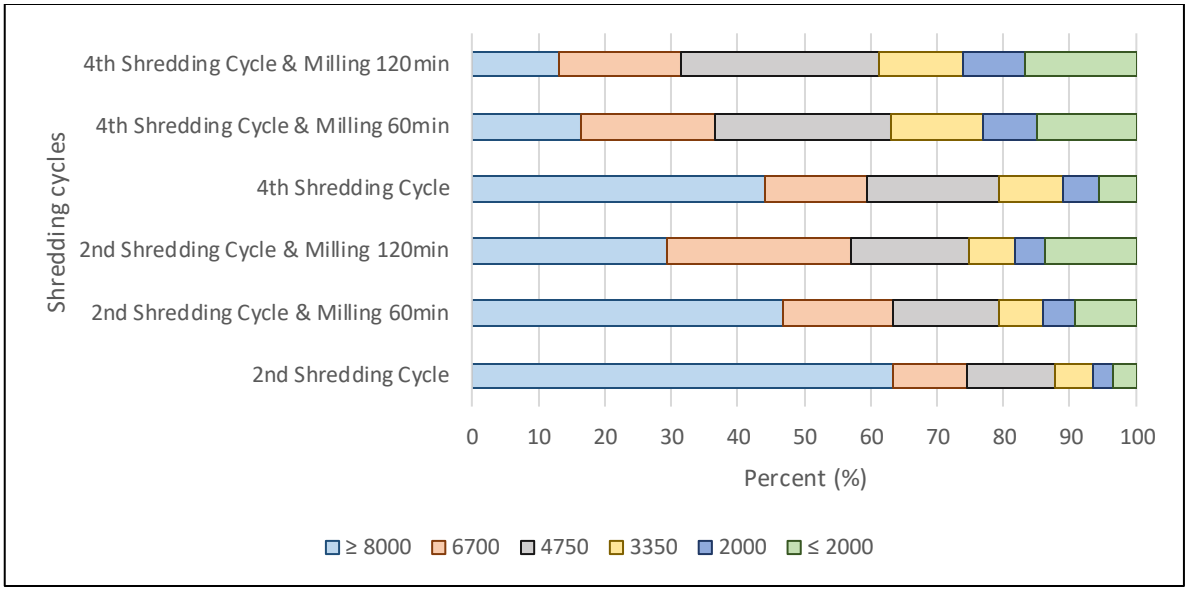

Figure IV-16: Particle size distribution of planetary ball milled PCBs

A distinctive difference in PSD can be observed between the milling of the two shredding cycles. For the 2nd shredding cycle, both milling times had a considerable effect on the PSD, causing the coarse size fraction to lose approximately 33.8 wt% of its mass in each of the milling times. The PSD change from one milling cycle to another is reported in Table IV-4. Negative values represent material loss while positive values indicate material gain for the respective size classes. This mass loss is distributed almost evenly between the two milling times, with intermediate size fraction gaining more throughout both milling times than the fine size fraction. The 4th shredding cycle's particles were more affected by 60 min of milling compared to the 120 min, losing 27.71 wt% and 3.31 wt% of its mass, respectively. Milling the 4th shredding cycle for 120 min results in mostly only fine particles to be generated, inferring that this milling time has a minimal effect on the PSD.

Table IV-4: Change in PSD for milled PCBs

Size classes	2nd cycle to 2nd cycle + 60 min	2nd cycle + 60 min to 2nd cycle + 120 min	4th cycle to 4th cycle + 60 min	4th cycle + 60 min to 4th cycle + 120 min
Coarse	-16.42	-17.33	-27.71	-3.31
Intermediate	8.89	12.89	15.55	0.55
Fine	7.53	4.45	12.17	2.76

iii. Copper Distribution

Planetary ball milling of the boards had a slightly different effect on the copper distribution than progressive shredding as indicated by Figure IV-17. Unlike progressive shredding where most of the copper was transferred by the coarse size fraction to the intermediate size classes, milling resulted in more Cu gain in the fine size fraction. This was primarily because of the impact nature of the PBM, grinding along the edges of the particles generating fine dust.

Milling of PCBs for 60 min that were shredded twice resulted in 8.8 % less copper in the coarse size fraction compared to PCBs that were shredded three times and a further 15.9 % was lost by milling the boards for 120 min. Most of this copper was gained by the ≤ 2000 µm and the 6700 µm size class, with minor changes in the other size classes. The material milled coming from the 4th shredding cycle again displayed a slightly different distribution. Milling for 60 min resulted in 17.7 % Cu loss from the coarse size fraction, of which 13 % was gained by the fine size fraction. Subsequent further milling of the PCBs for another 60 min (120 min total) only resulted in minor changes. The coarse size fraction lost 4 % of which 3.5 % was gained again by the fine size fraction.

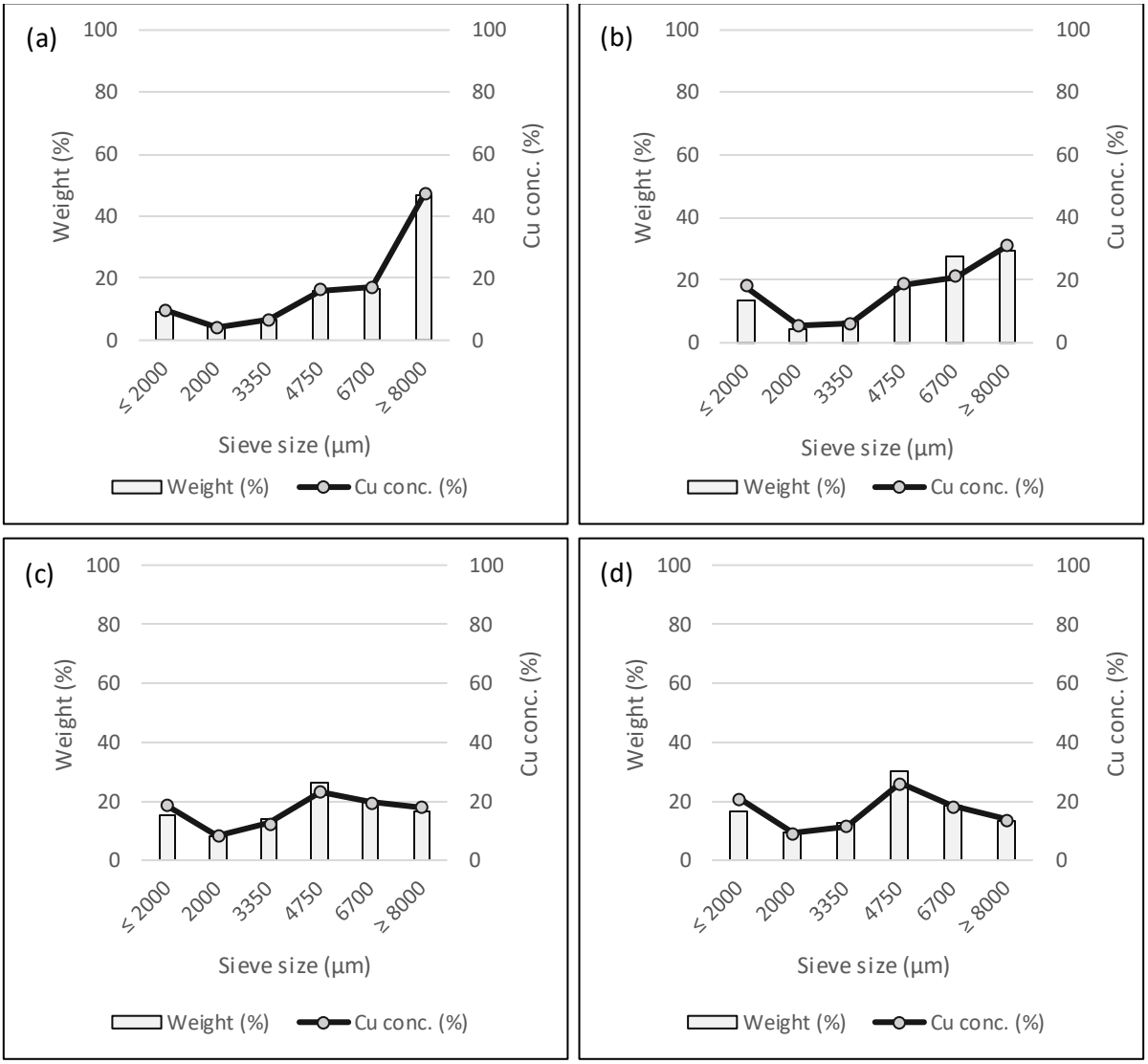

Figure IV-17: Copper concentration (g) and custom-made PCB weight % (a) – 2nd Shredding Cycle & 60 min milling; (b) – 2nd Shredding Cycle & 120 min milling; (c) – 4th Shredding Cycle & 60 min milling; (d) – 4th Shredding Cycle & 120 min milling

iv. Energy Consumption

Unlike the IGS, which ran for a short maximum period (± 2.5 min) to reduce the boards in size, the PBM ran for a considerably longer time period of up to 120 min. However, as opposed to the energy consumed by the IGS, the PBM drew considerably less power. Figure IV-18 displays this difference in power (J) and energy (kWh) required by the respective size reduction process.

Even though the power consumption for the 60- and 120-min milling times were relatively low, 93 W and 186 W, respectively, the long milling times resulted in total energy consumption considerably higher than those of the IGS. The IGS, as stated earlier, had a high-power consumption, but the shredding time is substantially shorter (on average ± 8.7 sec/cycle), thereby lowering the energy consumption.

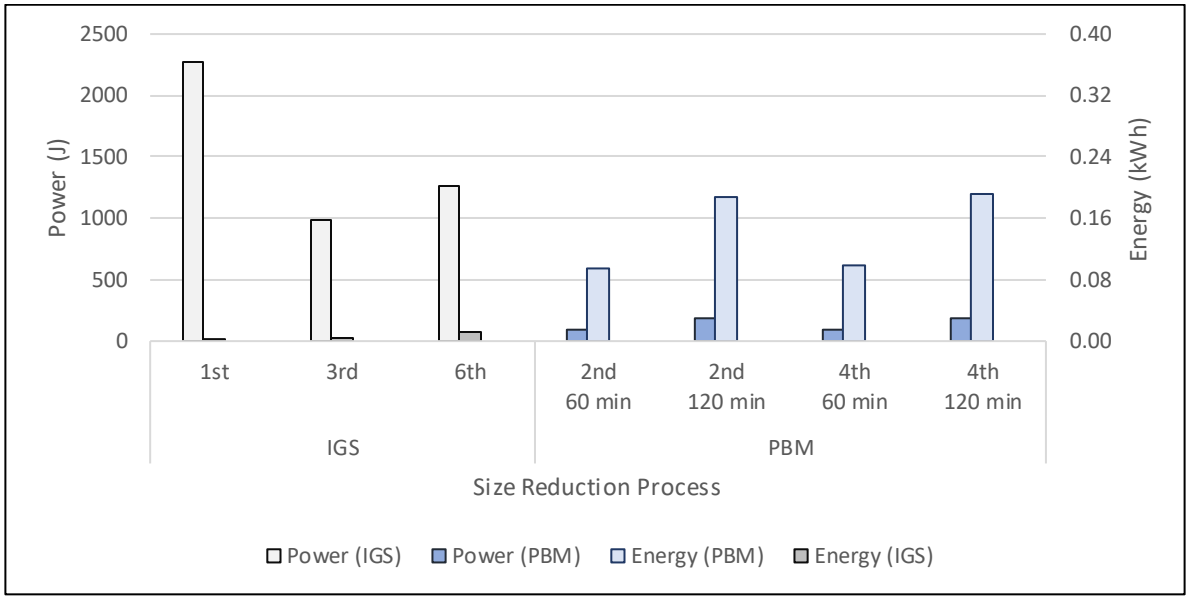

Figure IV-18: Power and Energy consumption of the IGS and PBM

v. Diagnostic Leach Test

The PCBs analysed for copper recoveries in this subsection were shredded as well as milled in the PBM. According to Hanafi et al., (2012), due to the high strength and resistance to the impact of the boards, higher milling times were recommended. Simple milling tests were then conducted in this research to determine the effect planetary ball milling had on the PCBs. It was found that significant size reduction was only achieved after prolonged milling. Therefore, 60 minutes, as well as 120 minutes, were chosen as milling times for the respective shredding cycles.

Two shredding cycles, as well as two milling times, were analysed to determine whether milling of shredded boards would have an impact on the copper liberation. For the comparison of shredding cycles, the 2nd, as well as the 4th cycles, were chosen. The 2nd cycle was chosen as it represents a cycle with minor delamination and larger particle sizes. The generated particles by the 4th shredding cycle, on the other hand, contained a higher number of delaminated and finer

particles. The impact the PBM then had on these two shredding cycles in terms of milling effect and ultimate copper extraction was analysed in this section.

1. Leach results

All planetary ball milled PCBs showed similar leaching trends with little deviation from one another (Figure IV-19 and Table VIII-6 in appendix B). All four milled boards recovered ± 2.40 g of Cu after 48 hrs, with the 4th shredding cycle milled boards marginally outperforming the 2nd cycle boards. This however changed after 72 hrs, with PCBs from both the 2nd and 4th shredding cycles that were milled for 60 min recovered higher concentrations of Cu, 3.70 g (12.79 %) and 3.85 g (13.29 %) respectively, than the PCBs that were milled for 120 min. However, it must be noted that the extraction values are extremely similar, differing by not more than 0.20 g. If the error margins from the previous experiments are of any indication, it would infer that the results of the respective shredding cycles would fall within one standard deviation, inferring negligible differences in Cu recoveries throughout the entire leach process.

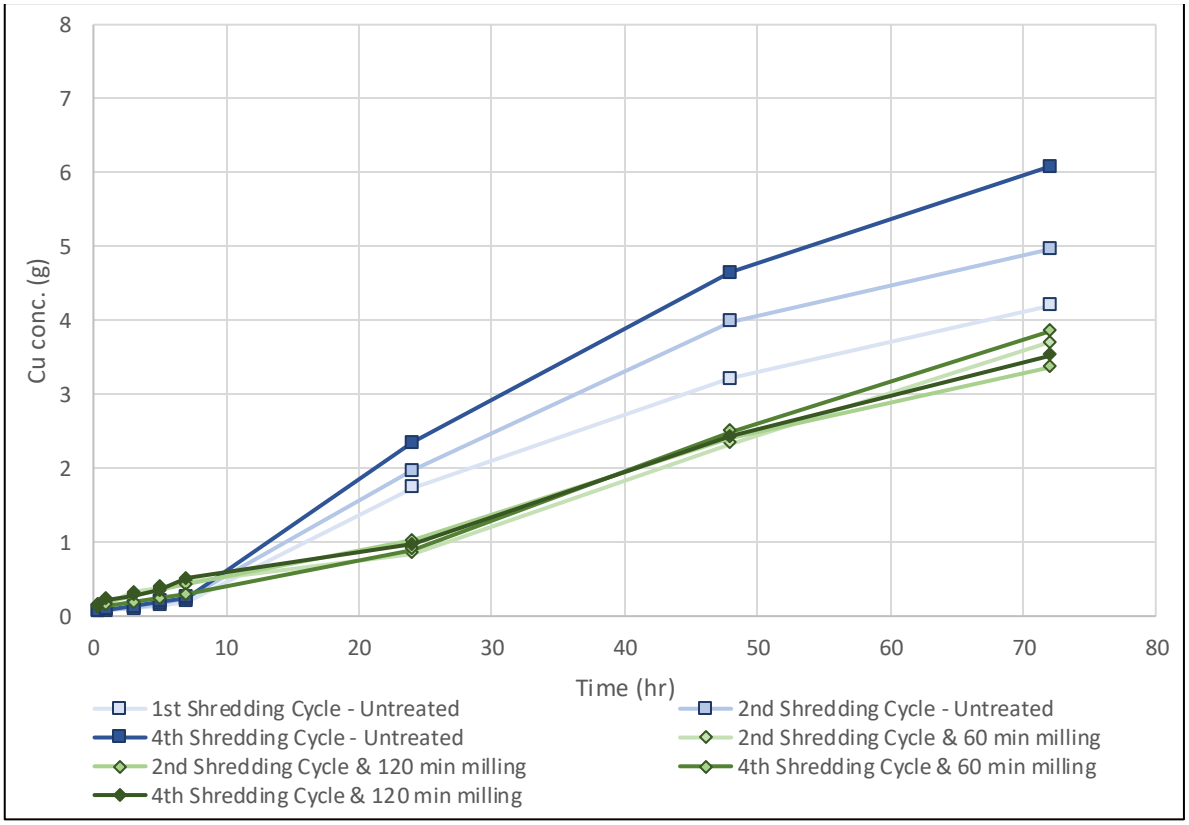

Figure IV-19: Cu concentration profile of shredded and subsequently ball milled PCBs

The Cu recovery graph in Figure IV-21 also displays the copper recoveries of the untreated PCBs that were shredded in the IGS once, four and six times. The untreated PCBs that were shredded once already outperformed the PBM milled boards in terms of copper recoveries. The untreated PCBs that underwent the 2nd and 4th shredding cycles achieved total Cu recoveries of 5.0 g and

6.1 g after 72 hrs, respectively. These recoveries are considerably higher than the average Cu recoveries (± 3.6 g) of the PBM milled PCBs after 72 hrs. In general, the PBM size reduced PCB only achieved higher recoveries during the initial 7 hrs. This can be related to the fine copper particles generated during the milling process, leaching quicker than the untreated PCBs.

However, during the milling process, fine plastic and fibreglass particles are also generated, which after the initial 7 hrs began to settle down on the bottom of the reactor on top of the larger PCB chips. The settling of the fine particles was mainly due to the slow agitation speed, not being able to hold the particles in suspension for the entire leach process. Figure IV-20 (a & b) visually show the settling of the fines after 48 and 72 hrs of the 4th shredding cycle, respectively. This resulted in an effective diffusion barrier, limiting the access of the lixiviant to those PCB chips, achieving poor Cu recoveries.

This also explains why the PCBs that were milled for 120 min performed worse in the long run than the ones that were milled for only 60 min, irrespective of the prior shredding cycles. Because the main constituent of the PCBs is the pre-preg and less the copper, prolonged milling preferentially generates finer plastic particles that inhibit the extraction of copper for longer periods of time.

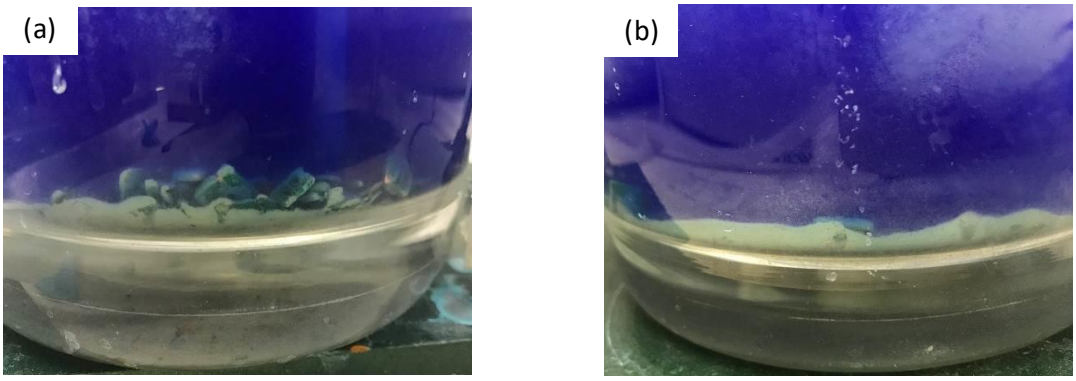

Figure IV-20: Planetary ball milled organic and inorganic material settling on the reactor floor after (a) 48 hrs and (b) 72 hrs respectively (4th shredding cycle and 120 min)

2. Reaction rates

The 4th shredding cycle and subsequent milling for 60 min resulted in a rate of reaction of 0.04 g/hr of copper for the early extraction phase (0 – 7 hrs). A slightly faster reaction rate was determined for the first seven hours (0.03 g/hr) if the boards underwent two shredding cycles and were milled for 60 min and 0.05 g/hr when milled for 120 min. The same extraction rate was recorded for the 4th shredding cycle and 120 min of milling with a rate of extraction of 0.05 g/hr. Regardless of the prior shredding cycles or the milling times, the PBM processed PCBs performed better than the untreated PCBs which displayed reaction rates of between 0.02 to 0.04 g/hr with increasing shredding cycles. This reflects the high efficiency of the leaching of the fine copper particles that was kept in suspension as indicated in Figure IV-21 (b).

However, unlike the untreated PCBs which displayed an increase in the reaction rates (0.09 – 0.16 g/hr), all of the PBM processed boards' rates decreased slightly by about 0.01 g/hr. This was the direct result of particle settling on the reactor floor, inhibiting faster Cu extractions. Moreover, the PBM milled PCBs' rate of reactions started to increase after the 24 hrs mark, reaching the its fastest rates after 72 hrs (0.05 g/hr). This contrasted with the untreated PCBs, which rates were decreasing after the 24 hrs mark to also 0.05 g/hr. It can be argued that the untreated PCBs had extracted most of the free available copper from the larger PCB chips, whereas the lixiviant in the PBM processed PCBs system were only reaching those chips now, effectively promoting Cu extraction.

Figure IV-21: Visual difference between generated untreated and PBM treated PCBs (a) Untreated 3rd shredding cycle; (b) 3rd shredding cycle, 120 min PBM milled

c. Pre- and Post-treated PCBs

This section included the analysis of three pre-and post-treated PCBs. Two pre-treatments were investigated, including the process recommended by Chirume (2018) solder mask removal by placing the PCBs in an 8 M NaOH solution and then shredding the boards up to six times. The other pre-treatment involved cooling the boards down in Liquid Nitrogen (Liq. N_2) to approximately -196 °C prior to shredding the PCBs once. Post shredding treatment involved the pulverization of the boards following the 1st shredding cycle.

i. Material Loss

Because the NaOH pre-treated PCBs underwent the same shredding cycles as the untreated processed PCBs, their material loss was measured and eventually found to be equal to that of the untreated PCBs. As indicated by the column graph in Figure IV-22, which displays boards that underwent the 1st, 3rd and 6th shredding cycles as comparisons, the material loss of the Liq. N_2 pre-treated PCBs is similar to that if the untreated 1st cycle processed PCBs. Of all treatments investigated, the pulverised PCBs recorded the highest material loss (± 1.12 g). The high error margin of the pulverised PCBs is due to the highly varying losses associated with the ring mill, as this comminution tool tends to retain considerable amounts on the equipment itself. In appendix A, the material losses of the pulverised and Liq.N_2 pre-treated PCBs are tabulated in Table VIII-3.

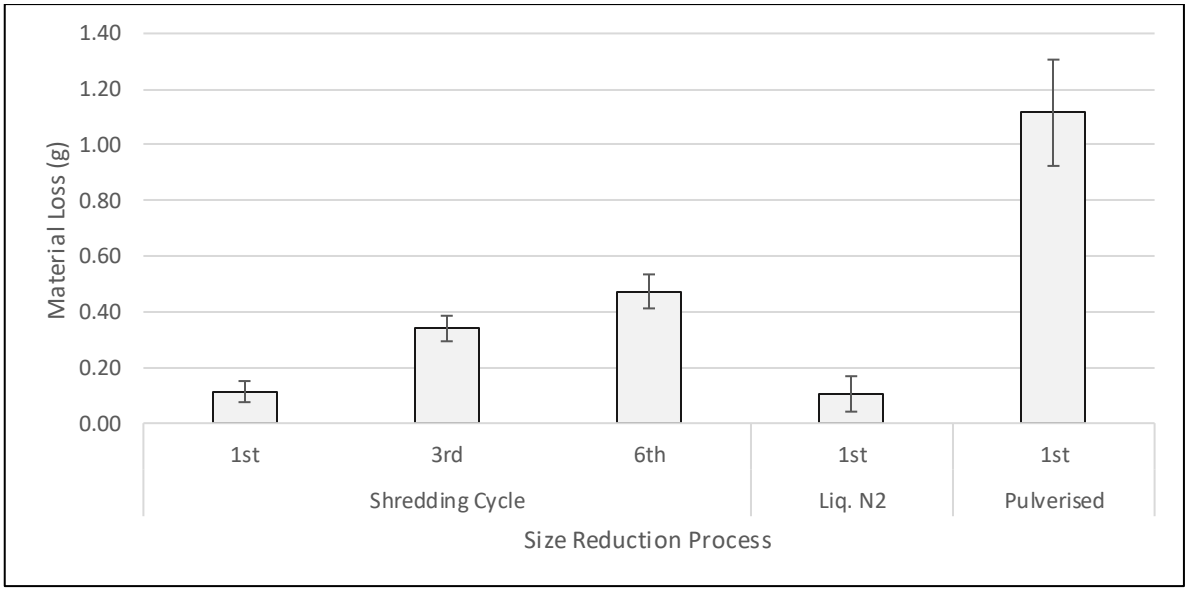

Figure IV-22: Material loss of shredded, Liq. N_2 pre-treated and pulverised PCBs

ii. Particle Size Distribution

The NaOH pre-treated PCBs followed the same shredding and screening process as the untreated PCBs and therefore follow the same OSD. The Pulverised PCB was milled for 3 min until the entire sample passed ≤ 1000 µm. The particle size distribution for the Liq. N2 pre-treated PCBs are depicted in Figure IV-2, chapter IV. From the Figure, it becomes apparent that the cooling of the

boards results in the presence of more particles in the coarse (≥ 8000 µm) size fraction (6.64 wt%) compared to PCBs that were shredded once at room temperature. This larger mass present in the coarse size fraction consequently causes the number of particles in the intermediate and fine size fractions to be lower, 6.33 wt% and 0.31 wt%, respectively.

iii. Energy Consumption

Again, as with the PSD, the energy consumption for the NaOH pre-treated PCBs was the same as with the untreated PCBs. As expected, the power consumed by the Liq. N_2 pre-treated PCBs are similar to that of the untreated and NaOH pre-treated PCBs with only minor neglecTable deviations from one another (Figure IV-23). This also directly translates and therefore applies to the total energy required, which is tabulated in Table VIII-10 in appendix C. The power for the pulverization process on the other hand, even though it drew similar amounts of energy, required approximately 3 min until complete size reduction was achieved. This resulted in higher energy consumptions (± 0.13 kWh) that are about 10-fold as much as the 6th shredding cycle (± 0.013 kWh).

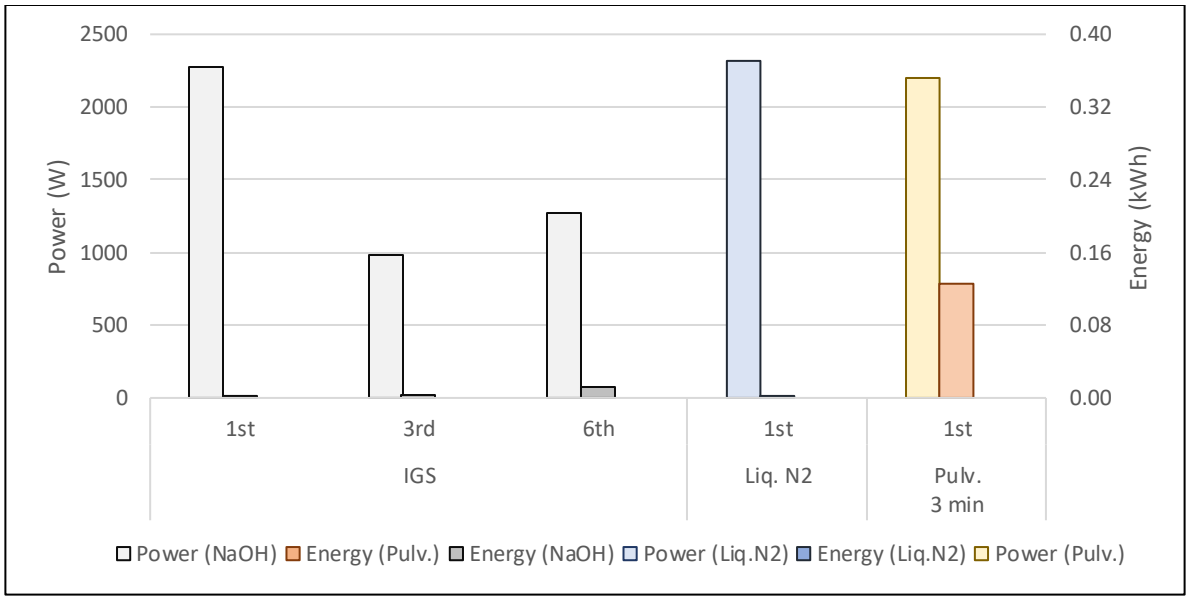

Figure IV-23: Power and energy consumption of NaOH, Liq. N2 and Pulverised PCBs

iv. Diagnostic Leach Test

The leach results for the NaOH pre-treated PCBs are presented in their own subsection due to the large number of parameters analysed. The Liq. N2 pre-treated and the post-shredding pulverised PCBs' results, on the other hand, are presented in the same subsection and compared to the 1st shredding cycles of the untreated and NaOH pre-treated PCBs to visually display the difference in leach kinetics.

1. NaOH Pre-treated PCBs

As mentioned in chapter II, printed circuit boards are generally covered with a solder mask to protect the upper- and lower-most copper layers from abrasion as well as oxidation. As indicated by Figure IV-11, this mask strongly inhibits the extraction of copper from those uppermost layers. As suggested by Adhapure et al., (2014) and Jadhav & Hocheng (2015) removal of the solder mask by soaking the boards in 10 M NaOH will effectively expose copper layers 1 and 4 (Figure III-14).

For this research, the methodology from Adhapure et al., (2014) was adapted but slightly changed by decreasing of the concentration of the NaOH solution from 10 M to 8 M. The shredding process remained the same as with the untreated PCBs, with a total of six shredding cycles analysed. Prior to the shredding process, the boards were soaked for 24 hrs in the 8 M solution at room temperature (25°C), successfully removing the solder mask as seen in Figures IV-24 (b & d).

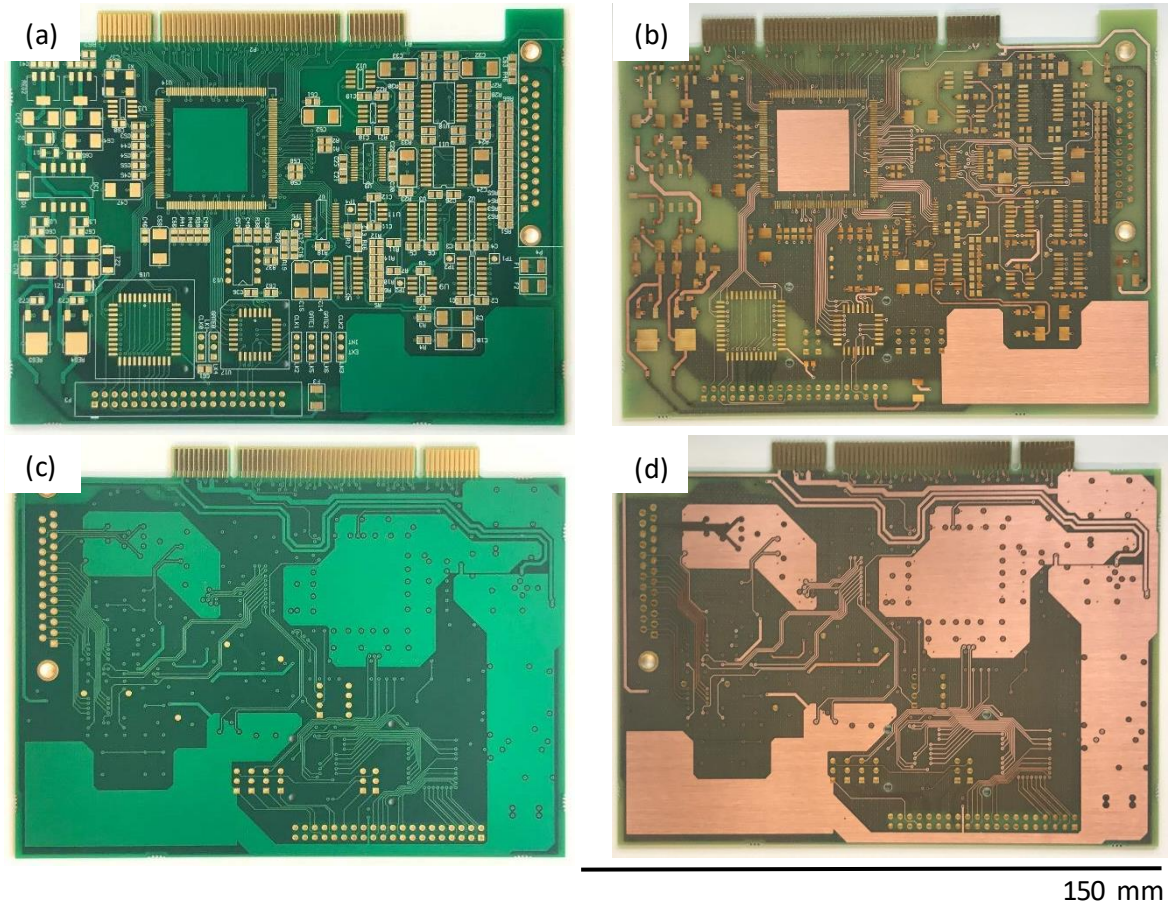

Figure IV-24: Untreated and NaOH pre-treated PCBs (a) – Top side of the original PCB with solder mask present; (b) – Topside of NaOH pre-treated PCB with solder masked removed; (c) – Bottom side of the original PCB with solder mask present; (d) – Bottom side of NaOH pre-treated PCB with solder masked removed

a. Leach results

Similar to the results from the leached untreated PCBs, the 1st shredding cycle mainly acted as a size reduction tool rather than aid copper liberation. However, because of the now exposed upper- and lowermost copper layers 1 & 4, the Cu recoveries are considerably higher for the later stages of the leaching experiment (24 - 72 hrs) as indicated by Figure IV-25. Table VIII-5 in appendix B lists the leach results. Compared to the untreated PCBs which recovered a maximum of 4.20 g (14.48 %) after 72 hrs (after shredding once), the NaOH pre-treated 1st shredding cycle achieved a maximum extraction of 6.58 g (22.70 %) over the same time period. This recovery is also higher than the 6.44 g (22.23 %) recovered by Chirume (2019) where the boards were soaked in a 2 M NaOH bath at 40 °C for 24 hrs after being cut into 5 x 5 cm squares. Chirume (2019) however reached higher Cu concentrations of 7.29 g (25.16 %) by drilling five holes into each of the 25 cm^2 squares, allowing lixiviant to enter and access the inner layers of the PCBs. This, therefore, needs to be considered when comparing the respective results.

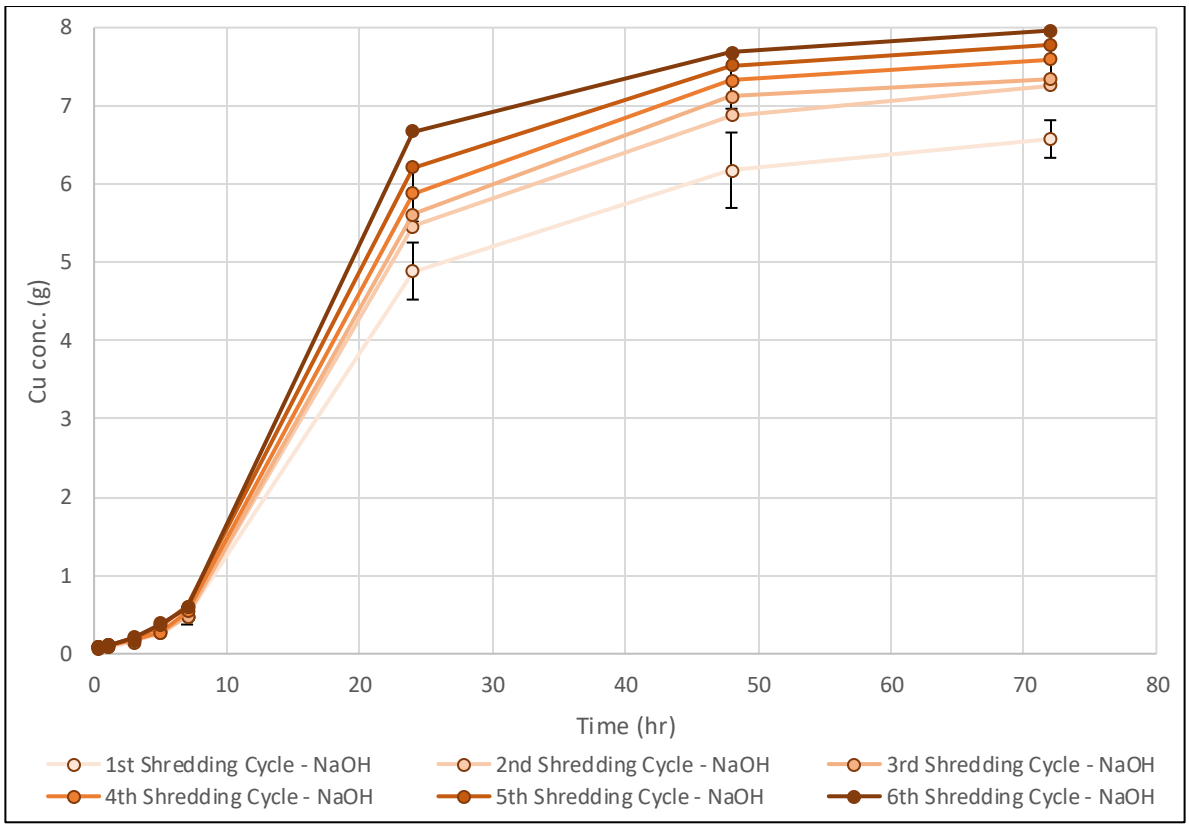

Figure IV-25: Cu concentration profile of NaOH pre-treated PCBs of six shredding cycles

The 2nd shredding cycle shows an increase in extractions for all samples compared to the 1st shredding cycle. Reaching a maximum Cu extraction of 7.26 g (25.04 %) after 72 hrs, the extractions are about 8 % higher after 72 hrs compared to untreated leached PCBs. This increase in Cu leaching is attributed exclusively to the exposed layers 1 & 4. The Cu extractions fall outside of the error bars of the 1st and 4th shredding cycle, indicating that the achieved Cu concentrations are significantly higher and lower than for the 1st and 4th cycles, respectively. As with the

untreated PCBs, the increase in Cu recoveries over the 1st shredding cycle is associated with the major increase in particle delamination but mainly due to the size reduction.

The 3rd and 5th shredding cycles fall within one standard deviation of the 4th shredding cycle, inferring that the increase in Cu recoveries for the individual shredding cycles are not significant. Nonetheless, the increase in Cu extractions of the three cycles over the 1st and 2nd cycles indicate that particle size decrease and delamination continue to play a major role in the liberation of copper from the inner two copper layers 2 &3. The maximum recoveries range from 7.34 g (25.34 %) for the 3rd shredding cycle to 7.78 g (26.86 %) for the 5th cycle, which is about 4.5 % more copper recovered from NaOH pre-treated boards compared to untreated leached boards.

A marked spike can be observed for the 6th and final shredding cycle, falling outside of the error bars of the 4th shredding cycle. Even though this cycle reaches a maximum copper extraction of nearly 8 g (27.49 %), it only achieves approximately 4 % higher recoveries than the untreated board's 6th shredding cycle.

Throughout the progressive leach recoveries of the respective shredding cycles, it became apparent that with an increase in the number of shredding cycles, the difference between the Cu extractions of the NaOH pre-treated and the untreated boards decreased systematically. For the first two shredding cycles, the difference in maximum Cu extraction between the NaOH pre-treated and the untreated boards was about 8 %. This difference decreased to approximately 5 % for 3rd and 4th cycles and eventually to 4 % for the 5th and 6th cycles. This decrease indicates that the exposure of the upper- and lowermost copper layers in the NaOH pre-treated boards play a greater role in copper extraction for a lower number of shredding cycles, exposing more metallic copper to the lixiviant for oxidation. Size reduction, on the other hand, has a greater influence on the Cu extraction on the leaching kinetics on the higher numbers shredding cycles. This is supported by the copper distribution determined by Chirume (2018), in which it is stated that the inner layers contain 69 % of the total copper content whereas the outer layers only make up 29 % of the total copper, with the remaining 2 % being allocated to Cu coatings of holes in the PCBs. Progressive shredding, therefore, liberates more of the copper stuck within the inner layers of the PCBs by means of size reduction.

b. Reaction rates

Overall, the reaction rates of the NaOH pre-treated PCBs occurred at a faster rate than those of the untreated PCBs or any other pre- or post-treated PCBs. The reaction rates for the initial phase (0 - 7 hrs) increased with the progressive shredding cycles, starting from a rate of 0.06 g/hr for the 1st, 2nd and 3rd shredding cycles over 0.07 g/hr for the 4th cycle to the highest rate of 0.08 g/hr for the last two cycles. The increase over the cycles is attributed to an increased number of finer particles as well as an increased number of delaminated particles generated by progressive shredding. Figure VIII-8 in appendix B displays these reaction rates.

As with the untreated PCBs, the highest extraction rate is recorded for the intermediate phase of the leaching process, from 7 – 24 hrs. However, the increase in the reaction rates for the NaOH pre-treated PCBs was more than double as for the untreated PCBs, attributed to the exposed copper layers, exposing more copper to the lixiviant for oxidation. Moreover, as stated by Koyama

et al., (2006), an increase in available Cu^0 results in higher Cu^{2+} generation, which in turn reacts with free ammonia in solution forming the $Cu(NH_3)_4^{2+}$. This compound acts as a catalyst, further driving the reaction and thereby amplifying the increase in reaction rates for the 7 – 24 hrs period. During this period, as with the untreated PCBs, there is a considerable increase in the rates of reactions with progressive shredding cycles, a direct result of more inner copper layers available for reaction.

A decrease in the rates of reactions for the final two leach periods from 24 – 48 hrs and 48 – 72 hrs is in coherence with the observed results from the untreated leached PCBs, dropping to on average 0.06 g/hr and 0.01 g/hr, respectively. As with the untreated PCBs, this is the result of limited copper available for extraction due to it being stuck within larger PCB particles. The NaOH pre-treated boards' reaction rates declined more compared to the untreated PCBs, as most of the available copper was extracted from the PCB chips. This indicates that the extraction process was close to completion after 72 hrs.

2. Liq. N_2 and Pulverised PCBs

A further aspect briefly investigated was the effect of cooling the boards down to -196 °C in Liq N_2 as well as completely pulveris

ing the boards has on copper liberation and eventual recovery. Both parameters were tested based on the 1st shredding cycle only. This was done for the pulverised boards primarily because this size reduction was sufficient for the PCBs to fit into the Pulveriser and to minimize further material loss during the shredding stages. Regarding the cooling of the PCBs in Liq. N_2, the PCBs only underwent the 1st shredding cycle because of the uncertainty of temperature increase.

The Liq. N_2 pre-treated PCBs temperature increase from -196 °C was determined by measuring the increase over time by attaching T-type thermocouples to four different areas of the PCBs. The results are displayed in Figure IV-26 and measurement procedure is outlined in section III-2. However, this does not include any potential change in temperature that may arise from thermal energy generated during the shredding process. The boards were therefore only shredded once.

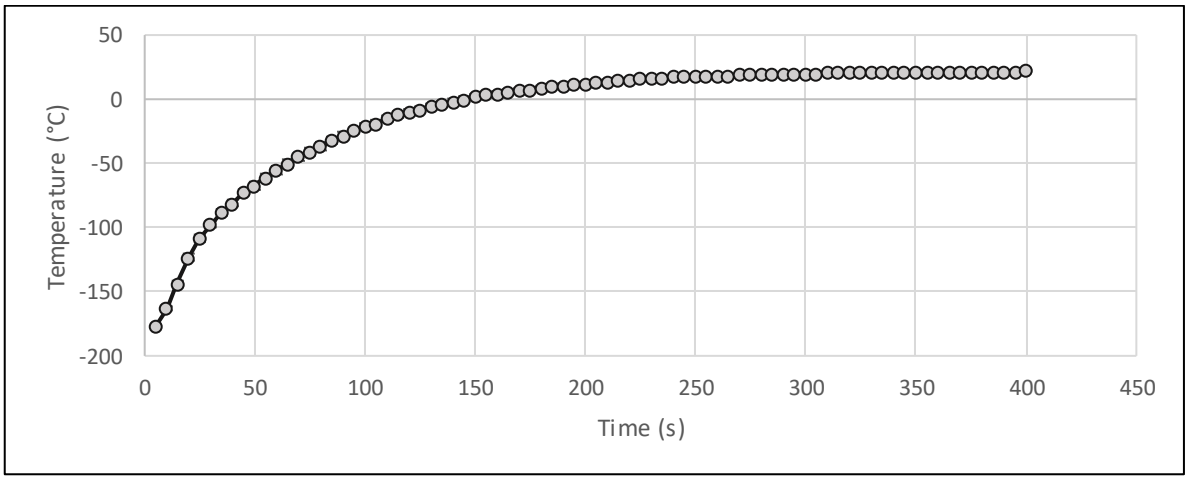

Figure IV-26: Liquid Nitrogen frozen PCBs temperature change of PCBs over time

The rate of temperature increase occurred rapidly for the first 30 sec. Even before the first measurement was taken after the PCBs were removed from the Liq. N_2 bath and the thermocouples were attached, the temperature had already risen from -196 °C to -176 °C in the span of approximately 10 sec. The rate of temperature change initially increased for all four areas from -196 °C until -123 °C and then began to slow down. The 1st shredding cycle on average took 14 sec to complete, indicating that the PCBs would have warmed up from -176 °C to -143 °C, neglecting thermal energy and incorporating 10 seconds for the referral time from Liq. N_2 bath to the IGS.

a. Leach results

Figure IV-27 compares several 1st shredding cycles investigated, including the 1st cycles for untreated boards, NaOH pre-treated, Liq N_2 pre-treated, and pulverised PCBs. Boards pre-treated in Liq N_2 displayed the lowest leach kinetics of the four 1st shredding cycles. Table VIII-7 in appendix B lists the results of the Liq.N_2 and pulverised samples.

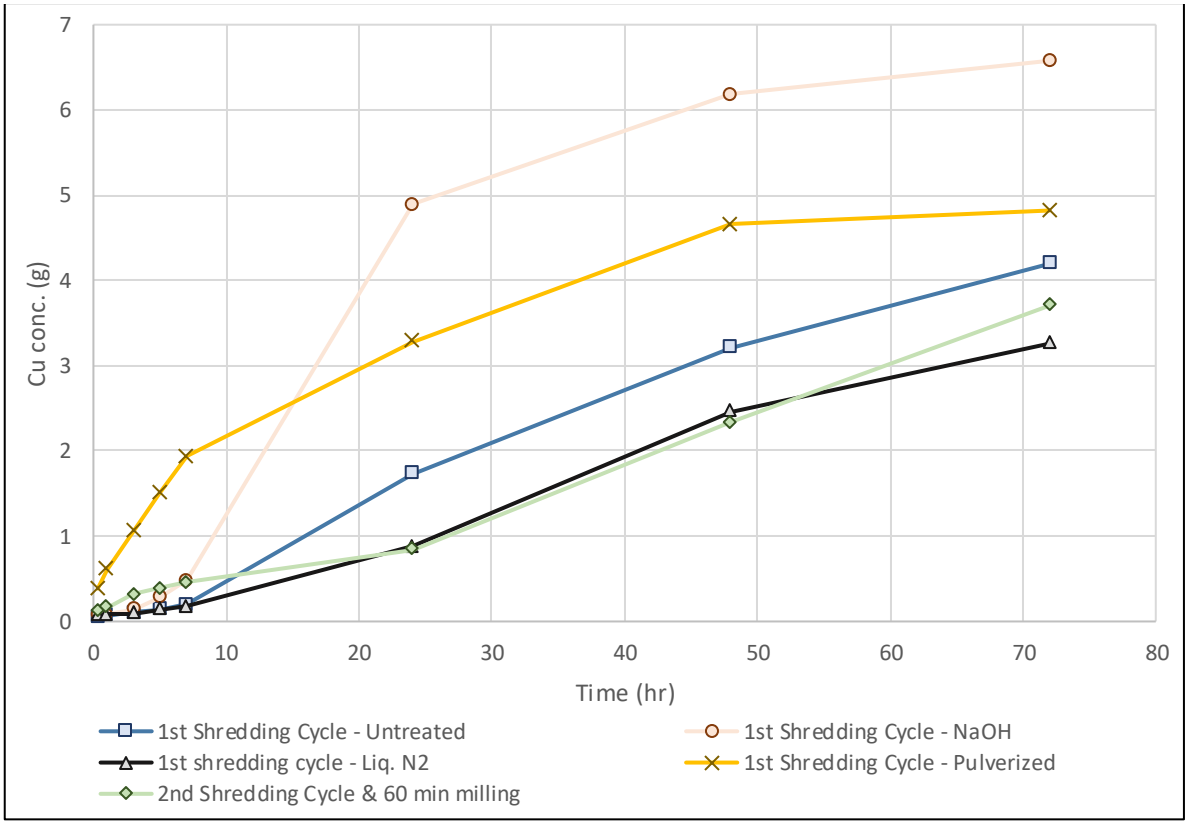

Figure IV-27: Cu concentration profile of 1st shredding cycle Liq. N_2 cooled, pulverised, untreated, NaOH pre-treated and 2nd cycle 60 min milled PCBs

The shredding of the cooled boards resulted in the largest particle sizes of all screened cycles as seen in the PSD in Figure IV-2, but also showed the highest degree of delamination and cracking of the PCB chips in comparison to untreated room temperature PCBs. Liq. N_2 pre-treated boards

reached a maximum copper recovery of 3.26 g (11.25 %) after 72 hrs, compared to the 4.20 g (14.48 %) and 6.58 g (22.70 %) of the untreated and NaOH pre-treated PCBs, respectively. These lower leaching rates are the result of the low amounts of easily accessible copper, with most of it stuck in larger particles and underneath the tightly woven fibreglass layers.

The PCB that was completely pulverised in the ring mill after the 1st shredding cycle showed better leach performance compared to the untreated PCB and Liq. N_2 pre-treated PCB, yet lower maximum extractions compared to the NaOH pre-treated PCB were recorded. These poor recoveries after 72 hrs are the result of settling of the pulverised material, a combination of copper, epoxy resin and fibreglass particles, at the reactor bottom. The settling of the particles and slow agitation speed effectively trapped the fine copper particles, inhibiting further extraction. The pulverised PCB reached maximum Cu extractions of 4.82 g (16.64 %) after 72 hrs. This is marginally more than the untreated PCB but considerably less than the NaOH pre-treated PCBs.

b. Reaction rates

The pulverised PCB, displayed in Figure IV-28 displayed the fastest initial leaching rates from all analysed samples, starting the Cu recovery profile with an average Cu extraction rate of 0.23 g/hr for the first seven hours. The high amount of fine copper particles in solution allows for rapid oxidation of the metallic copper to Cu^{2+}, producing $Cu(NH_3)_2^{+}$, which reacts with free ammonia in solution to produce $Cu(NH_3)_4^{2+}$. The presence of Cu^{2+} further acts as an oxidant in the solution, promoting higher Cu extractions. However, after the first seven hours, a significant drop in leach kinetics is recorded for this recovery curve. From 7 – 24 hrs, the rate of reaction drops to 0.08 g/hr, having recovered less copper (3.29 g) after 24 hrs than the NaOH pre-treated PCB (4.89 g). This decrease in reaction rates is attributed to the settling of the particles to the reactor bottom, only exposing the limited amount of Cu^0 to the lixiviant, effectively burying the copper under layers of fine glass fibre and epoxy resin particles. This settling of the fine particles was not an immediate effect as the overhead stirrers kept some particles in suspension for approximately 7 hrs. This limited amount of Cu^0 available to the solution slows the rate of reaction down. This drop-in Cu extraction is further amplified for the following 48 hrs, eventually dropping to 0.01 g/hr, essentially reaching termination of the reaction.

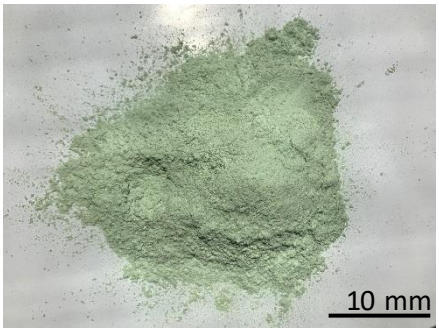

Figure IV-28: Pulverized PCBs after 1st shredding cycle in IGS and 3 min milling in ring mill/pulveriser

The Liq. N_2 pre-treated PCB performed similarly to the untreated 1st shredding cycle PCB in terms of reaction rate over the first seven hours, displaying a rate of 0.02 g/hr. As with the untreated PCB, this slow rate is attributed to the limited amount of Cu^0 exposed to the lixiviant. However, unlike the untreated PCBs, the reaction does not speed up considerably between 7 – 24 hrs, reaching a rate of only 0.04 g/hr in comparison to the 0.09 g/hr rate of the untreated PCB. The lower recovery rate for the Liq. N_2 board is primarily because of the poor accessibility of copper for dissolution, as can be seen in Figure IV-29. This is the direct result of cooling of the boards to – 196 °C, and subsequent shredding caused the boards to preferentially delaminate rather than be reduced in size. As a result, the tightly woven fibreglass remains above the copper layers, inhibiting the lixiviant from leaching the copper for dissolution and subsequent extraction. Unlike the untreated board which has 14.2 % of its total mass fraction distributed in the intermediate and fine size fraction, the Liq. N2 pre-treated board only has about 7.5 % distributed in the same size fractions after the 1st shredding cycle. The rate of reaction then increases to 0.07 g/hr after 48 hrs, as more of the copper from delaminated particles is oxidized by the now in Cu^{2+} enriched lixiviant, promoting the reaction. For the last 24 hrs the reaction rate slows down again to 0.03 g/hr as most of the Cu^0 available is used up and extracted in the lixiviant.

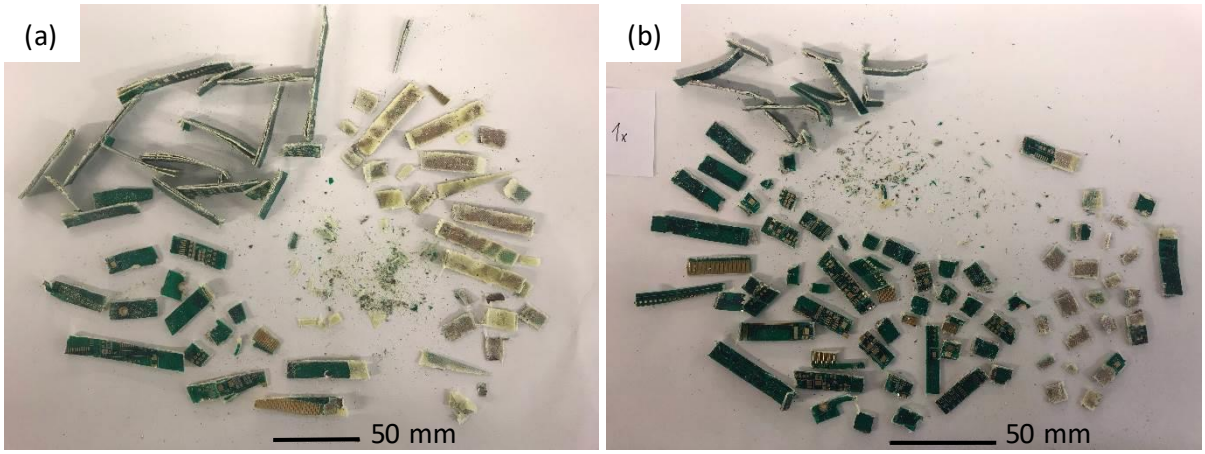

Figure IV-29: Visual analysis of the 1st shredding cycles (a) Liq. N_2 pre-treated PCB; (b) Untreated PCB

d. Comparison of Leach Results to Literature

As mentioned in the literature review in chapter II, few authors of published papers provided insights into the methods of size reduction. The journal articles that outlined these methods generally reported copper recoveries of 90 % or more. These high recoveries are the result of energy-intensive size reduction to particle sizes of ≤ 2 mm. This section compares the results obtained from this study to the recoveries from the literature review that used similar alkaline-based systems for copper recovery.

Table IV-5 highlights several research studies that were conducted on a similar basis to this study. Researcher conducted on precious metal (especially gold) recovery by far exceeds studies on copper recovery, which are only soluble in acid-based systems. As a direct result of this, most researchers use acidic lixiviants rather than alkaline-based systems. The studies presented in Table IV-5 were chosen based on their similarity to this study, but also to highlight the differences between methods of copper recoveries.

Table IV-5: Comparison of copper recoveries with literature

Author	PCB particle size (mm)	Leach solution	Molar conc. (M)	Leaching time (hrs)	Copper recoveries (%)	Temperature (°C)	Agitation speed (rpm)
(i)	-1.5	Ammonium Sulfate	1	2 4	67 82	25	200
(ii)	-0.06	Ammonium Carbonate	5 0	7	92.6 25.1	25	N/A
(iii)	Ultra-fine	Ammonium Sulfate	2	2	89.7	35	400
(iv)	0 to 8	Ammonium Carbonate	6	3.5	90	22	N/A
(v)	25	Ammonium Salts	1	24	72	25	300
(vi)	50	Ammonium Carbonate	2	45	11.5	25	500
(vii)	-8	Ammonium Carbonate	2	72	23.5	25	100

(i) (Koyama et al., 2006); (ii) (Bari et al., 2009); (iii) (Yang et al., 2012); (iv) (Xiao et al., 2013); (v) (Rudnik et al., 2016) (vi) (Chirume, 2019); (vii) This study

As indicated by Table IV-5, the first three authors achieved considerably higher Cu recoveries from ammonium-based systems by size reducing PCBs to ≤ 2 mm and leaching over shorter periods of time. This is because at this size fraction, copper tends to be completely liberated from the

Prepreg. Larger particle size fractions, such as the ones analysed in this study, tend to retain copper within the laminated layers, preventing Cu extraction from occurring.

Xiao et al. (2013) achieved considerably higher recoveries (± 90 %) compared to this study even though the PCB particle range generated by the mechanical size reduction was the same. This is because the majority of the larger pieces represented attachments to the boards which are copper rich in nature, leaving most of the actual PCB shredded to finer size fractions. The PCBs were furthermore mechanically pre-treated, resulting in little dielectric components present as well as highly liberated copper particles.

Rudnik et al. (2016) also managed to recover high amounts of copper (± 72 %) from PCBs that were cut into 2.5 x 2.5 cm chips. However, unlike the study by Chirume (2019) who cut the boards into 5 x 5 cm chips, the PCBs were pyrometallurgically pre-treated (no duration or temperature provided), in a furnace for a few hours in an industrial furnace. This resulted in delamination of the multi-layered PCBs and effectively removed the organic components (epoxy resin). The subsequent leaching process was therefore optimized, exposing copper to the solution which was agitated at 300 rpm.

It therefore becomes apparent that leaching of PCBs in ammonia-based systems is only effective when PCBs are reduced in size to ≤ 2 mm or are pyrometallurgically pre-treated to introduce delamination and remove organic compounds.

An additional note needs to be made on the peeling of copper off the PCBs during the ammonia-based leaching. As seen in Figure IV-30 (a & b), the gold is separated from the PCBs due to the oxidation of the copper. This is because the gold is plated on top of the copper on the surface of the PCBs, which, during the leaching process, is oxidized, thereby allowing the gold to peel of and be retained in solution.

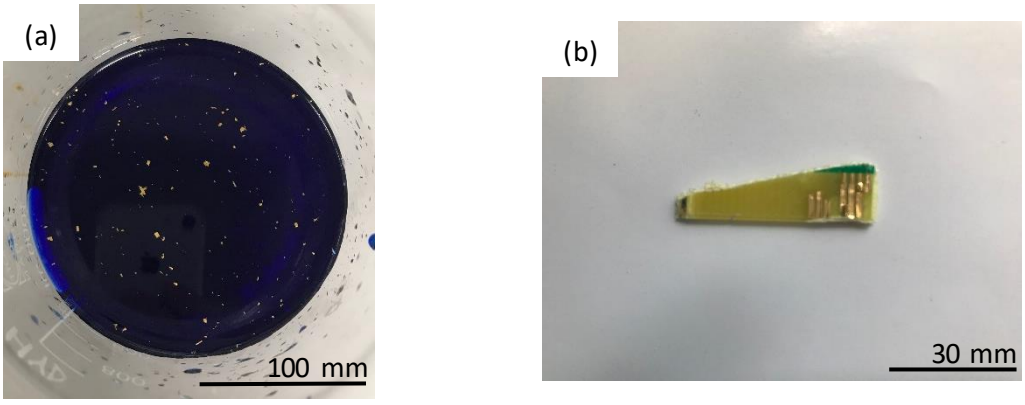

Figure IV-30: Peeling of gold off the shredded PCBs (a) in solution; (b) PCB particle

e. Techno-economic Evaluation

The aim of this section is to outline the costs that are associated with the separate size reduction processes. Subsection (i) outlines the shredding costs of each of the processes while subsection (ii) presents a cost-benefit analysis.

i. Cost of Size Reduction

The energy consumed as well as the time required for the shredding, milling and pulverising cycles can be utilized to determine the cost of each individual shredding cycle. As seen in Figure IV-31 (a & b), based on data calculated in eq. (III-2) – eq. (III-7) in chapter III, the cost of shredding increases with each consecutive shredding cycle. The same applies to the cost of milling. Table IV-7 presents the average shredding and milling times as well as the average power and final average energy consumed. As displayed in Figure IV-9 shredding, unlike the planetary ball mill, consumes considerably higher amounts of power. However, shredding is completed after a maximum of 2.5 min for a total of six shredding cycles. Milling in the PBM on the other hand can take up to two hours to complete. The pulveriser also consumed considerably higher amounts for the pulverization process (2.5 kW). However, because the milling time is rather short (± 3 min), the total consumption is comparable to that of the PBM. As a result of this, shredding of the boards costs only a fraction of the costs that are associated with the PBM.

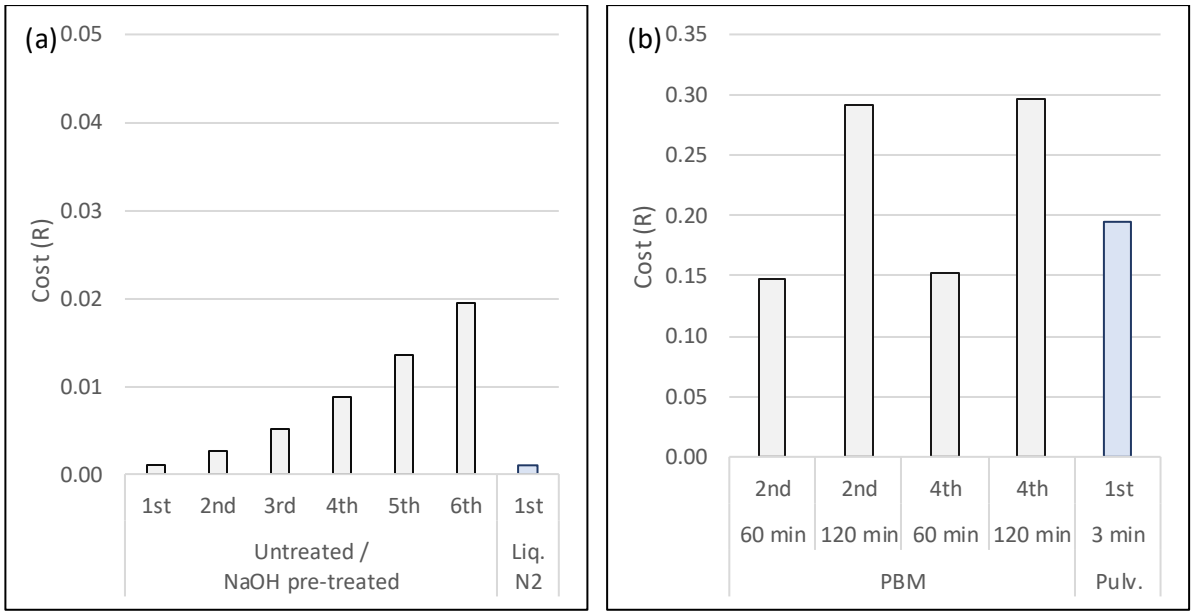

Figure IV-31: Cost of shredding of IGS, PBM and Pulveriser (a) Untreated, NaOH pre-treated and Liq. N_2 pre-treated PCBs; (b) Milled and pulverized

The cost of the 1st shredding cycle is considerably lower than that of the other five shredding cycles, primarily because it did not require a long time until the shredding is completed. The increase in cost from the 1st to the 2nd cycle was because of the necessity of a re-feeding stage, which consumed both energy and time, as well as the considerably longer shredding period for

the 1st cycle. From the 2nd shredding cycle onwards, the increase in cost was exponential as the successive number of re-feed time stayed the same as did the required amount of time for the respective shredding cycle.

Table IV-7: Running time and energy consumption of industrial grab shredder, planetary ball mill, Liq. N_2 and pulveriser

Treatment of PCB	Shredding Cycle	Shredding time (sec)	Milling time (min)	Power consumed (J)	Energy consumed (kWh)
IGS	1st	14	-	2.27	0.0006
	2nd	37	-	1.30	0.0017
	3rd	59	-	0.98	0.0033
	4th	81	-	0.95	0.0057
	5th	104	-	1.24	0.0088
	6th	128	-	1.26	0.0126
PBM	2nd	37	60	0.09	0.0947
	2nd	37	120	0.19	0.1877
	4th	81	60	0.09	0.0987
	4th	81	120	0.19	0.1917
Liq. N_2	1st	14	-	2.32	0.0006
Pulveriser	1st	14	3	2.50	0.1256

Table IV-7 further also presents the average energy consumed (kWh) of the separate size reduction processes, highlighting the importance the length of the size reduction has on the ultimate energy consumption. Shredding the boards twice and milling the generated particles for 60 min costs about R 0.15 per board, while simply shredding the boards six times costs about R 0.02 per board. Complete pulverization of the PCBs in the ring mill for 3 min consumed approximately 0.13 kWh which translates to about R 0.20 per board. This is slightly lower than milling a board in the PBM for 120 min after shredding it four times, costing approximately R 0.30 per board. Shredding of the PCBs in the IGS is therefore considerably cheaper than milling in the PBM of pulverization in the ring mill.

ii. Cost-benefit Analysis

Taking the information from the previous sections into consideration, a cost-benefit analysis can be constructed. This cost-benefit analysis was constructed by incorporating only the energy costs involved in the respective recovery processes, excluding any additional costs such as for example the pre-treatment costs of chemicals. Furthermore, for the cost-benefit analysis, copper price was determined to be valued at $6400/tonne as of 2018 (Bamber, 2019; Reemeyer, 2019). This equates to a copper value of approximately R 0.1/g, which is the value utilized for the following calculations.

Figure IV-32 aims to compare the cost-benefit breakdown by displaying the copper value recovered throughout the leaching period on the primary y-axis and the associated cost with the respective treatment of the PCBs on the secondary y-axis. It therefore displays the recovered value of copper recovered by the alkaline leaching process after 7, 24, 48 and 72 hrs for all size reduction processes. This data is furthermore tabulated in Table VIII-12 in appendix D.

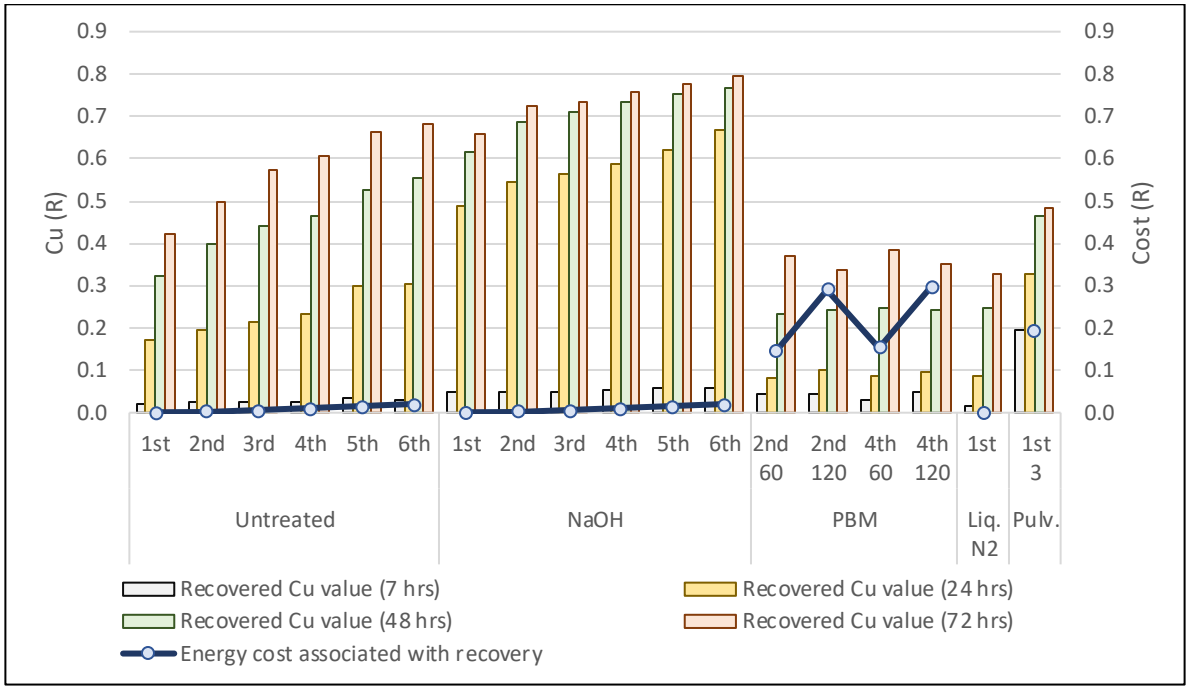

Figure IV-32: Cu value recovered vs cost of recovery of untreated, PBM and Pulverised PCBs

From graph in Figure IV-32 it becomes apparent that incremental increase in shredding and other comminution techniques' energy requirements does not yield the same incremental recovery in copper. Shredding in general is such an energy friendly way of reducing the PCBs in size, that already after 7 hrs of leaching the copper value recovered is higher than the associated energy costs. The NaOH pre-treated PCBs performed the best, recovering the most copper at the lowest energy costs. However, pre-treatment costs of the chemicals required to remove the solder mask need to be considered, thereby changing the cost-benefit situation. This also applies to the PCBs that were frozen in Liq. N_2 prior to shredding. However, this lies beyond the scope of this study.

PCBs that were milled in the PBM or pulverised in the ring mill showed different results in terms of cost-benefit. Energy costs of the PBM milling process are considerably higher than those of the IGS, resulting in copper recovery values only exceeding the energy costs after 48 hrs of leaching. Moreover, because of the flawed reactor system set-up, the Cu recovery values are considerably lower than those achieved by the IGS processed PCBs.

The pulverised PCBs again showed different Cu recovery values. Because of the ultrafine nature of the fine particles initially in solution, the cost-benefit analysis already breaks even after 7 hrs. However, as with the PBM milled PCBs, the flawed reactor set-up resulted in considerably lower Cu recovery values after 72 hrs which could have been optimized with improved leach systems.

f. Material Properties

As mentioned in the materials and methodology section, preliminary failure analysis was conducted with the purpose to gain an understanding regarding the responses of the custom-made PCBs to different stress environments. These three stress environments, impact, tensile and three-point bending, are discussed in the respective subsections (i – iii) as followed.

i. Drop-weight Impact Test

This test was carried out with the aim to determine the behaviour of the custom-made PCBs to impact stresses. The absorbed energies from the six areas recorded by the drop-weight impact are displayed in Figure IV-33, and the recorded energy profiles for the respective areas are reported in Figure VIII-2 (a-f) in appendix F. From the displayed results it becomes apparent that all areas record absorbed energies that fall within one standard deviation. Areas 1 and 3 recorded slightly higher amounts of absorbed energies than the other tested areas (1960.75 ± 77.75 J). As indicated by Figure III-3 (a & d) in chapter III, the top and lowermost outer copper layers are present in these two areas, whereas in the other areas the copper layers have been etched away. However, overall it can be concluded that the strength of the boards in impact environments is only marginally affected by the presence of the copper layers, but rather the presence of holes, notches and trace lines that introduce areas of weakness to the PCBs.

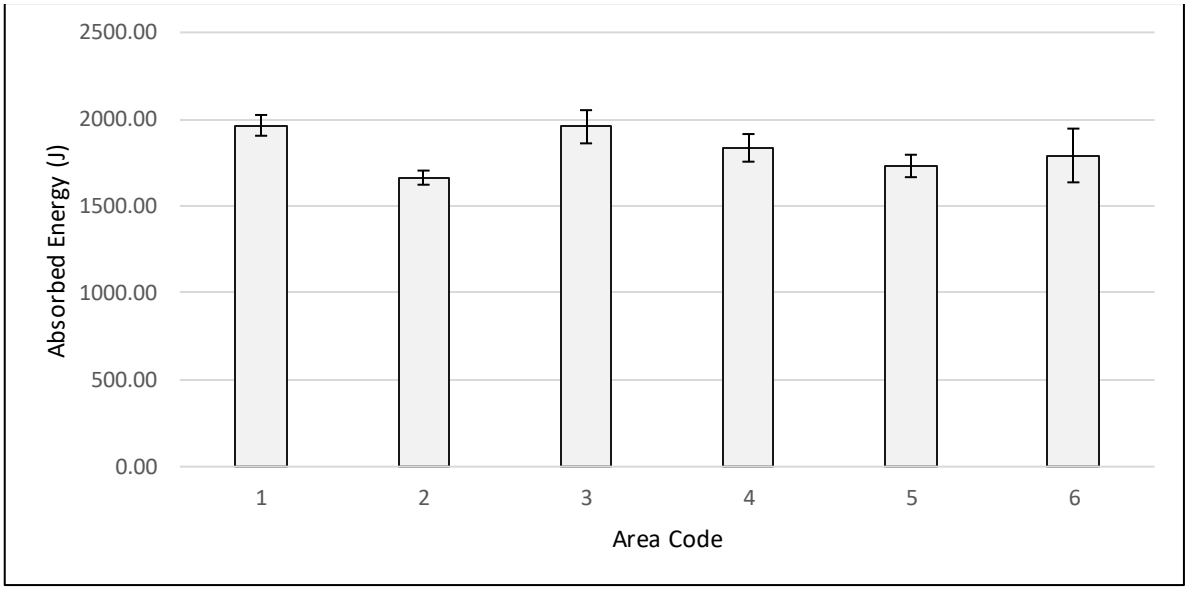

Figure IV-33: Absorbed energy by tested area of the custom-made PCBs

It must be further noted, as mentioned in chapter II-1, the minimum weight required of the impactor was not possible to be achieved as 5.0776 kg was the minimum weight attainable. As a result of this, none of the tested areas were able to withstand the drop-weight impact, resulting in complete failure of the respective areas. This is in line with the discussed observations by Ruan & Xu (2016). The authors concluded that mechanisms that utilize impact forces as a means of size reduction are most suitable for the pulverization of PCBs.

On the other hand, when comparing the impact generated samples to the PCB chips generated in the PBM in Figure IV-34 (b) & (a), respectively, considerable differences could be taken note off. The PBM milled PCBs displayed more abrasion on the sides rather than impact damage observed in the impact test which displayed clean breakage. This can be related to the poor set-up of the PBM, which operated with agate balls in an agate milling chamber. This resulted in poor breakage and more abrasion, therefore indicating that the PBM used performed poorly in terms of inflicting impact damage to the PCBs.

Figure IV-34: Visual comparison of samples from (a) 2nd shredding cycle 120 min PBM milled; (b) Impact test

ii. Three-point Bending Test

Another failure mode investigated involved the testing of the custom-made PCBs in a three-point bending environment. As discussed in the materials and methodology section, six areas based on the various copper layers within the PCBs were tested. Unlike the drop-weight impact test, for this type of failure analysis, it was hypothesized that the presence of copper in the PCBs plays a more important role. Areas 1, 2 and 5 are areas tested in vertical alignment to the PCBs, whereas areas 3, 4 and 6 are in horizontal alignment to the PCBs. The recorded flexural strengths and strains of the respective tested areas are reported in Figure IV-35.

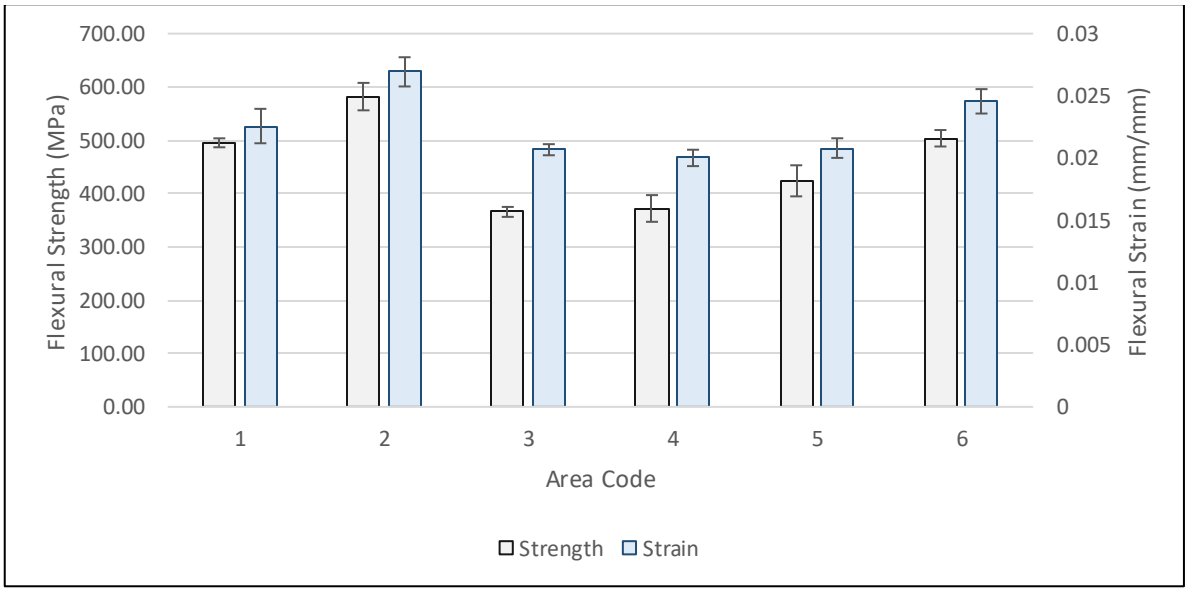

Figure IV-35: Flexural Strength by tested area of the custom-made PCBs

Areas 1 and 6 were selected based on their orientation in order to see if there is a difference in flexural strength based on 0° or 90° orientation. Both areas represent parts of the PCBs that have 3 out of 4 present copper layers as indicated by Figure III-3 (a-d). Both areas have recorded nearly identical results, 499.47 ± 11.91 MPa in flexural strength and 0.0236 ± 0.0012 mm/mm in flexural strain, indicating that there is negligible difference in flexural behaviour based on orientation. Areas 3, 4 and 5 reported similar results that fall within one standard deviation indicating that those areas are of similar flexural strength. Area 2 displayed the highest amount of resistance to flexural stress (581.82 ± 25.73 MPa), which can be explained by the fact that area 2 falls on a part of the PCBs that has all four copper layers present. Overall it can be concluded that, unlike the drop-weight impact test, the presence of the underlying copper layers rather than the orientation has a greater impact on the flexural strength of the custom-made PCBs.

In general, as seen in Figure VIII-3 in appendix F, in a three-point bending environment, the custom-made PCBs tend to behave in a ductile rather than brittle manner. This is because the glass fibres, which provide the PCBs with structural integrity, are capable of transmitting the experienced stress to the epoxy resin. This, in turn, allows the PCBs to withstand greater pressure in a bending environment, experiencing gradual failure rather than abrupt.

iii. Tensile Test

Due to the nature of the custom-made PCBs and to be as close to the recommended guidelines of the ASTM, the tensile tests were conducted on a set of three samples rather than six. The tensile strength of the three respective analysed samples is presented in Figure IV-36. Moreover, the stress-strain curves, as well as the failure codes of the respective areas, are presented in Figure VIII-4 and Table X in appendix F, respectively. It was unfortunately not possible to determine Poisson's ratio as the extensometer was not functioning during the testing time.

As seen in Figure IV-33, the tensile strength of the three different areas are similar to one another, all falling within the margins of one standard deviation (2.63 ± 0.08 MPa). Area 1 predominantly failed in the centre of the sample, in areas where there is an increased number of drilled holes as well as the absence of copper layers and along edging lines. Sample area 2 failed mainly closer to either the top or bottom grip. This failure, again as area 1, follows areas of weakness experienced by a decreased amount of copper layers and along holes. As expected, area 3 was no exception to this trend, failing in the centre of the sample, along planes of weakness introduced by holes and edging lines.

In tensile stress environments, as seen in Figure IV-36 and unlike to the flexural strength, the boards appear to fail in a brittle manner with no visible necking. The main reason for this is the fact that the glass fibres are unable to transmit the stress experienced in this type of environment effectively to the epoxy resin. The PCBs therefore once reaching their tensile threshold tend to experience abrupt rather than gradual failure.

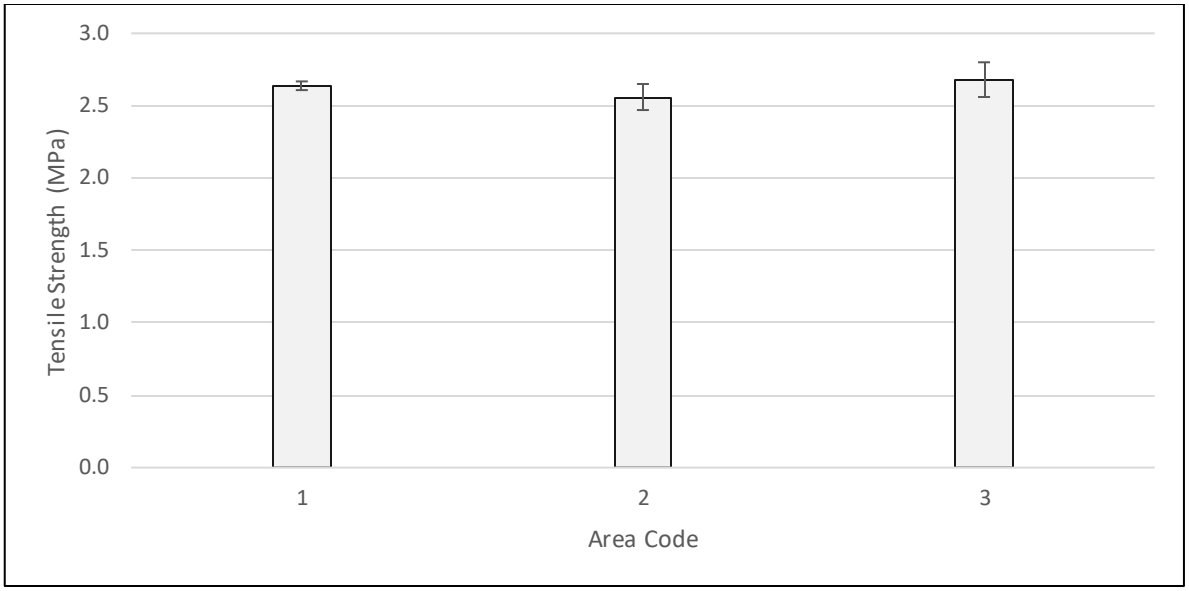

Figure IV-36: Tensile strength by tested area of the custom-made PCBs

When analysing the particles generated by the IGS, it becomes apparent that both tensile as well as bending forces are the predominant forces responsible for size reduction. The generated chips (Figure IV-37 (a)) display the same rough edges with ripped and split apart fibreglass that can also be observed in the failure areas of the tensile test (IV-37 (b)). Moreover, multiple particles form the IGS also displayed evidence of bending, inferring that the forces that act in the three-point bending test (IV-37 (c & d) also apply to the IGS shredding environment.

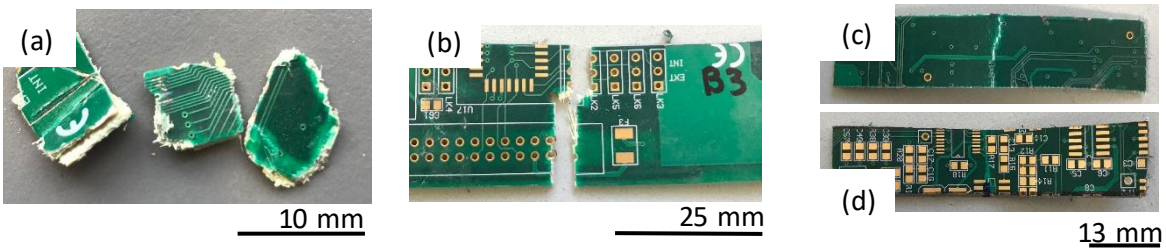

Figure IV-37: Visual comparison of samples from (a) 3rd shredding cycle IGS; (b) Tensile stress test; (c) Bottom of three-point bending test; (d) Top of three-point bending test

V. Conclusion

The overarching aim of this study was to understand the physical structure of the custom-made PCBs. This aim as carried out by evaluating how these characteristics can be exploited in an industrial grab shredder in terms of size reduction and metal by avoiding complete pulverization of the boards. The study further aimed to quantify and evaluate the effectiveness of various pre-treatment methods in terms of copper recovery by ammonia-based lixiviants in a batch stirred reactor. The experiments were designed with the aim to determine the copper liberation and subsequent recovery from custom-made PCBs, placing emphasis on the progressive clawing mechanics of an industrial grab shredder. Furthermore, pre- and post-treatments of the PCBs that included soaking in NaOH, freezing in Liquid Nitrogen, milling in the planetary ball mill and complete pulverization were evaluated in terms of their respective efficiencies when it comes to copper liberation and subsequent recovery. An additional aspect investigated involved an initial preliminary study into the material properties and failure behaviour of the custom-made PCBs in three different stress environments.

The clawing mechanics of the industrial grab shredder have proven to be ineffective in terms of the liberation of copper. It has been shown that with progressive shredding an increase in the number of delaminated particles occurs simultaneously with the generation of finer particles. However, delamination failed to effectively expose the copper that is situated underneath the tightly woven fibreglass layers. Most of the increase in copper extraction that is associated with progressive shredding by the ammonia lixiviant is the result of the generation of finer particles.

Pre-treating of the PCBs in an 8 M NaOH effectively removed the solder mask covering the upper- and lower-most copper layer, and this had a major effect on the Cu recovery behaviour over the 72 hours of extraction. However, ultimately only about 6 % more copper was extracted by the individual shredding cycles in comparison to the respective untreated processed PCBs. Post-shredding milling of the PCBs resulted in considerably lower recoveries (14 %) compared to the untreated leached PCBs over 72 hours, rendering this process inefficient. Moreover, milling for 120 min resulted in lower Cu recoveries than milling for 60 minutes. Similarly, shredding of frozen PCBs resulted in a higher degree of delamination but generated fewer fine particles than untreated shredding, which resulted in lower Cu recoveries. Complete pulverization proved to be effective in the initial stages of the leaching experiment, however, due to the low agitation the particles accumulated at the bottom of the reactors, hindering further additional Cu recoveries.

It was further determined that the copper distribution is closely dependent on the particle size distribution. This is because of the large size fractions of the resulting particles generated by the shredder, retaining the copper within the particles. After the 1st shredding cycle, most of the copper can be found in the largest size fraction, which is then transferred to the smaller size fractions with progressive shredding.

Considering the energy costs associated with the respective treatments, a cost-benefit analysis was carried out. This analysis concluded that the most beneficial treatment process for the investigated parameters includes no pre- or post-treatment but rather simply shredding the PCBs three times.

The industrial grab shredder mainly acts with tear and bending forces, achieving size reduction of the PCBs by biting into the boards, tearing them apart while simultaneously bending them. The tensile and three-point bending tests have confirmed this. The planetary ball mill has been shown to be ineffective for copper liberation, both in terms of recovery as well as costs.

VI. Recommendations

Several aspects have been noted throughout the study which needs further attention regarding additional research going into the extraction of copper from PCBs.

As seen by the untreated leached PCBs in Figure IV-11, the leaching process had not been completed by the time the experiment was terminated. By increasing the leaching time of the PCBs in the batch stirred reactors from 72 hours to 96 or 120 hours, higher recoveries will be achieved.

It has further become apparent that the agitation was a major factor limiting extractions, especially for the milled and pulverised PCB samples. Therefore, it is postulated that an increase of the rotational speeds of the overhead stirrer would be sufficient to keep the fine particles in suspension and extract more copper from those PCBs. There would be no difference in extractions for PCBs that were only shredded as the copper remains trapped underneath the fibreglass layers.

To achieve higher copper recoveries, improvement of the hydrodynamic design and/or increase the stirring rate when using finer particles would yield in higher recoveries.

Further NaOH treatment of post-shredding particles could be effective in removing the epoxy resin of the Pre-preg layer as it did with the solder mask. This could potentially loosen the tightly woven fibreglass, allowing the lixiviants to access and extract copper more efficiently.

Moreover, during the leaching, it became evident that due to the oxidation of copper, the above-plated nickel-gold complex peeled off. Further research should be conducted involving the subsequent recovery of the gold as the economic value of said gold considerably outweighs the value of copper. By investigating the recovery of gold without the costs of strong lixiviants major economic benefits can be achieved.

The effect freezing of the PCBs in Liq. N_2 has on the recovery of copper was only investigated for the 1st shredding cycle. However, as outlined by Figure IV-21, the temperature is expected to be considerably lower than room temperature. Therefore, subsequent shredding could be investigated to determine if the recoveries increase.

The research conducted for this study can further help to develop more efficient pre-treatment flowsheets for hydrometallurgical extraction operations. By increasing the degree of exposure of the inner copper layers, more copper and other valuable metals can be extracted and recovered from the waste PCBs. This can increase the effectiveness of the extraction process, allowing small-scale operations to extract more valuable metals, specifically copper, at the lowest possible cost while simultaneously preserving the environment.

Assessment of the efficiency and effectiveness of various size reduction process of PCBs within the recycling chain can significantly help semi-formal hydrometallurgical recycling business to find the most cost-effective recycling process. These semi-formal businesses, specifically in developing nations such as South Africa, can draw from the learning of this study to develop a pre-treatment flowsheet for their hydrometallurgical operations in order to recover the most Copper with the lowest possible amount of energy input and associated costs.

VII. Bibliography

Adhapure, N.N., Dhakephalkar, P.K., Dhakephalkar, A.P., Tembhurkar, V.R., Rajgure, A. V. & Deshmukh, A.M., 2014. Use of large pieces of printed circuit boards for bioleaching to avoid "precipitate contamination problem" and to simplify overall metal recovery. *MethodsX,* 1, pp.181–186.

Ayres, R., 1997. Metals recycling: economic and environmnetal implications. *Resources, conservation and recycling*, 21(3), pp.145-173.

Baldé, C.P., Forti, V., Gray, V., Kuehr, R., & Stegmann, P., 2017. The global e-waste monitor 2017: Quantities, flows and resources. *United Nations University, International Telecomunication Union, and International Solid Waste Association.*

Bamber, A. 2019. Co-dependencies in copper: Production, prices and innovation trends 1900 - 2018. In *Proceedings of the 58th conference of metallurgists hosting copper 2019*.

Bari, F., Begum, M.N., Jamaludin, B. & Hussin, K. 2009. Selective Leaching for the Recovery of Copper From PCB. In *Proceedings of the malaysian Metallurgical Conference '09 (MMC09), December. pp. 1-2*

Barontini, F., Marsanich, K., Petarca, L. & Cozzani, V., 2005. Thermal Degradation and Decomposition Products of Electronic Boards Containing BFRs. *Industrial & engineering chemistry research*, 44(12), pp.4186–4199.

Behnamfard, A., Mehdi, M. & Veglio, F., 2013. Process development for recovery of copper and precious metals from waste printed circuit boards with emphasize on palladium and gold leaching and precipitation, *Waste Management*, 33(11), pp.2354–2363.

Birloaga, I., De Michelis, I., Ferella, F., Buzatu, M. & Vegliò, F., 2013. Study on the influence of various factors in the hydrometallurgical processing of waste printed circuit boards for copper and gold recovery, *Waste Management*, 33(4), pp.935–941.

Bizzo, W.A., Figueiredo, R.A. & De Andrade, V.F., 2014. Characterization of printed circuit boards for metal and energy recovery after milling and mechanical separation, *Materials*, 7(6), pp.4555–4566.

Calvo, G., Mudd, G., Valero, A. & Valero, A., 2016. Decreasing ore grades in global metallic mining: A theoretical issue or a global reality? *Resources*, 5(4), pp.1–14.

Campbell, F.C., 2010. Introduction to Composite Materials. *Structural Composite Materials*, 1, pp.1–29

Castro, L.A. & Martins, A.H., 2009. Recovery of tin and copper by recycling of printed circuit boards from obsolete computers, *Brazilian Journal of Chemical Engineering,* 26(4), pp.649–657.

Chatterjee, S. & Kumar, K., 2009. Effective electronic waste management and recycling process involving formal and non-formal sectors. *International Journal of Physical Sciences*. 4(13), pp.893–905.

Chirume, B.H., 2019. *Investigation of a Hydrometallurgical Process Route to Recover Metals from Waste Printed Circuit Boards*. MSc (Eng) thesis, University of Cape Town.

Coombs Jr., C.F., 2008. *Printed Circuits Handbook*. 6th ed.

Coonrod, J., 2007. Bending, forming and flexing printed circuits. *IPC - IPC Printed Circuits Expo, APEX and the Designers Summit 2007*, 1, pp.594–615.

Coonrod, J. 2012. Different Copper Foils for Different Reasons. *The PCB magazine*, pp6.0–64.

Corporation, S.L., 2019. *Substrate's Dynes/cm*. Available: http://www.stevenlabel.com/resources/dyne-levels.

Creamer, N.J., Baxter-Plant, V.S., Henderson, J., Potter, M. & Macaskie, L.E., 2006. Palladium and gold removal and recovery from precious metal solutions and electronic scrap leachates by Desulfovibrio desulfuricans. *Biotechnology Letters*, 28(18), pp.1475–1484.

Cui, H. & Anderson, C.G., 2016. Literature Review of Hydrometallurgical Recycling of Printed Circuit Boards (PCBs). *Journal of Advanced Chemical Engineering*, 6(1), pp.1–11.

Cui, J. & Forssberg, E., 2003. Mechanical recycling of waste electric and electronic equipment: A review. *Journal of hazardous materials,* 99(3), pp.243–263.

Cui, J. & Zhang, L. 2008., Metallurgical recovery of metals from electronic waste: A review. *Journal of hazardous materials,* 158:(2-3), pp.228–256.

Das, A., Vidyadhar, A. & Mehrotra, S.P., 2009. A novel flowsheet for the recovery of metal values from waste printed circuit boards. *Resources, Conservation and Recycling*, 53(8), pp.464–469.

Department of Environmental Affairs., 2018. South Africa State of Waste Report: 2nd Draft. Available: http://sawic.environment.gov.za/documents/9066.pdf.

Eskom., 2019. Tariffs & Charges Booklet. (April 2019).

Feldman, A.V., 1993. Method for processing scrap of electronic instruments. *U.S. Patent No. 5,217,171*.

Ghosh, B., Ghosh, M.K., Parhi, P., Mukherjee, P.S. & Mishra, B.K., 2015. Waste Printed Circuit Boards recycling: An extensive assessment of current status. *Journal of Cleaner Production*, 94, pp.5–19.

González, E. V, Maimí, P., Camanho, P.P., Turon, A. & Mayugo, J.A., 2012. Simulation of drop-weight impact and compression after impact tests on composite laminates. *Composite Structures,* 94, pp.3364–3378.

Grant, R. & Oteng-Ababio, M., 2012. Mapping the invisible and real "african" economy: Urban e-waste circuitry. *Urban Geography*, 33(1), pp.1–21.

Guo, C., Wang, H., Liang, W., Fu, J. & Yi, X., 2011. Liberation characteristic and physical separation of printed circuit board (PCB). *Waste Management,* 31(9–10), pp.2161–2166.

Hadi, P., Xu, M., Lin, C.S.K., Hui, C.W. & McKay, G., 2015. Waste printed circuit board recycling techniques and product utilization. *Journal of Hazardous Materials*, 283, pp.234–243.

Hagelüken, C., 2007. Metals Recovery from e-scrap in a global environment. In *6th Session of OEWG Basel Convention, Geneva.*

Hanafi, J., Jobiliong, E., Christiani, A., Soenarta, D.C., Kurniawan, J. & Irawan, J., 2012. Material recovery and characterization of PCB from electronic waste. *Procedia - Social and Behavioral Sciences*, 57, pp.331–338.

Havlik, T., Orac, D., Petranikova, M., Miskufova, A., Kukurugya, F. & Takacova, Z., 2010. Leaching of copper and tin from used printed circuit boards after thermal treatment. *Journal of Hazardous Materials*, 183(1–3), pp.866–873.

Hino, T., Agawa, R., Moriya, Y., Nishida, M., Tsugita, Y. & Araki, T., 2009. Techniques to separate metal from waste printed circuit boards from discarded personal computers. *Journal of Material Cycles and Waste Management*, 11(1), pp.42–54.

Iji, M. & Yokoyama, S., 1997. Recycling of Printed Wiring Boards with Mounted Electronic Components. *Circuit World*, 23(3), pp.10–15.

Ilankoon, I.M.S.K., Ghorbani, Y., Chong, M.N., Herath, G., Moyo, T. & Petersen, J., 2018. E-waste in the international context: A review of trade flows, regulations, hazards, waste management strategies and technologies for value recovery. *Waste Management*, 82, pp.258–275.

Jadhav, U. & Hocheng, H., 2015. Hydrometallurgical Recovery of Metals from Large Printed Circuit Board Pieces. *Scientific Reports*, 5(101), pp.1–10.

Kasper, A.C., Berselli, G.B.T., Freitas, B.D., Tenório, J.A.S., Bernardes, A.M. & Veit, H.M., 2011. Printed wiring boards for mobile phones: Characterization and recycling of copper. *Waste Management*, 31(12), pp.2536–2545.

Kaya, M., 2016. Recovery of metals and nonmetals from electronic waste by physical and chemical recycling processes. *Waste Management*, 57, pp.64–90.

Khaliq, A., Rhamdhani, M.A., Brooks, G. & Masood, S., 2014. Metal Extraction Processes for Electronic Waste and Existing Industrial Routes: A Review and Australian Perspective. *Resources*, 3(1), pp. 152-179.

Kim, Y., Seo, H. & Roh, Y., 2018. Metal Recovery from the Mobile Phone Waste by Chemical and Biological Treatments. *Minerals,* 8(1), pp.8.

Konishi, H., Bitoh, T., Ono, H., Oishi, T., Koyama, K. & Tanaka, M., 2014. Behavior of Copper Dissolution in an Ammonia Solution Containing Ammonium Chloride or Sulfate. *Journal of the Japanese Society for Experimental Mechanics*, 14, pp.s205–s209.

Koyama, K., Tanaka, M. & Lee, J.C., 2006. Copper leaching behavior from waste printed circuit board in ammoniacal alkaline solution. *Materials Transactions*, 47(7), pp.1788–1792.

Kridiotis, P. & Rogerson, C., 2019. *Leaching kinetics of waste printed circuit boards prepared in an industrial grab shredder*. BSc (Eng) thesis, University of Cape Town.

Kumar, A., Holuszko, M. & Espinosa, D.C.R., 2017. E-waste: An overview on generation, collection, legislation and recycling practices. *Resources, Conservation and Recycling*, 122, pp.32–42.

Li, J., Shrivastava, P., Gao, Z. & Zhang, H., 2004. Printed Circuit Board Recycling : A state of the Art survey. *IEEE transactions on electronics packaging manufacturing,* 27(1), pp.33–42.

Li, Y., Chen, H., Zhang, X., Tan, C. & Ding, Y., 2010. Renewable energy carriers: Hydrogen or liquid air/nitrogen? *Applied Thermal Engineering*, 30(14–15), pp.1985–1990.

Long, L., Sun, S., Zhong, S., Dai, W., Liu, J. & Song, W., 2010. Using vacuum pyrolysis and mechanical processing for recycling waste printed circuit boards. *Journal of Hazardous Materials*, 177(1–3), pp.626–632.

Luda, M.P., 2011. Recycling of Printed Circuit Boards. *Integrated Waste Management - Volume II*, pp.285–299.

Maguyon, M.C.C., Alfafara, C.G., Migo, V.P., Movillon, J.L. & Rebancos, C.M., 2012. Recovery of copper from spent solid printed-circuit-board (PCB) wastes of a PCB manufacturing facility by two-step sequential acid extraction and electrochemical deposition. *Journal of Environmental Science and Management,* 15(1), pp.17–27.

Menad, N. & Van Houwelingen, J., 2011. Identification and recovery of rare metals in electric and electronic scrap: a review. In *Tirtheenth International Waste Management and Landfill Symposium*, pp. 10-p.

Menetti, R.P. & Tenorio, S.A.J., 1995. Recycling of Precious Metals from Electronic Scraps. In *In Proceedings of the 50th Annual Congress of ABM*, *Sao Pedro, SP, Brazil.*, pp.625–634.

Mereco., 2019. *What makes epoxy resin good adhesives? Why do they bond so strongly to surfaces?* Available: http://www.mereco.com/resources/ask-the-doctor/what-makes-epoxy-resins-good-adhesives-why-do-they-bond-so-strongly-to-surf.

Oguchi, M., Murakami, S., Sakanakura, H., Kida, A. & Kameya, T., 2011. A preliminary categorization of end-of-life electrical and electronic equipment as secondary metal resources. *Waste Management*, 31(9–10), pp.2150–2160.

Oh, C.J., Lee, S.O., Yang, H.S., Ha, T.J., Kim, M.J., Oh, C.J. & Lee, S.O., 2003. Selective Leaching of Valuable Metals from Waste Printed Circuit Boards, *Journal of the Air & Waste Management Association,* 53(7), pp.897-902.

Oliveira, P.C., Cabral, M., Nogueira, C.A. & Margarido, F., 2010. Printed Circuit Boards Recycling: Characterization of Granulometric Fractions from Shredding Process. In *Materials Science Forum,* 636–637, pp.1434–1439.

Ongondo, F.O., Williams, I.D. & Cherrett, T.J., 2011. How are WEEE doing? A global review of the management of electrical and electronic wastes. *Waste Management*, 31(4), pp.714–730.

Oyelami, H.I., Hammed, T.B. & Sridhar, M.K.C., 2016. Characterization of Elements in the Printed Circuit Boards of Television to Enhance Managing E-Waste through Resource Recovery. *Nature & Science*, 14(10), pp.114–118.

Patel, S., Patel, R., Gautam, A. & Gautam, S., 2017. Influence of oxidizing Agant on recovery of metals including gold and silver from printed circuit boards. *International Research Journal of Engineering and Technology, 4(1), pp.830-834.*

Petter, P.M.H., Veit, H.M. & Bernardes, A.M., 2014. Evaluation of gold and silver leaching from printed circuit board of cellphones. *Waste Management*, 34(2), pp.475–482.

Pietrelli, L., Pietrantionio, M., Piozzi, A., Flammini, R. & Francolini, I., 2014. Material Recovery From Printed Circuit Boards: Characterization and Recycling Strategy. *Proceedings SUM.*

Radmehr, V., Koleini, S.M.J., Khalesi, M.R. & Mohammadi, M.R.T., 2012. Ammonia leaching in the copper industry: A review. In *XXVI international mineral processing congress (IMPC) proceedings, New Delhi, India, 24–28 September,* pp. 02512-02523

Ravikumar, S., 2008. *Characterization of FR-4 printed circuit board laminates before and after exposure to lead-free soldering conditions.* MSc (Eng), University of Maryland.

Reemeyer, H.C.L., 2019. Going Coarser: Is It Worth It? In *Proceedings of the 58th conference of metallurgists hosting copper 2019*.

Rötzer, N. & Schmidt, M., 2018. Decreasing metal ore grades - Is the fear of resource depletion justified? *Resources,* 7(4), pp.88.

Ruan, J. & Xu, Z., 2016. Constructing environment-friendly return road of metals from e-waste: Combination of physical separation technologies. *Renewable and Sustainable Energy Reviews,* 54, pp.745–760.

Rudnik, E., Pierzynka, M. & Handzlik, P., 2016. Ammoniacal leaching and recovery of copper from alloyed low-grade e-waste. *Journal of Material Cycles and Waste Management*, 18(2), pp.318–328.

Singh, J.P., Singh, D. & Sutaria, M., 1999. Ceramic composites: roles of fiber and interface. *Composites Part A: Applied Science and Manufacturing,* 30(4), pp.445–450.

Sohaili, J., Muniyandi, S.K. & Mohamad, S.S., 2012. A Review on Printed Circuit Boards Waste Recycling Technologies and Reuse of Recovered Nonmetallic Materials. *International Journal of Scientific & Engineering Research*, 3(2), pp.1–7.

Standard, A.S.T.M. "D3039/D3039M"., 2017. Standard test method for tensile properties of polymer matrix composite materials. *Annual Book of ASTM Standards*, pp.1–13.

Standard, A.S.T.M. "D7136/D7136M"., 2015a. Standard test method for measuring the damage resistance of a fiber-renforced polymer matrix composite to a drop-weight impact, pp.1–16.

Standard, A.S.T.M. "D7264/D7264M"., 2015b. Standard Test Method for Flexural Properties of Polymer Matrix Composite Materials. *ASTM Standards*, pp.1–11.

Sum, E., 1991. The Recovery of metals from electronic scrap. *The Journal of The Minerals, Metals and Materials Society*, 43(4), pp.53–61.

Terena, L.M., Neto, A.F.D.A., Gimenes, M.L. & Vieira, M.G.A., 2017. Characterisation of printed circuit boards of mobile phones discarded in Brazil. *Chemical Engineering Transactions*, 56, pp.1945–1950.

Theo, L., 1998. Integrated recycling of non-ferrous metals at Boliden Ltd . Ronnskar Smelter. In *Proceedings of the 1998 IEEE International Symposium of Electronics and the Environment, ISEE 1998*, pp.42–47.

Tuncuk, A., Stazi, V., Akcil, A., Yazici, E.Y. & Deveci, H., 2012. Aqueous metal recovery techniques from e-scrap: Hydrometallurgy in recycling. *Minerals Engineering*, 25(1), pp.28–37.

Tunsu, C., Petranikova, M., Gergori, M., Ekberg, C. & Retegan, T., 2015. Hydrometallurgy Reclaiming rare earth elements from end-of-life products : A review of the perspectives for urban mining using hydrometallurgical unit operations. *Hydrometallurgy,* 156, pp.239–258.

Veit, H.M., de Pereira, C.C. & Bernardes, A.M., 2002. Using mechanical processing in recycling printed wiring boards. *Jom*, 54(6), pp.45–47.

Veit, H.M., Diehl, T.R., Salami, A.P., Rodrigues, J.S., Bernardes, A.M. & Tenório, J.A.S., 2005. Utilization of magnetic and electrostatic separation in the recycling of printed circuit boards scrap. *Waste Management,* 25(1), pp.67–74.

Vidyadhar, A., 2016. A Review of Technology of Metal Recovery from Electronic Waste. *E-Waste in Transition - From Pollution to Resource*.

Vijayaram, R. & Chandramohan, K. 2013., Chemical Engineering & Process Technology Studies on Metal (Cu and Sn) Extraction from the Discarded Printed Circuit Board by Using Inorganic Acids as Solvents. *Journal of Chemical Engineering & Process Technology,* 4(2), pp.4-6.

Wang, H., Gu, G.H. & Qi, Y.F., 2005. Crushing performance and resource characteristic of printed circuit board scrap. *Journal of Central South University of Technology,* 12(5), pp.552–555.

Widmer, R., Oswald-Krapf, H., Sinha-Khetriwal, D., Schnellmann, M. & Böni, H., 2005. Global perspectives on e-waste. *Environmental Impact Assessment Review*, 25(5), pp.436–458.

Wu, S. & Cheng, L., 2014. Approach to evaluation of the overall strengthening and toughening effect of continuous fiber-reinforced ceramic matrix composites. *International Journal of Materials Research,* 105(4), pp.365-368.

Xiao, Y., Yang, Y., Van Den Berg, J., Sietsma, J., Agterhuis, H., Visser, G. & Bol, D., 2013. Hydrometallurgical recovery of copper from complex mixtures of end-of-life shredded ICT products. *Hydrometallurgy*, 140, pp.128–134.

Yamane, L.H., de Moraes, V.T., Espinosa, D.C.R. & Tenório, J.A.S., 2011. Recycling of WEEE: Characterization of spent printed circuit boards from mobile phones and computers. *Waste Management,* 31(12), pp.2553–2558.

Yang, J.G., Wu, Y.T. & Li, J., 2012. Recovery of ultrafine copper particles from metal components of waste printed circuit boards. *Hydrometallurgy*, 121, pp.1–6.

Yoo, J., Jeong, J., Yoo, K., Lee, J. & Kim, W., 2009. Enrichment of the metallic components from waste printed circuit boards by a mechanical separation process using a stamp mill. *Waste Management,* 29(3), pp.1132–1137.

Zhang, L. & Xu, Z., 2016. A review of current progress of recycling technologies for metals from waste electrical and electronic equipment. *Journal of Cleaner Production*, 127, pp.19–36.

Zhang, S. & Forssberg, E., 1998. Optimization of electrodynamic separation for metals recovery from electronic scrap. *Resources, Conservation and Recycling*, 22(3–4), pp.143–162.

Zhang, S. & Forssberg, E., 1999. Intelligent Liberation and classification of electronic scrap. *Powder technology,* 105(1-3), pp.295–301.

VIII. Appendix

a. Appendix A

Table VIII-1: Material loss of shredded PCBs

Shredding cycle	1st	2nd	3rd	4th	5th	6th
PCB 1	0.14	0.20	0.29	0.33	0.40	0.42
PCB 2	0.13	0.18	0.38	0.42	0.52	0.54
PCB 3	0.07	0.24	0.35	0.37	0.41	0.46
Average	0.11	0.21	0.34	0.37	0.44	0.47
Standard Dev.	0.04	0.03	0.05	0.05	0.07	0.06
CV	33.41	14.78	13.48	12.08	15.02	12.91

Table VIII-2: Material loss of planetary ball milled PCBs

Shredding cycle + Ball milling time (min)	2nd	2nd + 60	2nd + 120	4th	4th + 60	4th + 120
PCB 1	0.20	0.50	0.55	0.33	0.47	0.56
PCB 2	0.18	0.42	0.49	0.42	0.51	0.47
PCB 3	0.24	-	-	0.37	-	-
Average	0.21	0.46	0.52	0.37	0.49	0.51
Standard Dev.	0.03	0.06	0.04	0.05	0.03	0.06
CV	14.78	12.30	8.16	12.08	5.77	12.36

Table VIII-3: Material loss of Liq. N2 and Pulverised PCBs

Shredding cycle + Type of treatment	1st + Liq. N2	1st + 3 min pulverising
PCB 1	0.15	0.98
PCB 2	0.06	1.25
PCB 3	0.10	1.12
Average	0.10	1.12
Standard Dev.	0.05	0.14
CV	60.61	17.12

b. Appendix B

The percentage of leaching in most literature is determined based on the following equation.

$$Copper\ recovered\ (\%) = \frac{Amount\ of\ \text{copper}\ in\ leached\ solution\ (mg/g)}{Initial\ amount\ of\ \text{copper}\ in\ PCB\ (mg/g)} \quad \textit{Eq. (VIII-1)}$$

Table VIII-4: Leaching data for untreated PCBs

Shredding cycle		Treatment conditions	Leach time (hrs)	pH	Copper recovered (g)	Copper recovered (%)
Untreated	1st	-	0.2	10.07	0.06	0.21
			1	10.04	0.07	0.24
			3	10.00	0.10	0.36
			5	9.95	0.14	0.49
			7	9.92	0.20	0.68
			24	9.86	1.74	6.01
			48	9.93	3.21	11.09
			72	9.99	4.20	14.48
	2nd	-	0.2	10.08	0.07	0.24
			1	10.06	0.08	0.29
			3	10.02	0.12	0.43
			5	9.99	0.17	0.59
			7	9.93	0.24	0.84
			24	9.97	1.97	6.78
			48	10.01	3.98	13.74
			72	10.04	4.96	17.12
	3rd	-	0.2	9.94	0.08	0.26
			1	10.04	0.09	0.30
			3	9.96	0.12	0.41
			5	10.02	0.16	0.54
			7	10.02	0.23	0.79
			24	9.95	2.14	7.38
			48	9.90	4.39	15.16
			72	9.90	5.75	19.85

			0.2	10.06	0.08	0.27
			1	10.07	0.09	0.32
			3	10.02	0.14	0.47
			5	10.02	0.19	0.67
	*4th	-	7	10.02	0.26	0.88
			24	10.01	2.35	8.11
			48	10.02	4.64	16.02
			72	9.99	6.08	20.99
			0.2	10.06	0.08	0.28
			1	10.09	0.10	0.34
			3	10.06	0.14	0.49
			5	10.01	0.22	0.77
Untreated	*5th	-	7	10.02	0.33	1.12
			24	9.94	2.99	10.32
			48	10.02	5.26	18.14
			72	10.03	6.63	22.89
			0.2	10.03	0.08	0.28
			1	10.09	0.11	0.39
			3	10.06	0.15	0.53
			5	10.00	0.22	0.76
	6th	-	7	10.02	0.32	1.11
			24	9.91	3.05	10.54
			48	10.00	5.56	19.19
			72	9.98	6.80	23.49

(*) indicates repeats in triplicates; average of three samples

Table VIII-5: Leaching data for NaOH pre-treated PCBs

Shredding cycle		Treatment conditions	Leach time (hrs)	pH	Copper recovered (g)	Copper recovered (%)
			0.2	10.06	0.07	0.23
			1	10.04	0.08	0.29
			3	10.02	0.14	0.49
			5	9.98	0.28	0.97
NaOH	*1st	-	7	9.98	0.48	1.64
			24	10.03	4.89	16.88
			48	9.99	6.18	21.32
			72	10.00	6.58	22.70

NaOH	2nd	-	0.2	10.12	0.08	0.28
			1	10.1	0.11	0.37
			3	10.02	0.17	0.60
			5	10.02	0.26	0.91
			7	10.00	0.47	1.63
			24	10.06	5.46	18.84
			48	10.02	6.88	23.75
			72	10.06	7.26	25.04
	3rd	-	0.2	10.13	0.08	0.28
			1	10.10	0.10	0.36
			3	10.03	0.18	0.61
			5	10.10	0.28	0.97
			7	9.98	0.48	1.64
			24	10.05	5.62	19.39
			48	10.02	7.11	24.56
			72	10.10	7.34	25.34
	*4th	-	0.2	10.08	0.09	0.30
			1	10.07	0.10	0.36
			3	10.00	0.17	0.60
			5	10.04	0.28	0.96
			7	9.97	0.53	1.84
			24	10.02	6.03	20.82
			48	9.99	7.37	25.44
			72	10.03	7.57	26.14
	5th	-	0.2	10.10	0.07	0.26
			1	10.06	0.09	0.32
			3	10.02	0.19	0.65
			5	9.94	0.36	1.23
			7	9.97	0.60	2.08
			24	9.94	6.21	21.44
			48	10.01	7.51	25.94
			72	10.03	7.78	26.86
	6th	-	0.2	10.01	0.08	0.29
			1	10.03	0.10	0.36
			3	9.91	0.21	0.71
			5	10.04	0.38	1.32
			7	9.90	0.59	2.04
			24	9.99	6.67	23.03
			48	10.03	7.69	26.54
			72	9.97	7.96	27.49

(*) indicates repeats in triplicates; average of three samples

Table VIII-6: Leaching data for planetary ball milled (PBM) PCBs

Shredding cycle		Treatment conditions	Leach time (hrs)	pH	Copper recovered (g)	Copper recovered (%)
PBM	2nd	60	0.2	10.09	0.13	0.44
			1	10.07	0.17	0.57
			3	10.02	0.32	1.11
			5	10.00	0.39	1.35
			7	10.02	0.46	1.59
			24	10.02	0.84	2.91
			48	9.94	2.34	8.07
			72	10.03	3.70	12.79
	2nd	120	0.2	10.19	0.14	0.49
			1	10.17	0.19	0.65
			3	10.12	0.28	0.97
			5	10.08	0.36	1.26
			7	10.04	0.43	1.48
			24	10.04	1.02	3.52
			48	10.05	2.42	8.34
			72	9.94	3.36	11.61
	4th	60	0.2	10.16	0.11	0.38
			1	10.15	0.14	0.49
			3	10.10	0.18	0.62
			5	10.05	0.23	0.80
			7	10.03	0.29	1.01
			24	9.97	0.89	3.09
			48	10.05	2.49	8.60
			72	9.92	3.85	13.29
	4th	120	0.2	10.10	0.15	0.52
			1	10.07	0.22	0.76
			3	9.98	0.29	0.99
			5	9.99	0.34	1.18
			7	9.99	0.51	1.75
			24	10.02	0.97	3.34
			48	9.94	2.43	8.40
			72	10.03	3.52	12.15

Table VIII-7: Leaching data for Liq.N_2 pre-treated and pulverised PCBs

Shredding cycle		Treatment conditions	Leach time (hrs)	pH	Copper recovered (g)	Copper recovered (%)
Liq.N_2	1st	-	0.2	10.24	0.07	0.23
			1	10.20	0.08	0.26
			3	10.18	0.10	0.34
			5	10.14	0.14	0.49
			7	10.15	0.18	0.61
			24	10.06	0.87	3.02
			48	10.03	2.46	8.51
			72	10.05	3.26	11.25
Pulverised	1st	3	0.2	10.23	0.39	1.33
			1	10.21	0.61	2.12
			3	10.17	1.06	3.65
			5	10.14	1.50	5.17
			7	10.12	1.93	6.66
			24	10.13	3.29	11.35
			48	10.02	4.65	16.06
			72	10.02	4.82	16.64

Table VIII-8: Reaction rate of the Cu recovery curves

Type of pre – or post-treatment	Shredding Cycle	Milling time (min)	Rate of reaction (g/hr)			
			0-7	7-24	24-48	48-72
Untreated	1st	-	0.02	0.09	0.06	0.04
	2nd	-	0.03	0.10	0.08	0.04
	3rd	-	0.03	0.11	0.09	0.06
	4th	-	0.03	0.12	0.10	0.06
	5th	-	0.04	0.16	0.09	0.06
	6th	-	0.04	0.16	0.10	0.05
NaOH	1st	-	0.06	0.26	0.05	0.02
	2nd	-	0.06	0.29	0.06	0.02
	3rd	-	0.06	0.30	0.06	0.01
	4th	-	0.07	0.31	0.06	0.01
	5th	-	0.08	0.32	0.06	0.01
	6th	-	0.08	0.36	0.04	0.01
Planetary Ball Mill	2nd	60	0.03	0.02	0.06	0.06
	2nd	120	0.05	0.03	0.06	0.04
	4th	60	0.04	0.04	0.07	0.06
	4th	120	0.05	0.03	0.06	0.05
Liq. N_2	1st	-	0.02	0.04	0.07	0.03
Pulverised	1st	-	0.23	0.08	0.06	0.01

c. Appendix C

Table VIII-9: Industrial grab shredder power consumption

Time (sec)	Avg. power consumed (W)	STD
1st Shredding Cycle		
0	118.50	0.00
1	123.91	0.11
2	137.34	4.08
3	170.56	6.31
4	196.16	3.09
5	209.55	6.56
6	217.24	5.20
7	214.66	6.49
8	212.14	7.45
9	197.59	8.30
10	165.50	9.40
11	139.61	7.41
12	125.55	4.01
13	120.26	1.62
14	118.50	0.00
2nd Shredding Cycle		
0	118.50	0.00
1	128.92	9.82
2	173.46	8.64
3	234.34	11.03
4	206.34	5.51
5	159.54	14.29
6	142.04	3.66
7	124.61	3.43
8	119.20	1.22
9	118.50	0.00
3rd Shredding Cycle		
0	118.50	0.00
1	135.93	8.83
2	165.09	3.01
3	194.28	9.86
4	156.46	15.29
5	131.05	10.29
6	121.32	3.23
7	118.50	0.00

Time (sec)	Avg. power consumed (W)	STD
4th Shredding Cycle		
0	118.50	0.00
1	130.22	1.91
2	159.76	8.34
3	164.59	3.87
4	152.08	2.68
5	138.04	11.12
6	124.10	5.58
7	118.50	0.00
5th Shredding Cycle		
0	118.50	0.00
1	135.89	8.74
2	158.95	13.98
3	191.81	9.28
4	168.13	11.35
5	135.32	3.04
6	125.55	1.22
7	121.67	1.06
8	119.20	1.22
9	118.50	0.00
6th Shredding Cycle		
0	118.50	0.00
1	123.86	3.29
2	140.56	2.76
3	169.90	3.09
4	190.39	5.54
5	175.33	3.20
6	141.43	6.61
7	124.14	3.23
8	119.55	1.83
9	118.50	0.00

Table VIII-10: Liq.N_2, planetary ball mill & pulveriser power consumption

Time (sec)	Avg. power consumed (W)	STD	Time (min)	Avg. power consumed (W)	STD
1st Shredding Cycle + Liq. N_2			**Planetary Ball Mill**		
0	118.50	1.37	**2nd Shredding Cycle**		
1	127.49	4.14	60	93	-
2	164.24	4.95	120		
4	202.47	7.69	**4th Shredding Cycle**		
5	220.02	8.98	60	93	-
6	231.61	10.06	120		
7	234.77	6.13	**1st Shredding cycle + Pulveriser**		
8	224.81	5.10	3	2500	-
9	205.40	5.33			
10	160.65	2.18			
11	130.96	2.77			
12	123.08	1.22			
13	118.50	0.00			

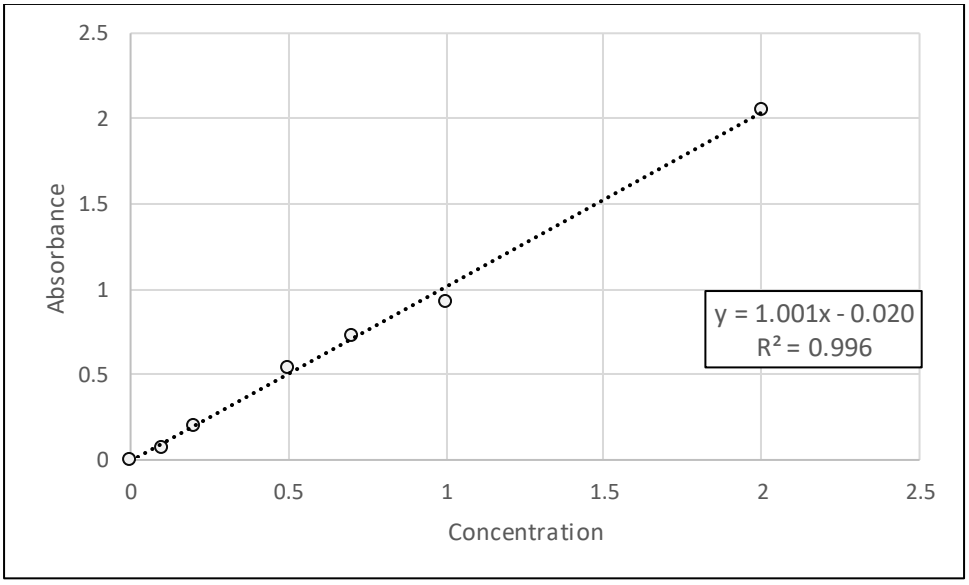

Figure VIII-1: Calibration curve for UV spectrophotometer

d. Appendix D

Table VIII-11: Copper concentrations for the individual shredding and milling cycles

			Sieve sizes (µm)						
	Shredding cycle	**Milling time (min)**	**≤2000**	**2000**	**3350**	**4750**	**6700**	**≥8000**	**Total**
Cu conc. (g)	1st	-	0.27	0.17	0.34	1.19	1.37	24.20	27.54
Cu conc. (%)			0.96	0.60	1.24	4.33	4.98	87.88	100.00
Cu conc. (g)	2nd	-	0.85	0.72	1.26	3.12	2.96	18.93	27.84
Cu conc. (%)			3.04	2.58	4.53	11.22	10.64	67.99	100.00
Cu conc. (g)	3rd	-	1.26	0.90	1.82	3.97	3.99	14.95	26.89
Cu conc. (%)			4.68	3.35	6.76	14.77	14.85	55.60	100.00
Cu conc. (g)	4th	-	1.67	1.29	2.34	4.78	4.21	12.68	26.97
Cu conc. (%)			6.19	4.77	8.69	17.72	15.60	47.03	100.00
Cu conc. (g)	5th	-	1.82	1.84	3.11	5.63	4.61	9.40	26.40
Cu conc. (%)			6.90	6.96	11.77	21.33	17.44	35.60	100.00
Cu conc. (g)	6th	-	1.90	1.95	3.81	5.40	6.38	7.49	26.93
Cu conc. (%)			7.05	7.25	14.15	20.07	23.68	27.80	100.00
Cu conc. (g)	2nd	60	2.57	1.11	1.73	4.28	4.51	12.52	26.73
Cu conc. (%)			9.63	4.16	6.47	16.03	16.87	46.84	100.00
Cu conc. (g)	2nd	120	4.86	1.49	1.65	5.01	5.67	8.38	27.07
Cu conc. (%)			17.96	5.52	6.11	18.49	20.96	30.95	100.00
Cu conc. (g)	4th	60	5.00	2.23	3.38	6.23	5.30	4.82	26.97
Cu conc. (%)			18.54	8.27	12.54	23.12	19.65	17.88	100.00
Cu conc. (g)	4th	120	5.73	2.53	3.11	7.12	4.95	3.80	27.25
Cu conc. (%)			21.01	9.29	11.43	26.14	18.18	13.95	100.00

Table VIII-12: Cu recovery (g) and associated costs of the investigated recovery processes

	Shredding	Cu Recovery (g)				Total Cost (R/PCB)				
	Cycle + Time	7	24	48	72	General	7	24	48	72
Untreated	1st	0.20	1.74	3.21	4.20	0.001	0.02	0.17	0.32	0.42
	2nd	0.24	1.97	3.98	4.96	0.003	0.02	0.19	0.40	0.49
	3rd	0.23	2.14	4.39	5.75	0.005	0.02	0.21	0.43	0.57
	4th	0.26	2.35	4.64	6.08	0.009	0.02	0.23	0.46	0.60
	5th	0.33	2.99	5.26	6.63	0.014	0.02	0.29	0.51	0.65
	6th	0.32	3.05	5.56	6.80	0.020	0.01	0.29	0.54	0.66
NaOH*	1st	0.48	4.89	6.18	6.58	0.047	0.05	0.48	0.62	0.66
	2nd	0.47	5.46	6.88	7.26	0.044	0.04	0.54	0.69	0.72
	3rd	0.48	5.62	7.11	7.34	0.043	0.04	0.56	0.71	0.73
	4th	0.53	5.89	7.33	7.59	0.044	0.04	0.58	0.72	0.75
	5th	0.60	6.21	7.51	7.78	0.046	0.05	0.61	0.74	0.76
	6th	0.59	6.67	7.69	7.96	0.039	0.04	0.65	0.75	0.78
PBM	2nd + 60 min	0.46	0.84	2.34	3.70	0.147	-0.10	-0.06	0.09	0.22
	2nd + 120 min	0.43	1.02	2.42	3.36	0.291	-0.25	-0.19	-0.05	0.05
	4th + 60 min	0.29	0.89	2.49	3.85	0.153	-0.12	-0.06	0.10	0.23
	4th + 120 min	0.51	0.97	2.43	3.52	0.297	-0.25	-0.20	-0.05	0.05
Liq. N_2*	1st	0.18	0.87	2.46	3.26	0.001	0.02	0.09	0.25	0.33
Pulveriser	1st + 3 min	1.93	3.29	4.65	4.82	0.195	0.00	0.13	0.27	0.29

*(-) indicates a cost-benefit deficit; *excluding chemical pre-treatment costs for NaOH and Liq. N_2*

e. Appendix E

Table VIII-13: Average Energy cost calculation according to Eskom (2019)

Sector	High Demand Season (Jun – Aug) (c/kWh)	Low Demand Season (Sep-May) (c/kWh)	Additional costs (c/kWh)	Average cost by sector (c/kWh)	Average cost of electricity in SA (R/kWh)
Urban (1)	152.65	97.79	3.84	140.58	
Residential (2)	244.30	149.75	0	197.02	1.55
Rural (3)	163.40	87.11	7.79	156.40	

(1) - Nightsave Large, Nightsave Small, Megaflex, Megaflex Gen, Miniflex, Business rate; (2) – Homepower standard, Homelight; (3) – Nightsave Rural, Ruraflex, Ruraflex Gen

f. Appendix F

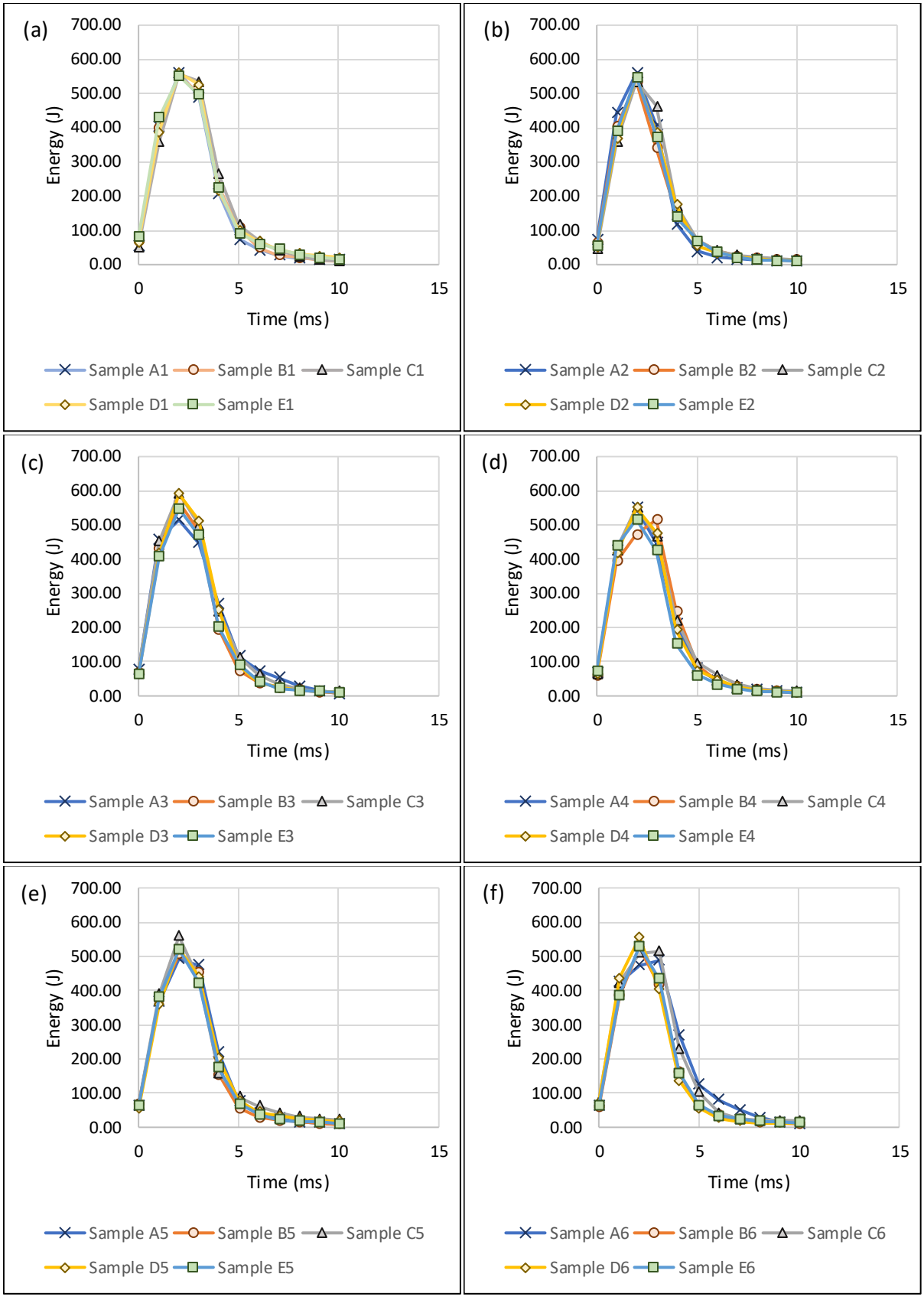

Figure VIII-2: Absorbed impact energy over time; (a) – Sample area 1; (b) – Sample area 2; (c) – Sample area 3; (d) – Sample area 4; (e) – Sample area 5; (f) – Sample area 6

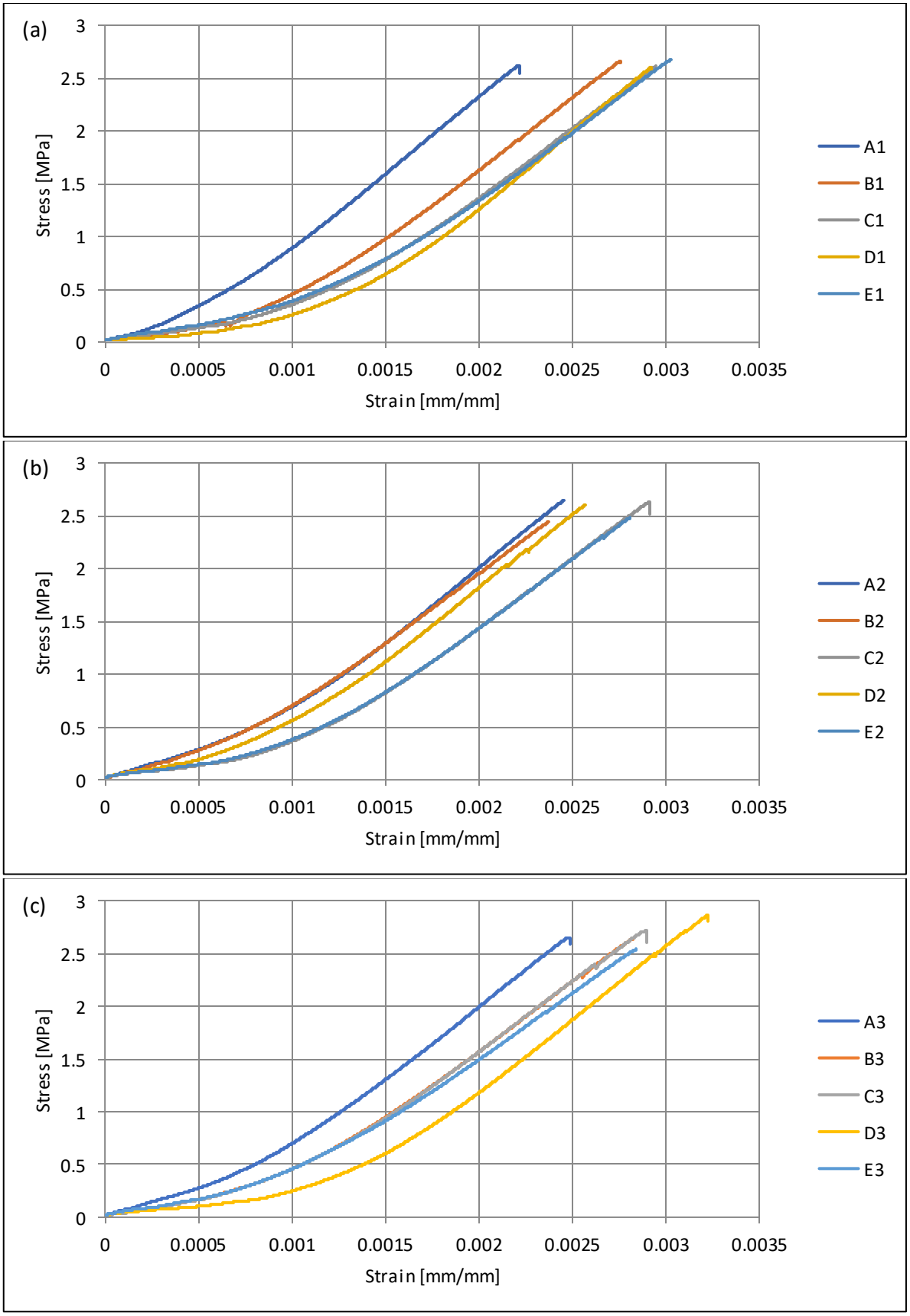

Figure VIII-3: Tensile stress response (MPa); (a) – Sample area 1; (b) – Sample area 2; (c) – Sample area 3

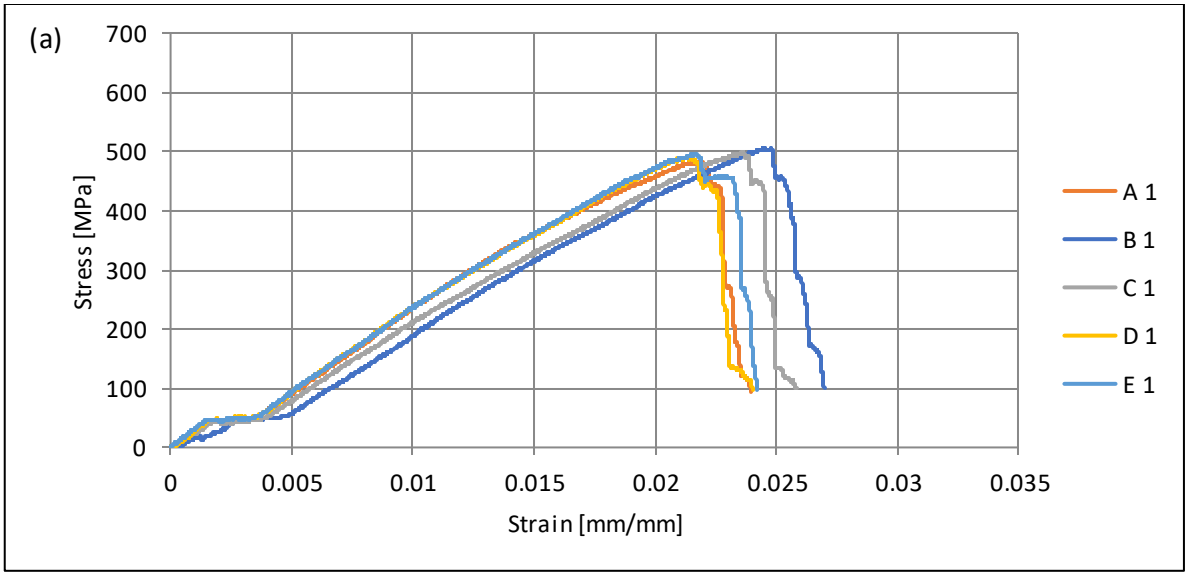
(a)
Stress [MPa]
700
600
500
400
300
200
100
0
0
0.005
0.01
0.015
0.02
0.025
0.03
0.035
Strain [mm/mm]
A 1
B 1
C 1
D 1
E 1

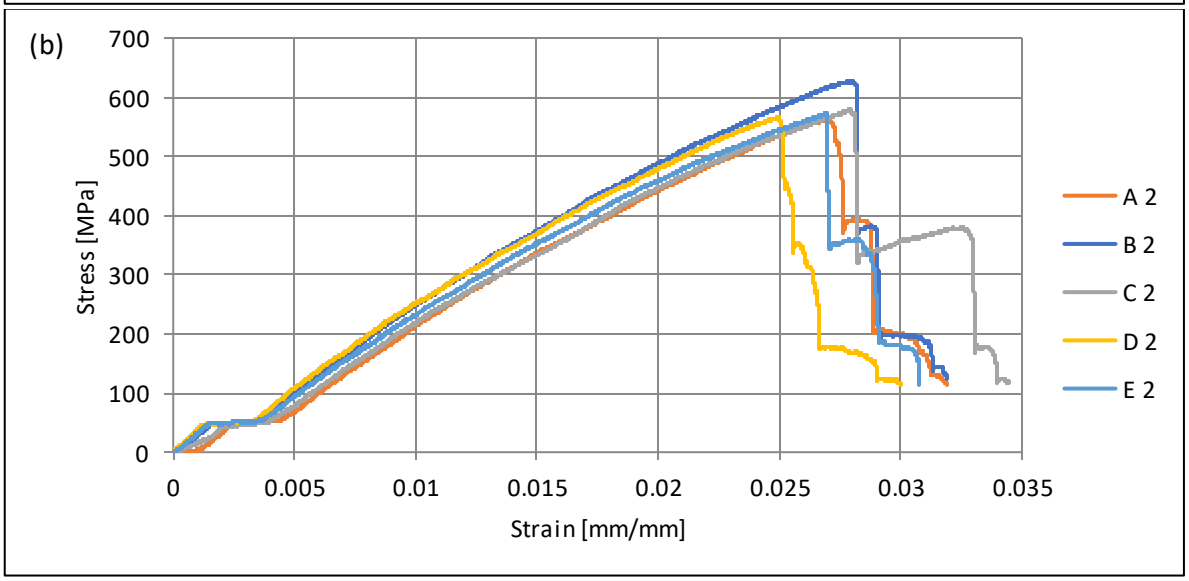
(b)
Stress [MPa]
700
600
500
400
300
200
100
0
0
0.005
0.01
0.015
0.02
0.025
0.03
0.035
Strain [mm/mm]
A 2
B 2
C 2
D 2
E 2

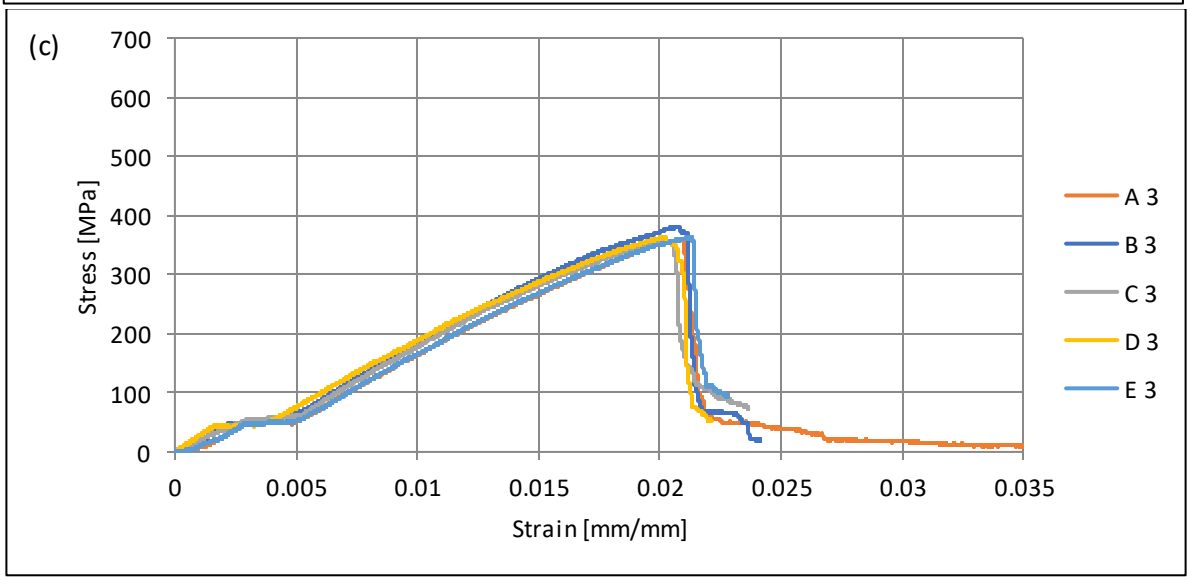
(c)
Stress [MPa]
700
600
500
400
300
200
100
0
0
0.005
0.01
0.015
0.02
0.025
0.03
0.035
Strain [mm/mm]
A 3
B 3
C 3
D 3
E 3

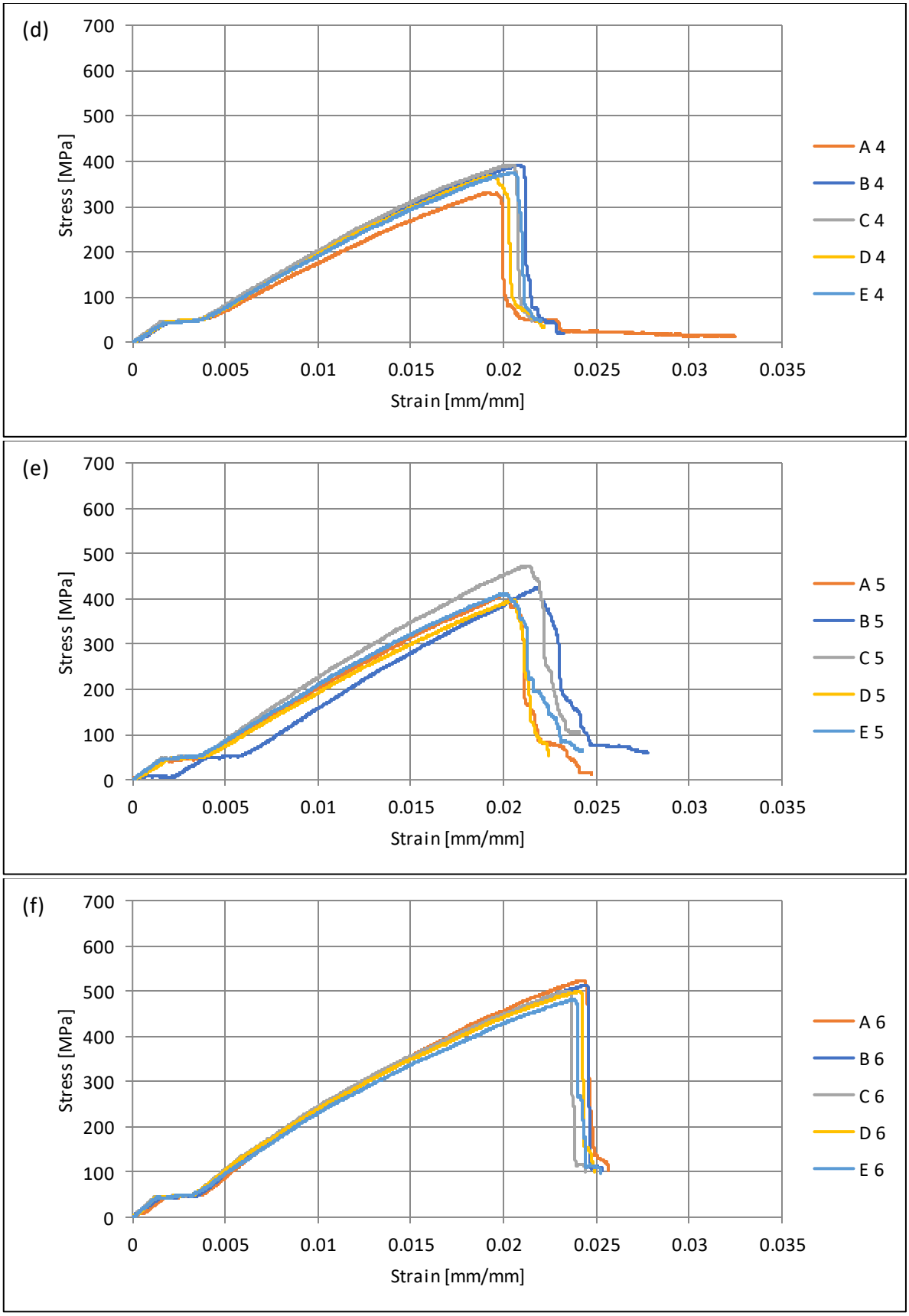

Figure VIII-4: Three-point bending stress respond (MPa); (a) – Sample area 1; (b) – Sample area 2; (c) – Sample area 3; (d) – Sample area 4; (e) – Sample area 5; (f) – Sample area 6